TECHNISCHE UNIVERSITÄT WIEN
Vienna | Austria

Signature Supervisor

Master Thesis

Chemical characterisation of PM 10 and PM 1 collected at the Sonnblick Observatory

Under Supervision of

Ao. Univ. Prof. Dipl.-Ing. Dr. techn. Anneliese Kasper-Giebl
(E164 Institute of Chemical Technologies and Analytics)

And
Mag.ª Marion Greilinger
(Zentralanstalt für Meteorologie und Geodynamik)

Submitted to TU Wien
Faculty of Technical Chemistry

By

Hanna Gureczny BSc
Korneuburgerstraße 157
2102 Bisamberg

Vienna, 2018

Hanna Gureczny

An educated person knows many things,

And one with much experience knows what he is talking about.

An inexperienced person knows few things,

But he that has travelled acquires much cleverness.

Sirach 34:9-11

Ein Mensch, der viel herumgekommen ist, hat viel gelernt;

er hat reiche Erfahrungen gesammelt und redet von Dingen, die er kennt.

Wer keine Erfahrungen gemacht hat, hat nur ein beschränktes Wissen;

wer aber viel herumgekommen ist, ist reich an Lebensklugheit.

Jesus Sirach 34,9-11

Acknowledgments

First of all, I want to thank Anneliese Kasper-Giebl, who gave me the possibility to join her great research group and to write my master thesis under her supervision. Thanks for guiding me on my journey through unknown depths of aerosol science.

Thanks to Julia Firmkranz, Bernadette Kirchsteiger, Peter Redl, Thomas Steinkogler and Hans Lohninger for answering patiently all my questions about measurement systems or data related concerns. Peter Redl, I want to thank for carrying out the PM 10 sugar and Sunset measurements, as well as preparing data of the Aethalometer and SHARP measurements at SBO. Furthermore, I am grateful that Marion Greilinger has established the measurements and introduced me to her work, including giving me tips and tricks of her practical experience. Additionally, I am grateful for the opportunity to measure XRF at the X-Ray Center (XRC – TU Wien) under the supervision of Johannes Zbiral from the Research Group for Powder Metallurgy. For maintaining of the sampling system, I want to thank Gerhard Schauer, who is responsible at the Sonnblick Observatory, where samples are being taken.

I would also like to thank the whole research group for the spirit of community, apparent while having lunch together and passing on relevant information as well. In addition, I appreciate all the small conversations, which brightened my days.

Finally, to finish my thesis I needed a lot of support from my family and friends, who pushed me forward and urged me to carry on. Thanks to all my beloved fellows, who endured my bad days as well. Special thanks to Karin, Erwin, Diana, Esther, Sarah and Ralf, who read my thesis and gave me feedback to improve my text and make it better understandable. Thank you all for believing in my abilities, at times when I could not do so.

Abstract

Since 2016 weekly samples of aerosols (PM 1 and PM 10) are taken at Sonnblick Observatory (SBO; 3106 m a.s.l.) in cooperation with ZAMG (Zentralanstalt für Meteorologie und Geodynamik). These filter samples were analysed for the time period from June 2016 to May 2018. X-Ray fluorescence analysis (XRF), ion chromatography (IC) as well as Transmissiometer and Sunset measurements were used to characterise the composition of these aerosol samples. Ions, sugars, carbonaceous compounds, as well as metals, were measured and compared with available online measurements of aerosols at SBO (Aethalometer, SHARP).

In case that analytes were determined with more than one analytical method an intercomparison was performed.

Typical annual cycles of analytes could be observed over the two-year time period. Higher concentration in summer than in winter were found at the height of the sampling station due to different mixing of the troposphere for most of the compounds. In summer the mixing layer reaches higher up, transporting boundary layer air masses up to the site. Summer to winter ratios reach up to 7.

Concentrations of PM 1 mostly lay below the concentrations of PM 10, as expected.

Kurzfassung

Im Rahmen dieser Arbeit wurden PM 10 und PM 1 (PM steht für Particulate Matter, zu deutsch: Feinstaub), welche als Wochenproben am Sonnblick Observatorium (3106 m ü.N.N.) in Zusammenarbeit mit der ZAMG (Zentralanstalt für Meteorologie und Geodynamik) gesammelt wurden, analysiert. Die Zusammensetzung der Aerosolproben wurde von Juni 2016 bis May 2018 mittels Röntgen-Fluoreszenz-Analyse (RFA), Ionenchromatographie (IC), sowie Transmissiometer und Sunset Messungen untersucht. Ionen, Zucker, kohlenstoff-haltige Bestandteile, sowie Metalle wurden gemessen und mit Messungen vom Sonnblick, welche online zur Verfügung standen (Aethalometer, SHARP), verglichen.

Messergebnisse von Analyten, die mit mehr als einer Methode bestimmt wurden, wurden miteinander verglichen.

Über die beiden Jahre der Probenahme hinweg konnten bei allen Analyten die typischen Jahresgänge beobachtet werden. Auf dieser Höhe sind höhere Konzentrationen an Aerosolen im Sommer im Vergleich zum Winter gefunden worden, was auf eine unterschiedliche Durchmischung der Troposphäre zurück zu führen ist. Im Sommer reicht die Mischungsschicht höher hinauf und transportiert so Luftmassen aus der bodennahen Grenzschicht zur Messstation empor. Das Verhältnis von Sommer zu Winter Konzentrationen steigt auf bis zu 7.

Die Konzentration der PM 1 Fraktion lag meistens erwartungsgemäß unterhalb jener der PM 10 Fraktion.

Nomenclature

%rH ..... percentage of relative humidity
Al ..... aluminium
Ca/Ca^{2+} ..... calcium/calcium ion
CO_2 ..... carbon dioxide
CO_3^{2-} ..... carbonate (-ion)
BC ..... black carbon measured with transmissometry
BL ..... Blank values
Cl ..... chloride (-ion)
Digitel ..... abbreviation for sampling system of PM 10 called Digitel DHA-80 (high volume sampler)
EBC ..... equivalent BC measured with aethalometer
EC ..... elemental carbon measured with Sunset
Fe ..... iron
h ..... hour(s)
HCl ..... hydrochloric acid
IC ..... ion chromatography
ICP-MS ..... inductively coupled plasma mass spectroscopy
K/K^+ ..... potassium/potassium ion
LOD ..... limit of detection
µl ..... microliter
Mg/Mg^{2+} ..... magnesium/magnesium ion
MSA ..... methane sulfonic acid
Na^+ ..... natrium ion
NH_4^+ ..... ammonium
NO_2^- ..... nitrite (-ion)
NO_3^- ..... nitrate (-ion)
OC ..... organic carbon
P ..... phosphor
PM ..... Particulate Matter
PM mass ..... mass of Particulate Matter
PM 1 ..... Particulate Matter with an aerodynamic diameter of less than 1 µm
PM 10 ..... Particulate Matter with an aerodynamic diameter of less than 10 µm
PM coarse ... Particulate Matter with an aerodynamic diameter between 1 and 10 µm (fraction between PM 1 and PM 10)
S ..... sulphur
Si ..... silicium
SBO ..... Sonnblick Observatory
SD ..... Saharan dust
SDE ..... Saharan dust event
SHARP ..... Synchronized Hybrid Ambient Real-time Particulate (Monitor)
SO_4^{2-} ..... sulfate (-ion)
TC ..... total carbon
TSP ..... total suspended particles
XRF ..... X-Ray fluorescence analysis
ZAMG .....Zentralanstalt für Meteorologie und Geodynamik

1. What are we doing?

This thesis contributes to the FFG-project DUSTFALL, which is investigating Saharan dust events (SDEs), Particulate Matter (PM) concentrations and the impact of SDEs on air quality. At the present time, ZAMG (Zentralanstalt für Meteorologie und Geodynamik) predicts Saharan dust (SD) concentration in the atmosphere and near-ground Particulate Matter (PM) concentration twice a day. SBO offers the opportunity for comparative analysis between model results and in-situ measurements. To evaluate the online measurements for predictions at the Sonnblick Observatory (SBO), comparative analysis is carried out in this project. [1] Since June 2016, aerosols are sampled weekly at the SBO to gather chemical information of the composition of aerosols. For this thesis data from June 2016 to May 2018 is used. Methods of sampling and measurements of compounds, as well as beginning data analysis is outlined in the present work.

2. Why are we doing this?

Aerosols play a relevant role in earth radiation processes, climate change, cloud formation, nutrient circles, visibility and finally in human health [2], [3]. These various reasons lead to a great interest of diverse research groups. One of the aims of the project DUSTFALL is to increase knowledge about the occurrence of SD in Austria [1].

PM has two sources. On one hand, natural sources supply sea salt aerosols, water droplets, bacteria, pollen, mineral dust and others. On the other hand, manmade aerosols emerge for example by combustion or other production processes. [2]

One of the main contributors to global natural PM load is mineral dust. Mineral dust may originate in the Saharan desert and therefore sometimes is called Saharan dust (SD) - for details see chapter 2.2. Here, time periods, where SD arrives at a special receptor point, are called Saharan Dust events (SDEs). ZAMG gives a prediction of Saharan dust concentrations and near-ground PM concentrations in Austria twice a day. For April 2016 a good prediction of a SDE with up to 70 % contribution of SD to PM concentration could be made for SBO by Baumann-Stanzer et al (2019) [4].

PM and SD are relevant for the public as recently published newspapers show. In March 2018 big headlines were dedicated to the topic of aerosols and especially mineral dust transport. In Ukraine, Russia, Bulgaria and Romania a major sand, dust and pollen event was observed, which is occurring roughly every 5 years in such a high extent. “The Independent” for example wrote about orange snow in Eastern Europe:

> *“According to Russia’s environmental watchdog, however, the snow was possibly the result of chemical pollution as it contained large amounts of iron, acids and nitrates.”* [5]

If the snow contains iron (Fe), acids and nitrates, does it have to be anthropogenically polluted? In this work samples representing a remote site are considered. Anthropogenic pollution is possible but limited. At least in some cases events with Fe, acids and nitrates in large amounts can be traced back to a natural origin. Nevertheless, our atmosphere is anthropogenically influenced as seen for example in elevated CO_2 concentrations, but discussion hereof would exceed this work, where focus is laid upon chemical characterisation of PM.

Composition of PM 1 and PM 10, as well as their concentration ratio, provides data for further evaluations in respect to SDEs and comparison with previous measurements.

2.1. What are aerosols?

Aerosols are a colloidal mixture. They consist of small solid or fluid particles suspended in gases. Solid particles suspended in air are called Particulate Matter (PM). PM is an atmospheric aerosol, which is discussed in this work. The atmosphere is the air accumulated around the earths’ surface on a global scale. The atmospheric aerosols are mainly of natural origin except in urban ambience and underlie

strong regional variations in concentration. Depending on their composition, their influences around the world vary as well. [6]

As atmospheric aerosols are spread around the world, one of the major effects is their influence on radiation balance, which means the amounts of radiation reaching the earth's surface and leaving it, thus influencing the temperature homeostasis. Particles either absorb light, which leads to a warming effect on the climate, or they scatter light, which tends to have a cooling effect on the earth due to enhanced reflection. Furthermore, aerosols can serve as condensation nuclei as well as ice nuclei and can link the radiative effects of particles to those of clouds and cloud formation processes. One of the remaining uncertainties concerning the overall global effects of aerosols on the radiative balance is due to black carbon, because black carbon induces a complex cloud response in addition to its absorption. Black carbon is formed during incomplete combustion of biomass or fossil fuel. [7]

Additionally, to their influence on solar radiation and cloud formation as condensation- or ice nuclei, aerosols play a role in atmospheric chemistry and biogeochemical cycles. For example, nutrients like Fe and P are transported from the Sahara to the Amazonian rain forest. The interaction and dependency of two ecosystems, which are separated by the ocean but connected through the atmosphere, is part of understanding and forming the functions of the global system earth. [7], [8]

Aerosols also show direct impact on humans. PM concentration has been correlated to symptoms in the cardiovascular system and premature deaths. The effect of PM on humans differ with their size as the particles penetrate deeper lying parts of the body with decreasing size. [9]–[11] PM 10 for example, shows an increase of cardiovascular daily mortality of 0.9 % per 10 µg/m³ PM enhancement [12], [13], whereas PM 2.5 even showed an increase of 1.4 % per 10 µg/m³ PM rise [13].

Concerning children enhanced PM concentration may lead to reduced lung function. Generally, elderly people above 65 years, children and people already suffering from cardiovascular diseases are more affected by exposure to PM. [10], [11], [14], [15]

Often traffic and industry, as well as biomass burning, or other anthropogenic aerosols are correlated with health impacts. [16] Nevertheless, also natural sources like pollen could show an impact especially concerning allergies or asthma patients, especially increasing allergic diseases in synergy with air pollutants. [17]

Highly relevant is a decrease in PM concentration for every case mentioned above, as there could not be found a lower limit for PM concentration beneath no effects on human health were observed. [18], [19]

The timely influence of aerosols depends on their different lifetimes due to their size and composition. Additionally, aerosols have different lifetimes, depending on the layer aerosols are suspended in. In the troposphere usual lifetime of particles lies between one day and two weeks, whereas in the stratosphere they last up to one year. Size, composition and shape of aerosols vary greatly, as well as their origin. [7]

2.2. Where do aerosols come from?

The source of aerosols depends on the kind of aerosols which are concerned. Generally, aerosols are subdivided into natural and anthropogenic ones. In this study we focus on natural sources, as the sampling site at SBO is located in a remote area. Due to low concentration on this remote site, transportation processes of natural sources are visible. Simultaneously, anthropogenic influences can be observed depending on the current weather situation. [20]

Natural sources are diverse. As one source, volcanic eruptions carry aerosols up into the stratosphere. Another mainly natural source is mineral dust, which accounts for approximately 45 % of global aerosol emissions [21]. Mineral dust mainly consists of silicates including clay minerals, feldspars and quartz. Sometimes carbonates, sulphates, oxides and hydroxides of iron (and occasionally aluminium) contribute to the mineral dust fraction to a smaller extent [22]. With an annual estimate of 300 to 700 megatons per year, the Sahara is the most important emitter. SD transport is correlated to meteorological conditions like the location of high-pressure centres [21]. But stating that the Sahara is the biggest emitter does not necessarily mean, that all mineral dust originates in the Sahara Desert.

Nevertheless, in this work the terms mineral dust and Saharan dust are used equally, even if it is not verified, that all of this mineral dust events actually originate in the Sahara. Looking at the SDE in April 2016, Baumann-Stanzer et al (2019) show that approximately 20 to 30 % of air masses originates in western or eastern Sahara.

There are three major source regions specified for Saharan dust: [21]

- Sahel sector
  includes Senegal, south Mauritania, south Mali
- South and central Sahara sector
  includes Mauritania, north Mali, south Algeria
- North and west Sahara sector
  includes Spanish Sahara, Morocco, west Algeria

There are different approaches of defining the origin of Saharan dust. Caquineau et al (1998) found that the ratio between relative abundance of illite and kaolinite (both clay minerals) is a good tracer for the regional origin of SD, because the relative abundance is different in other regions. This ratio remains unchanged over a long-distance transport. Other methods use elemental ratios of Si, Al, Fe, Ca and K combined with air-mass trajectories to distinguish Saharan dust. Other mineral indicators for SD, originating from the Northern part, are calcite and palygorskite. [22]

Chiapello et al (1997) found high intensities of SDEs originating in the Sahel sector, when transport to the Sal Island (Cape Verde) is observed [21]. Thinking of deserts, this source may not only be a natural source, if natural source is interpreted as “not influenced by human activity”. Production of mineral dust increases in areas of disrupted soil surfaces [23]. Agricultural activities or deforestation as well as desert shifting, both of which offer new surfaces to wind erosion, count as disrupted soil surface [23]. In the Saharan region a seasonal shift of the dust plume is observed [24]–[27]. During summer the plume shifts to the Sahel region. This shift could not be reproduced in a transport model based only on natural sources. In addition, this transport model overestimates the amount of export of mineral dust from Australia, where primary vegetation types are desert and shrub land. This enforces the assumption of anthropogenic influence on mineral dust loads in the Saharan and Sahel region. [23]

3. Methods and Calculation

Here analytical methods are summarized. Furthermore, a limited number of results is shown to explain the methodical approach.

3.1. Where and when did we sample?

Filter samples were taken at the Sonnblick Observatory (SBO), which is located at 3106 m above sea level in the midst of the mountain range called Hohe Tauern (12°57'E, 47°03'N) [20]. The subsurface consists of gneiss. The gneiss core attaches in the North, the North-East and in the East to a schistose sub-surface. [28] In the East and South the ground is covered with large glacier fields. [20] Therefore, the influence of the sub-surface plays a minor role, unless the snow cover is blown off or construction work reaches beyond it.

The sampling system is situated on the roof-top of SBO. Weekly samples were taken from June 2016 to May 2018. In summer 2017 measurements were stopped for several weeks due to construction work at SBO (marked as red week of 27.7.2017). For detailed information of sampling times see Table 1.

Table 1: Weeks of sampling at SBO. Green marked weeks are sampled properly, and red marked weeks are excluded from calculation due to sampling system errors, interruption of the sampling due to constructions at the site* or wrong filter material.**

	02.06.2016	09.06.2016	16.06.2016	23.06.2016	30.06.2016	07.07.2016	14.07.2016	21.07.2016	28.07.2016	05.08.2016	11.08.2016	18.08.2016	25.08.2016	01.09.2016	08.09.2016	15.09.2016	22.09.2016	29.09.2016	06.10.2016	13.10.2016	20.10.2016	27.10.2016	03.11.2016	10.11.2016
PM 10																								
PM 1																								
	17.11.2016	24.12.2016	01.12.2016	08.12.2016	15.12.2016	23.12.2016	29.12.2016	05.01.2017	12.01.2017	19.01.2017	26.01.2017	02.02.2017	16.02.2017	23.02.2017	02.03.2017	09.03.2017	10.03.2017	16.03.2017	23.03.2017	30.03.2017	06.04.2017	13.04.2017	20.04.2017	27.04.2017
PM 10																						**		
PM 1																								
	04.05.2017	12.05.2017	18.05.2017	25.05.2017	01.06.2017	08.06.2017	15.06.2017	22.06.2017	29.06.2017	06.07.2017	14.07.2017	27.07.2017	21.09.2017	28.09.2017	05.10.2017	12.10.2017	19.10.2017	26.10.2017	02.11.2017	11.11.2017	16.11.2017	23.11.2017	30.11.2017	07.12.2017
PM 10												*									**			
PM 1												*												
	14.12.2017	21.12.2017	28.12.2017	04.01.2018	11.01.2018	18.01.2018	25.01.2018	01.02.2018	08.02.2018	15.02.2018	22.02.2018	01.03.2018	08.03.2018	15.03.2018	22.03.2018	29.03.2018	06.04.2018	12.04.2018	19.04.2018	26.04.2018	03.05.2018	10.05.2018	17.05.2018	24.05.2018
PM 10																**								
PM 1																								

3.2. How did we sample?

Aerosols were sampled for chemical analysis on a weekly basis in different size fractions. The aerosol fraction containing the largest particles, PM 10, was sampled with a high-volume system (Digitel DHA-80) on quartz fibre filters having a diameter of 15 cm. PM 1 was sampled on quartz fibre filters with a diameter of 47 mm. The coarse fraction was collected before sampling of PM 1. Sampling substrates were aluminium foils and quartz fibre filters. PM 1 and PM coarse were collected with a home built Berner impactor installed at the whole air inlet operated at SBO. The inlet has an upper cut-off size for

particles of 20 µm at a wind speed of 20 m/s and its temperature is controlled and stabilised at 20 °C. The air flow is distributed to different measurement devices via an isokinetic flow splitter. Aethalometer AE33 and SHARP measurements are performed after the whole air inlet. Aethalometer values are labelled as PM 10 measurements in this work. SHARP measurements are referred to as total suspended particles (TSP).

Blank values (BL) were generated by blank filters, which were treated in the same way as the sampled filters, including transport and loading into the measurement device. In difference to samples, they were exposed to air for one minute only to imitate the influence of contamination of the sampling system and handling. These BL were subtracted from each sample value to get correct values, furthermore they were used to determine the LOD via standard deviation of blanks.

3.2.1. PM 10

For PM 10 measurements PALL Life Science Membrane Filters (Pallflex Tissuequartz; 2500 QAT-UP; size 150 mm) were used in the high-volume sampler Digitel DHA-80. The filter holders were washed with Milli-Q water and afterwards the filters (150 mm diameter) were placed into the sample holders without treatment. Sample holders were piled for transportation to SBO in an airtight container.

After transport of the Digitel filters (PM 10) to or from the SBO, the airtight container had to be aerated properly due to pressure differences between sampling station (700 mbar) and analysis at TU Wien (1013 mbar). Therefore, the small opening in the lid, which is closed with a plug or adhesive strip, was opened slowly. The lid should not be pulled off with force, as the filters inside may rip if the air flows from bottom to top. If the air flows from top to bottom there is no problem as the filters are pressed to the grid on which they are lying.

At a few occasions, glass fibre filters were used by mistake. Due to a lack of sufficient number of blank glass fibre filters the LOD could not be calculated for these cases. Providing more blank filters will enable a correct calculation of measured glass fibre filters in the future. For this work all values measured on glass fibre filters were excluded from calculations and graphs. Additionally, Sunset measurement is not possible with glass fibre filters.

3.2.2. PM 1

For correct sampling of PM 1 aerosols, the PM coarse fraction had to be separated. Here separation took place at the first stage of the impactor. Coarse particles were collected for chemical analysis on an aluminium foil and on a quartz fibre half ring (see Figure 2). The second stage guaranteed the full separation of coarse fraction from the fine fraction by using a greased aluminium foil to deposit all coarse particles which had been blown off the first impactor step (see Figure 1).

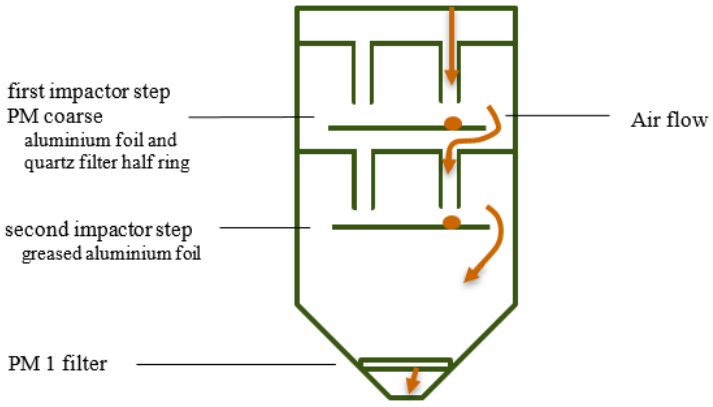

Figure 1: Sampling scheme of PM coarse and PM 1.

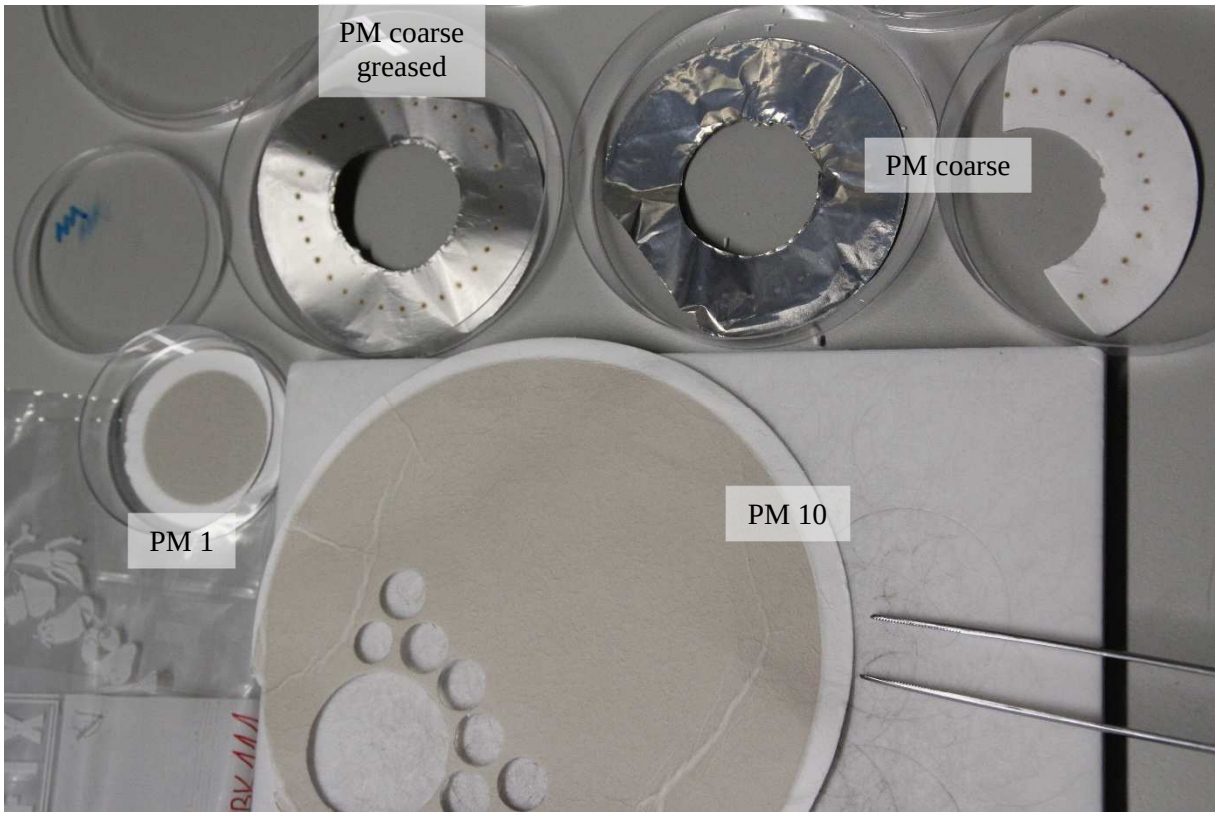

Figure 2: PM 1 and PM 10 sampled on filters and PM coarse sampled on filter and aluminium foil.

Sample preparation included cleaning of the substrates. The small quartz fibre filters (47 mm in diameter) for PM 1 measurements, as well as the quartz and the aluminium substrates for PM coarse were treated in the oven at a temperature of about 550 °C overnight. Afterwards, they cooled down on the oven door for five min and finished cooling to room temperature in a humid atmosphere i. e. in a desiccator containing deionised water. They were left at room temperature for about 12 hours. Aluminium foils and PM 1 filters were weighed before the transportation to SBO for sampling.

Before weighting (see chapter 3.5), filters were equilibrated for at least 48 h at 19 – 21 °C and 45 – 50 %rH. After weighing, they were placed in PS (polystyrene) petri dishes and sealed with Parafilm® M Laboratory film [29] for transport to SBO and storage until the time of sampling. After sampling, the filters were transported to the Lab in Vienna and stored in laboratory film-sealed petri dishes as well.

Greased aluminium foil for the safety of the separation of coarse and PM 1 fraction (second impactor step) was treated equally to the description above except for weighing. Additional greasing (Merck Art. 4318. Desiccator fat. melting range: 45-53 °C) took place before sealing the petri dishes with laboratory film for transport. Greasing of the foils didn't contaminate the filter for PM 1 sampling as pre-experiments of Marion Greilinger showed (pers. comm.).

3.3. What kind of information is extracted?

Different methods were used to determine sampled aerosols. Aerosol mass was only determined for PM 1 on quartz fibre filters and PM coarse on aluminium foils (not greased). After weighing of filters, punches for other analyses were taken. Therefore, the Teflon plate and the tweezer were cleaned with milli-Q-water. The punching tool was cleaned by wiping it on a clean filter material. Sample material was only touched with cleaned tweezers and always laid on a clean plate. Non-destructive analyses were carried out in the first place including X-Ray Fluorescence Analysis (XRF – PM 10 filters only) and transmissometer measurements (soot scan OT21). Afterwards ion chromatography (IC) was conducted for anions, cations and sugars and other destructive analyses like thermal-optical carbon measurement (Sunset Inc.) were performed. The PM 1 samples have not been analysed with all methods due to limited

filter area. Table 2 presents an overview of undertaken measurements. Besides weighing, analysis of PM coarse was not performed within this work.

Table 2: sampled fractions of aerosols and performed measurements.

Methods	PM 1	PM coarse	PM 10
Gravimetric Analysis	✓	✓	×
Transmissometry	✓	×	✓
X-ray fluorescence analysis	×	×	✓
Thermal-optical carbon measurement (Sunset)	✓	×	✓
Ion chromatography	✓	×	✓

As mentioned above, punches were taken from the filters for destructive analysis. As PM 1 filter material had a smaller area than PM 10 filters, it was important to split the area properly. PM 1 filter material was needed for Transmissometer, IC and Sunset measurements (see following chapters). The remaining half was spared and reserved for subsequent ICP-MS analysis, which is not described here. The area was divided as listed in Table 1 and shown in Figure 1).

Table 3: Area distribution of PM 1 filters for analysis given in mm².

	Area [mm²]
Sampled	1075
12 mm stamp (IC cations)	113
1 x 1.5 stamp (Sunset)	150
Leftover half (IC anions and sugars)	274
Remaining half reserved for ICP analysis	537

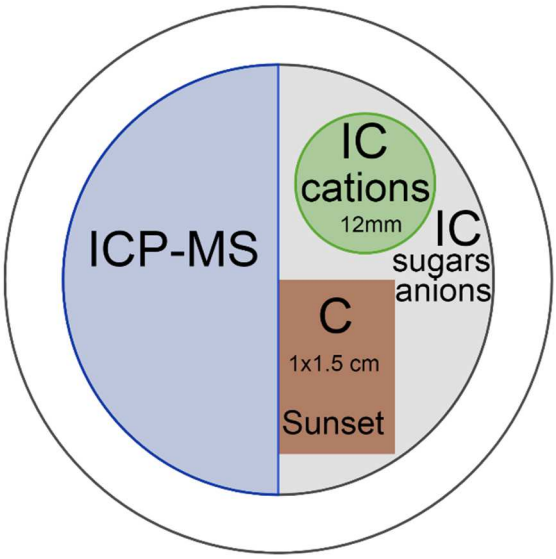

Figure 3: Distribution of PM 1 filter material for analysis.

3.4. Volumes and Times

For PM 10 filters the Digitel sampling system provided the volume of air sampled (at ambient conditions and normalised to 1013 hPa, Temp); as well as the sampling time in minutes in a logfile. For some filters the data was not available due to manual shut offs or power outages. For such cases, the sampling time was retrieved from a hand-written protocol, which was also available for all filters, to allow further calculations. To derive the missing volumes, an average of the air flow rate was multiplied with the manually recorded sampling time. The average air flow rate was deduced from the automatically recorded normalised volumes and sampling times of the previous 24 filters.

For PM 1 and PM coarse samples the sampled air volume was not recorded, but the flow rate was measured instead. Until summer 2017 (14.07.2017) a flowmeter, based on the rotameter principle was used. For that time period (Q_{dis}) was set (approximately at 52 L/min, recorded manually at every sample change) and the respective normalised air flow (Q_{STP}) was calculated according to Equation 1 [30], yielding an average value of 43.6 L/min. In summer 2017 a mass flow controller was installed to set the flow rate at 32.2 L/min (at 1013 mbar, 273 K).

$$Q_{STP} = Q_{dis} \cdot \sqrt{\frac{p_r}{p_{STP}}}$$

Equation 1

Q_{STP}.....flow at standard conditions [L/min]
Q_{dis}.....flow displayed on measurement device [L/min]
(43.6 L/min until mid of 2017 and 32.2 L/min afterwards)
p_r.....pressure of actual working conditions (=700 mbar at SBO) [mbar]
p_{STP}.....pressure under standard conditions (=1013 mbar) [mbar]

The normalised air volume sampled for PM 1 and PM coarse was calculated according to Equation 2, by multiplying the normalised flow rate with the recorded time. Due to the parallel sampling of the PM 10 (Digitel) and the PM 1/PM coarse fractions the automatically recorded sampling time of the Digitel was also used to define the sampling time of the PM 1/PM coarse fractions, missing values could be replaced as described above.

$$V_N = Q_{STP} \cdot t$$

Equation 2

V_N.....normalised volume [L]
Q_{STP}.....flow at standard conditions [L/min]
t.....sampling time of Digitel [min]

3.5. Analytical methods

Here, methods for characterisation, as well as calculation and data treatment are described. First, an overview of relevant parameters concerning all methods is given. Afterwards, the methods are presented one by one.

The active sample area on the filter material was needed for all calculations. The area of PM loaded filter material for PM 10 was 154 cm² (circle with a diameter of 14 cm), for PM 1 filters 1075 mm² (circle with a diameter of 37 mm).

Sometimes the Digitel sampling system had disorders. Therefore, the week of 9.3.2017 was excluded from calculation (see also section B in the Appendix). In addition, samples on glass fibre filters instead of quartz fibre ones were excluded, due to insufficient data for field blanks and as thermal-optical analysis cannot be performed from glass fibre filters (week 13.4. and 16.11.2017; 29.3.2018).

All the calculations for this thesis were performed in R. [31] For linear regression the geom_smooth model was used, which uses a confidence interval of 95% to show a grey background pointing out the uncertainty of the regression model.

3.5.1. Limit of detection (LOD)

Here LOD for samples was calculated as mean value of field blanks plus three times standard deviation of field blanks (Equation 3) in measurement units depending on the measurement device without further modification, except for XRF. XRF values were converted into µg/(π*cm²) for the calculation of LOD. Here, the LOD always refers to the instrumental LODs and not atmospheric concentration. All sample values lying below the LOD were excluded of further calculations and are highlighted with specific symbols, if they are displayed in time lines.

$$LOD = m_{BL} + 3 \cdot s_{BL}$$

Equation 3

LOD.....limit of detection
m_{BL}.....mean value of field blanks
s_{BL}.....standard deviation of field blanks

LODs in atmospheric concentrations are given additionally in Table 17 and Table 18. These were calculated using the instrumental LOD and multiplying it with the used filter area for the specific method and dividing through the average air volume for all samples (3440 m³ for PM 10 and 386.4 m³ for PM 1).

3.5.2. Weighing of Filters

Evaluation of the aerosol mass was carried out by weighing the filters three times before and after sampling, respectively. Reference filters (unloaded filters) were measured several times and over a long-time horizon (20 months) to ensure the stability of the used scale, Sartorius MC210P analytical balance, itself. Table 4 lists the number of measurements, the mean value and the standard deviation for each reference filter. The values were noted after two min, when the scale showed a constant value for at least 10 seconds.

Table 4: Mean and standard deviation of reference quartz filters and aluminium foil (Jan 17 to May 18) measured with Sartorius MC210P analytical balance.

Reference filter	Number of measurements	Mean [mg]	Standard deviation [mg]
Quartz 1	33	112.96	0.064
Quartz 2	24	108.57	0.061
Quartz 3	30	109.31	0.074
Quartz 4	18	150.33	0.155
Aluminium 1	15	104.09	0.028
Aluminium 2	3	79.60	0.026

Previous experiments showed, that weighting of PM 10 filters is not possible due to material losses. For PM 1 filters and PM coarse the installation of sampling substrates behind the whole air inlet made sampling less sensitive to humidity or even the input of hydrometeors. Thus, the possibility of gravimetric analyses was tested within this work.

3.5.2.1. PM coarse mass

The aluminium foils were weighted for the time period of June 2016 to May 2017 (n = 52). Some masses weighed before sampling outranged the masses after sampling and thus resulted in “negative masses” (two masses around -7 µg/m³ (week of 23.06.2016 and 02.03.2017). These “negative masses” are bigger than the estimated error of the balance (a difference in weighing of 0.2 mg leads to an error of about 0.06 µg/m³ for PM 10, 0.5 µg/m³ for PM 1). Hence, lower mass after sampling are rather due to foil material losses during the transport and handling than to errors in gravimetric measurements. All “negative masses” outranging the estimated error of the balance (weeks in 2016: 23.06; 24.12; 29.12; weeks in 2017: 12.01; 19.01; 02.03) were excluded from figures and further calculations. Although the occurrence of these false low reading already demonstrates the limitations of the method, the results of the gravimetric analyses are given below.

The weighted mass was divided by the air volume to get the concentration of mass per volume [µg/m³]. The mass of PM coarse fraction collected on the aluminium foil [µg/m³] is compared with TSP measured continuously with a SHARP monitor at the SBO in Figure 4. Some of the higher masses in TSP were also found in PM coarse for example in September 2016 and end of March 2017. On other occasions the mass of PM coarse rises while there is no increase in the mass of TSP. Generally mass concentrations of PM coarse stay below the mass concentrations of TSP, as assumed, because PM coarse is a sub-fraction of TSP. During the winter period of 2016/2017 from November to January (n = 13) PM coarse mass concentrations rise above TSP masses. This is theoretically impossible, because PM coarse, as already stated above, is a sub-fraction of TSP. Possible reasons are again errors in the gravimetric measurement as explained above, but also errors in mass concentrations determined with the SHARP monitor are possible. Note that these differences were determined during time periods with very low mass concentrations.

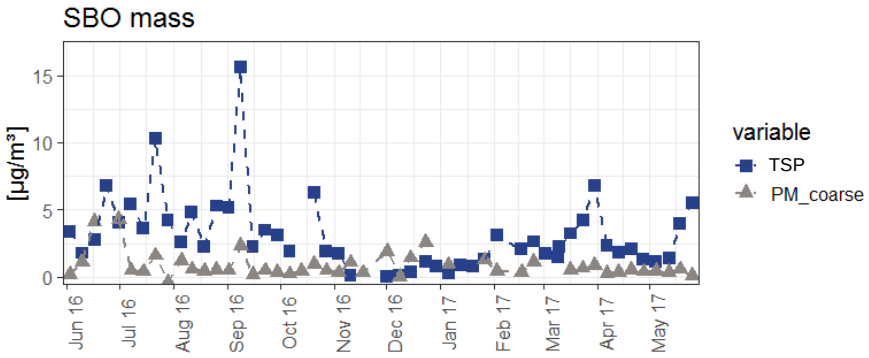

Figure 4: Mass of PM coarse sampled on aluminium foil [µg/m³] measured with MC210P and TSP [µg/m³] measured with SHARP monitor.

Correlation of mass concentrations of TSP and PM coarse is shown in Figure 5. Here two groups can be seen. One of the groups shows a PM coarse to TSP ratio of about 0.13, the other group a ratio of about 1. The sampling weeks of the smaller second group are listed in Table 5. The first assumption was, that these filters represent weeks with an elevated contribution of the coarse aerosol fraction. However, this need not be the case as most of these data point represent the winter period with the mismatch of mass concentrations, as already discussed above. A mass closure with data obtained from chemical analyses could help to evaluate the difference of mass concentrations given by the impactor and the on-line monitor. A first evaluation of the other data point did not reveal any specialities of the chemical composition.

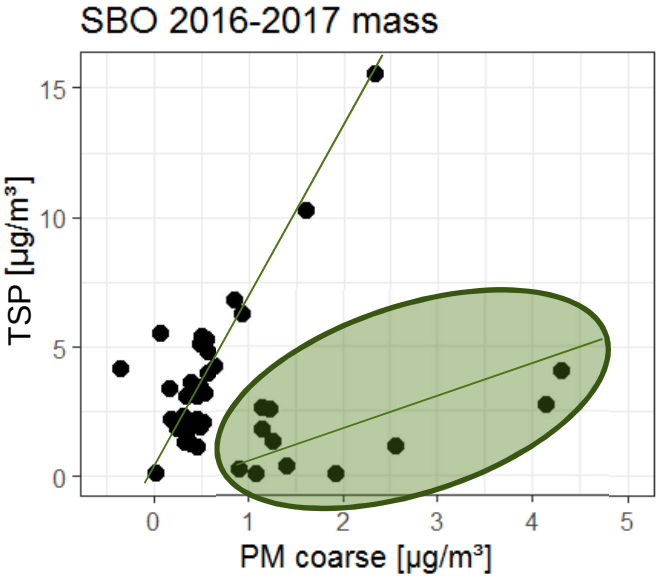

Figure 5: Correlation between mass concentrations of PM coarse [µg/m³] and TSP mass [µg/m³] measured online with a SHARP monitor.

Table 5: Weeks having a PM coarse to PM 10 ratio of about 1 – group 2.

09.06.2016	15.12.2016
16.06.2016	23.12.2016
30.06.2016	05.01.2017
05.08.2016	26.01.2017
10.11.2016	23.02.2017
01.12.2016	

3.5.2.2. PM 1 mass

Gravimetric determination of PM 1 mass showed a similar problem. 19.5 % of quartz filter samples weighed less after sampling, thus resulting in "negative masses" as discussed above. As samples are taken in a remote area, only a small amount of aerosol is sampled, resulting in a small mass and just a greyish colour of the PM load on the filters. But "negative masses" occurred not alone when the filter load looked light grey, but also if the load had a medium greyish colour, when mass loadings tend to be higher. Note that the decrease of the mass of the filters was markedly higher than it could be expected due to the deviations of the balances. These false readings are most likely due to a material loss of the sampling substrate, which can be expected more easily for quartz fibre filters than for aluminium foils. As such losses are possible for both, low and heavily loaded filters, PM 1 mass determined here has to be regarded as approximate values and weighing of PM 1 filters will not be continued.

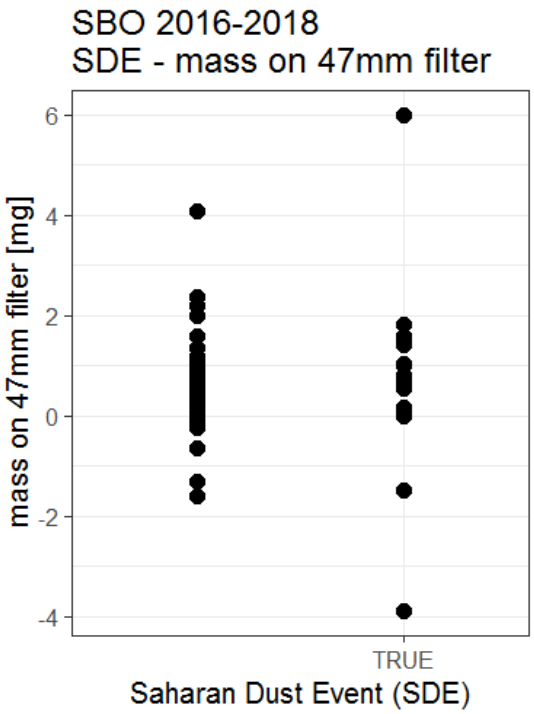

Figure 6: Mass of aerosols on 47mm diameter quartz-filters observed without SD transport (left side) and during a week with SD transport (right side – TRUE).

If the mass of PM 1 is compared with the SD report of SBO it is apparent, that filters in SD-periods have more often a positive mass than filters without an SDE (see Figure 6.). Three filters out of 20 filters during SDE showed a negative mass. The other negative masses (12 occurrences) were observed without reported SD transport (57 filters). The negative masses represent 15 % of the filters during SDE and 21 % of the filters without SDE. This is likely as high mass loadings can be expected for SDEs, still these evaluations will be heavily effected by errors due to loss of filter material as well.

Nevertheless, the data set obtained within this work allows some evaluations. In Figure 7 the time trend of PM 1 mass is compared with TSP as well as TC and SO_4^{2-}, determined from PM 10 filters. The pattern of TSP to PM 1 looks similar to the one observable for TSP to PM coarse. Again, most of PM 1 mass

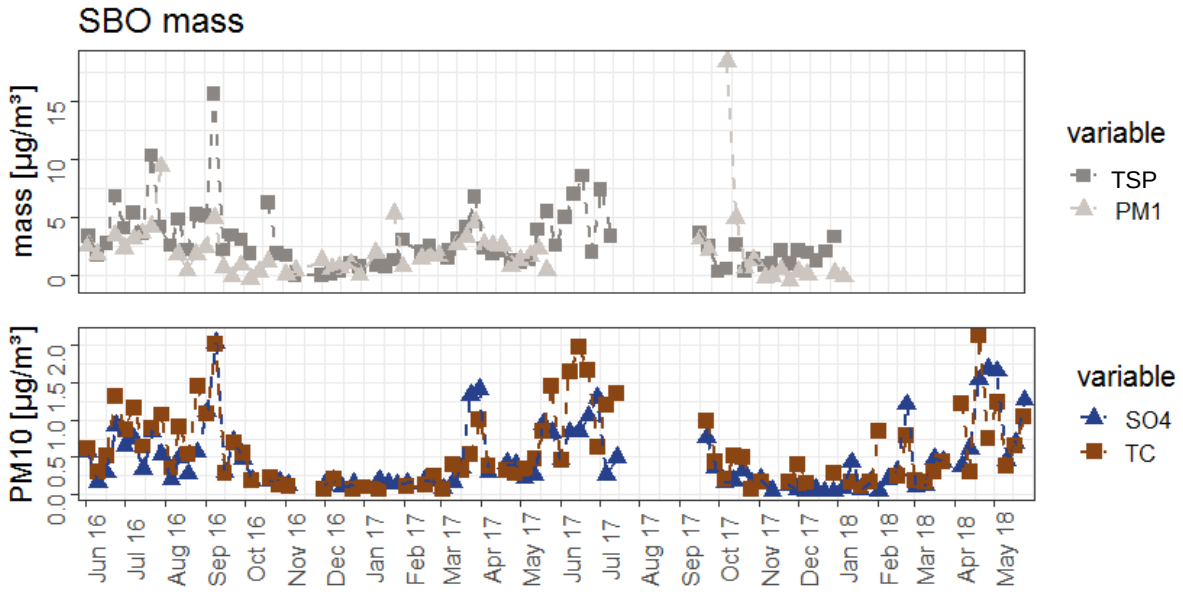

Figure 7: masses of TSP and PM 1 fraction, as well as SO_4^{2-} and TC values of PM 10 fraction, displayed in µg/m³ from June 2016 to May 2018.

concentrations lay below TSP mass concentrations, as expected, because PM 1 is a sub-fraction of PM 10. Two outliers become visible in autumn 2017. Generally, the contribution of PM 1 to TSP (PM 1/TSP about 1/3) is higher than the contribution of PM coarse to TSP (PM coarse/TSP about 1/7.5). Correlation of PM 1 mass to SO_4^{2-} and TC concentrations within the PM 10 fraction as well as to TSP were calculated. All three correlations lay below 0.3 (see Appendix Figure 53 to Figure 55), again highlighting the problems related to PM 1 mass concentrations.

Summarizing it has to be highlighted again, that gravimetric determination of PM 1 mass concentrations is prone to errors and mass concentrations results can only be regarded as an approximation of the actual conditions. Weighing of the filters will not be continued.

3.5.3. Preparing aliquots of PM 1 filters

PM 1 filters were cut in half for analyses (see chapter 3.3). To ensure that the cutting device yields a correct and constant partitioning of the filters, PM 1 filters were weighed before and after cutting. The difference between weighted halves and calculated halves (half of weight of whole filter) was related to the calculated half and multiplied by 100. To get the relative standard deviation equivalent, the standard deviation thereof was calculated (see Equation 4).

$$RSD = sd\left(\frac{|m_{ex} - m_{th}|}{m_{th}} \cdot 100\right)$$

Equation 4

RSD.....relative standard deviation
sd .....standard deviation of expression in brackets
m_{ex}.....experimentally determined mass of filter half [mg]
m_{th}.....theoretically determined mass of filter half [mg] – halved value of whole weighted filter
|.....taking the absolute value in between

In parallel the variability of the mass of sample aliquots obtained by a circular punching tool was determined. Therefore, 25 punches of 20 mm diameter were taken out of a 15 cm diameter quartz fibre filter. Each punch was weighed. The statistical results are shown in Table 6.

The filter halves showed a RSD of 1.46 %, which is lower compared to the RSD of PM 10 filter material (RSD 3.14 % - Table 6).

The punches should vary only due to inhomogeneous nature of filter material and variance of the balance. Assumed that the PM 1 filter material shows the same variance as PM 10 filter material, the smaller variance of PM 1 filter halves compared to the PM 10 punches show that the areas produced by cutting the filters are sufficiently accurate operating with the cutting device. Therefore, the PM 1 filter halves were not further weighed.

Table 6: Statistics of 25 20 mm quartz filter punches concerning their weight.

minimum	12.90 mg	Average	13.984 mg
q1	13.675 mg	s^2 variability	0.1929
median	13.98 mg	s standard deviation	0.4392
q3	14.33 mg	corr. Variance (s-1)	0.2009
maximum	14.94 mg	(s-1) standard deviation	0.4482
Span width	2.04 mg	RSD – relative standard deviation	3.14 %
delta q	0.62		

3.5.4. Aethalometer AE33

This method analyses carbonaceous particles. The defined fraction is named EBC for equivalent black carbon. Calculations are based on simultaneously measured attenuation at seven different wavelengths

(370, 470, 525, 590, 660, 880 and 940 nm). The beam is focused on a filter belt on which aerosols are sampled. A blank filter material spot is used as reference. [32], [33]

The aethalometer measures the absorption on a filter band. To get the EBC value, the absorption coefficient is divided through the MAC (mass absorption cross section) value (Equation 5). Standardized methods use the absorption at 880 nm. At this wavelength absorption of other carbonaceous or mineral aerosol is lower. The absorption coefficient is extracted out of the attenuation coefficient and parameters to correct the influence of filter loading and multiple scatter in the filter material (Equation 6). The attenuation coefficient is calculated out of flow rate, active sampling area and the difference of ATN over a small time interval (Equation 7). [32]

$$EBC = \frac{b_{abs}(\lambda)}{MAC(\lambda)}$$

Equation 5

EBC .....equivalent black carbon [µg/m³]
$b_{abs}(\lambda)$.....absorption coefficient [Mm^{-1}]
MAC(λ).....mass absorption cross section [m²/g] (SBO 880 nm: 7.77 m²/g)

$$b_{abs}(\lambda) = \frac{b_{ATN}(\lambda)}{C_\lambda \cdot R(f_\lambda, ATN_\lambda)}$$

Equation 6

$b_{abs}(\lambda)$..... absorption coefficient [Mm^{-1}]
$b_{ATN}(\lambda)$..... attenuation coefficient [Mm^{-1}]
C_λ ..... specific scatter coefficient of filter material (SBO: 1.57)
$R(f_\lambda, ATN_\lambda)$ ..... influence of filter loading (DualSpot™ technology)

$$b_{ATN}(\lambda) = \frac{A}{Q} \cdot \frac{\Delta ATN}{\Delta t}$$

Equation 7

$b_{ATN}(\lambda)$..... attenuation coefficient [Mm^{-1}]
A ..... active sampling area [m²]
Q..... flow rate [m³/min]
ΔATN ..... attenuation
Δt ..... time interval [min]

3.5.5. Transmissometer – Soot SNn Model OT21

This method measures light attenuation of particles like the Aethalometer. To distinguish the values, the carbonaceous particle fraction determined by transmissometry is named BC. A punch area of 36 mm diameter of each filter of PM 10 and the whole area of PM 1 filters were analysed. [34]

The transmissometer measures the transmission of light at two wavelengths. One lies in the IR-range (880 nm), the other in the UV-range (370 nm). The attenuation (ATN) is calculated out of transmission intensities of a loaded (I) and unloaded filter (I_0 - Equation 8). Here only measurements at 880 nm are evaluated. The ATN determined at 880 nm is divided through a station specific mass attenuation cross section σ (33.7 cm²/µg). [35] To get atmospheric concentrations of BC, the value is multiplied with the filter area and divided through the sampled air volume (Equation 9). Blank measurements were only

available for PM 10 measurements. The mean of ATN_{IR} of blanks was subtracted from the sample values.

$$ATN = 100 \cdot \ln\left(\frac{I}{I_0}\right)$$

Equation 8

ATN.....attenuation
I.....intensity of transmission of loaded filter
I_0.....intensity of transmission of unloaded filter

$$BC\left[\frac{\mu g}{m^3}\right] = \frac{ATN_{IR}}{\sigma} \cdot \frac{A}{V_N}$$

Equation 9

BC.....concentration of BC measured with Transmissometer [µg/m³]
ATN_{IR}.....attenuation of sample in the IR-range (880 nm)[ ]
σ.....specific mass attenuation cross section (33.7 cm²/µg) [cm²/µg]
A .....area of filter loading [cm²]
V_N.....normalized air volume [m³]

All values above the LOD were used for further calculation. For PM 1 no blanks were measured, so all values were taken for further calculations.

3.5.6. X-Ray Fluorescence Analysis (XRF)

XRF measurements were carried out at the XRC (X-Ray Center of TU Wien) under the supervision of Johannes Zbiral.

In XRF analysis absorption of X-rays leads to an excited ion. By returning to their ground state, ions emit X-rays of longer wavelengths than the absorbed ones, which are characteristic for each element. Calibration for quantification was carried out with standard reference material 2709 (San Joaquin Soil, National Institute of Standards & Technology) and was available from previous work (Neuwirth 2016) [36]. Quartz filters have been loaded with different amounts of this soil, which has a specified composition (shown in Table 7). The loaded filters were measured with XRF (aperture for exposure: 20 mm diameter; exposure time: 2.5 s; X-ray generation: 50 kV, 50 mA). During the procedure some filters lost weight and therefore were excluded from the calibration. Figure 8 to Figure 14 show the calibration curves for each element [36]. Silicon was excluded for further calculations as the filter itself contains Silicon. The calibration shows a negative slope (Figure 15), as increasing mass loadings shield the signal of the substrate.

Table 7: Composition of San Joaquin Soil. Only elements measured with XRF are listed.

Fe	3.50 m%
Ca	1.89 m%
K	2.03 m%
S	0.089 m%
P	0.062 m%
Si	29.66 m%
Al	7.50 m%
Mg	1.51 m%

Iron, calcium and potassium have a calibration curve with a calibration coefficient above 0.99. As shown in Figure 10, Figure 11, Figure 13 and Figure 14, the other calibrations (Mg, Al, S, P) show only a correlation coefficient above 0.8. If there is a negative offset on the y-intercept, the calibration curve is forced through zero (for Ca, Mg, Al, K, S and P; see Figure 9 to Figure 14).

The linear fits have been calculated with R [31], using lm and geom_smooth, which shows a confidence interval of 0.95 shaded in grey.

Via the calibration (Equation 10) an area related concentration [µg/(π*cm²)] was obtained. The mean of blank values (equally calculated like sample values) was subtracted from the sample values for blank

value correction. Afterwards the corrected sample values were converted into µg/m³ with the scaling factor for the active sample area and the normalised air volume (Equation 11).

$$f(x) = k \cdot x + d$$

Equation 10

*f(x) .....[µg/(π*cm²)]*
*k .....specific slope[µg/(π*cm²*kcps)]*
x .....measured value [kcps]
*d .....y-intercept [µg/(π*cm²)]*

$$c = \frac{\left[f\left(x_{Sample}\right) - m_{BL}\right] \cdot S}{V_N}$$

Equation 11

c .....concentration [µg/m³]
*f(x_{Sample})..value of sample [µg/(π*cm²)]*
*m_{BL} .....Average value of blanks (average of: $f(x_{Blank})$) [µg/(π*cm²)]*
S .....=d²/4=r² (d: diameter of active sample area, r: radius of active sample area) [cm²]
Scaling factor for the area
V_N.....normalised volume [m³]

The XRF measurements were performed after the Transmissometer measurements, thus enabling the usage of the 36mm diameter punches. Samples were placed in brackets with an aperture of 27 mm or 20 mm diameter (for blanks). The beam passed a mask inside the measurement system with an aperture of 20 mm in diameter. Therefore, both sample holders result in the same measured values.

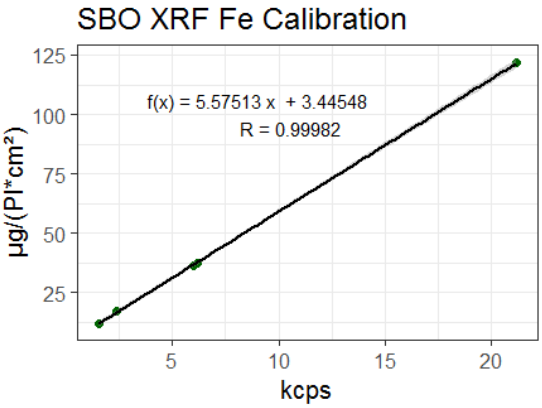

Figure 8: XRF Calibration of Iron (Fe).

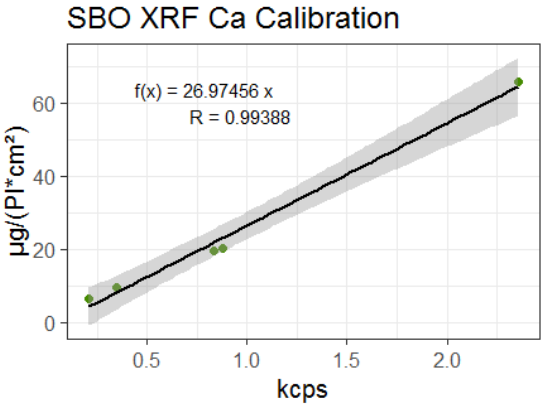

Figure 9: XRF Calibration of Calcium (Ca).

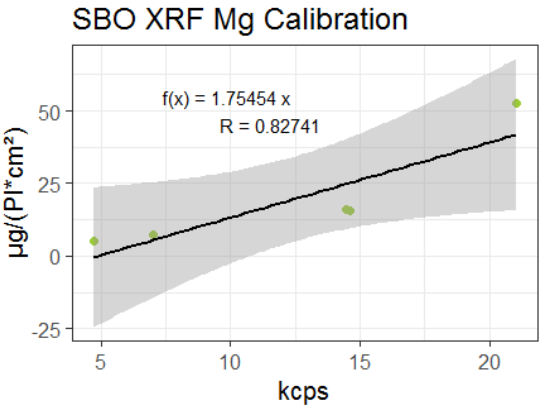

Figure 10: XRF Calibration of Magnesium (Mg).

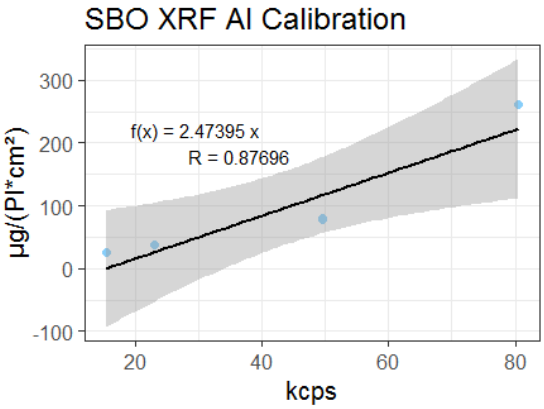

Figure 11: XRF Calibration of Aluminium (Al).

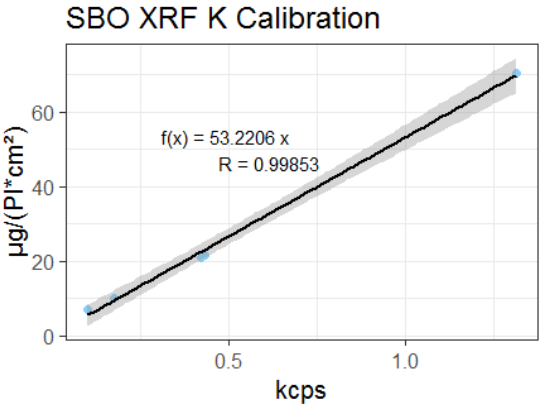

Figure 12: XRF Calibration of Potassium (K).

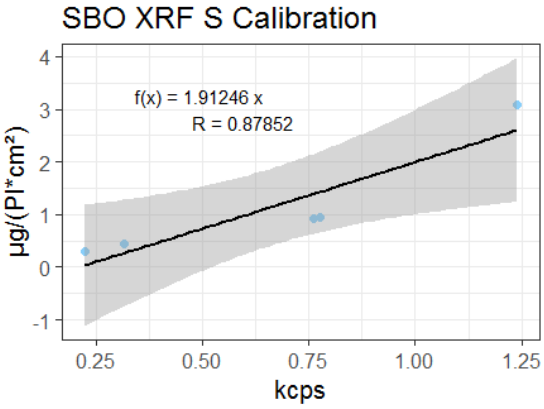

Figure 13: XRF Calibration of Sulphur (S).

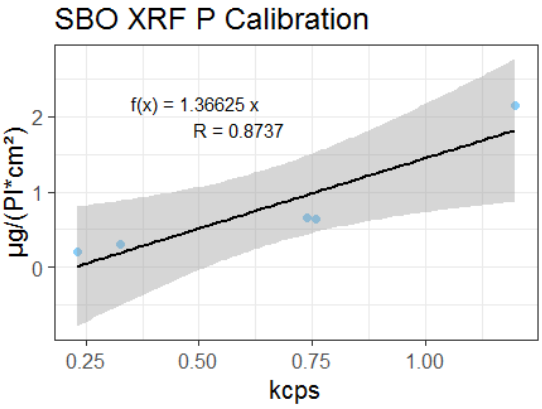

Figure 14: XRF Calibration of Phosphor (P).

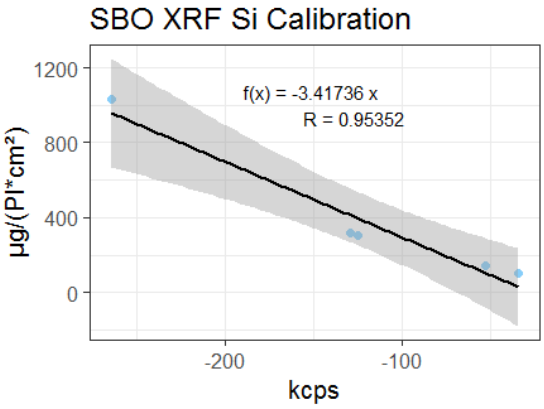

Figure 15: XRF Calibration of Silicon (Si).

3.5.7. Thermal-optical Carbon measurement

The thermal-optical method was carried out with the instrument Sunset Laboratory "Lab OC-EC Aerosol Analyzer". [37] It allows to measure TC, EC and OC by combining the thermal oxidation with an optical device to distinguish between OC and EC while simultaneously determining the evolving gases. During the oxidation there are two major phases. In the first one, the oven is flushed with helium (non-oxidising atmosphere) with a maximum temperature of 650 °C. In this phase, only OC, containing oxygen itself, burns. Burning of OC forms pyrolytic carbon among others. The laser beam, pointing through the filter, monitors the darkening of the filter due to pyrolytic carbon building. In the second phase of the temperature profile, a helium-oxygen mixture (2 % oxygen) flows through the oven (oxidising atmosphere). During this step, the temperature rises to 860 °C, EC oxidises, and the filter gets brighter again. The split point, separating OC and EC, is set at the time, when the laser transmission signal is equal to the value at the start of the measurement. Therefore, pyrolytic carbon developed in the first step of oxidising OC is count to OC and just EC measured after the split point accounts for EC. The method is comparable with other studies carried out with the EUSAAR2 protocol (standard method for carbon measurement of European aerosols). [38]

For analysis of the filters a punch area of 10 mm diameter (78.5 mm²) for PM 10 and 1x1.5 cm (150 mm²) for PM 1 samples was used. As stated previously (chapter 3.2.1) glass fibre filters were used occasionally by mistake (e.g. week 29.3.2018). These filters could not be measured with the Sunset as the filter material melts during the measurement.

Values of Sunset measurement were recorded in µg/cm². These values were converted via the active sampling area and the normalized air volume to µg/m³. As the concentrations were very low, they were converted into ng/m³ values (multiplied by 1000 – see Equation 12).

$$TC\left[\frac{ng}{m^3}\right] = TC\left[\frac{\mu g}{cm^2}\right] \cdot \frac{A}{V_N} \cdot 1000$$

Equation 12

TC.....concentration of TC measured with Sunset [ng/m³]
TC.....TC measured with Sunset [µg/cm²]
A .....area of filter loading [cm²]
V_N.....normalized volume [m³]

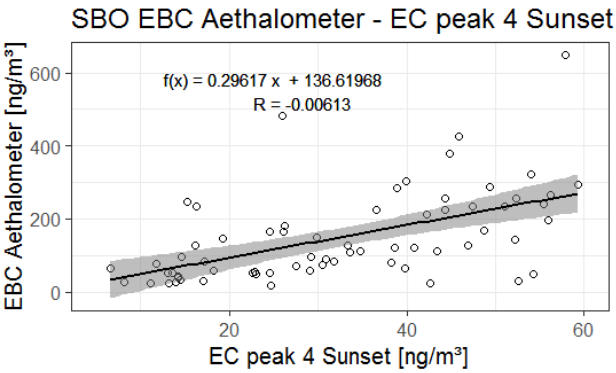

Figure 16: linear regression between EC (Sunset Laboratory) Peak 4 of PM 10 fraction and EBC (Aethalometer) of PM 10 fraction.

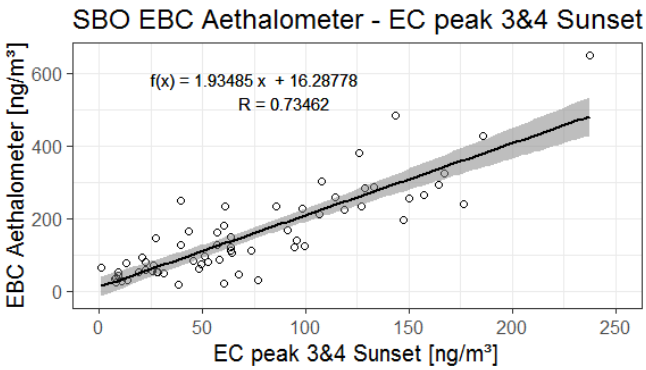

Figure 17: linear regression between EC (Sunset Laboratory) as summary of Peak 3 and Peak 4 of PM 10 fraction and EBC (Aethalometer) of PM 10 fraction.

Besides the automatic determination of the split-point the Sunset Analyser allows a manual split-point correction as well. Thus, the differentiation between OC and EC can be changed. The automatically set split-point was at exactly the same transmission during the measurement as in the beginning of the measurement. During the measurement there was a defined temperature profile due to the method used (EUSAAR2). In this protocol there were two peaks (peak 3 and peak 4) in the second half of the measurement, which were concluded to be EC, as the split point was always set at various points between

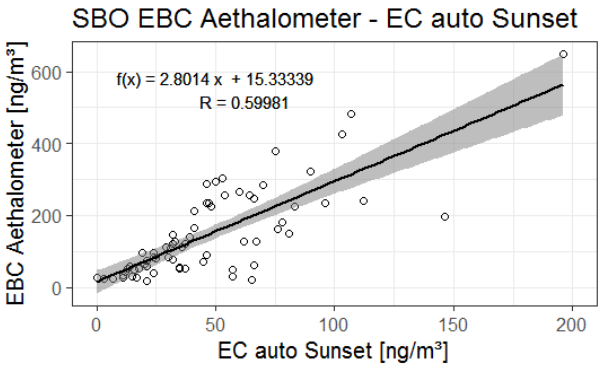

Figure 18: linear regression between EC (Sunset Laboratory) of PM 10 fraction with automatically set split point and EBC (Aethalometer) of PM 10 fraction.

peak 3 and 4. Three different possibilities to calculate EC were compared for PM 10 measurements concerning their correlation to EBC measured with the Aethalometer. The comparison of the correlation between EC-auto, EC34, EC4 and EBC (see Figure 16, Figure 17 and Figure 18) showed the best correlation (R of 0.70626) for EC calculated out of peak 3 and peak 4. For further calculations and figures EC was calculated out of both peaks EC3 and EC4.

On one of the measurement days (13.7.2018), the calibration area of the internal calibration peak of the Sunset Analyser was too low. Consequences were drawn too late and therefore, some PM 1 filters were already measured. These values may be too low due to the small calibration area (week 30.11.2017 and 14.12.2017 until 11.1.2018). Since there were no other errors, and the obtained values lay in the usual measurement range, the values remain in the data set for further calculation.

3.5.8. Ion Chromatography

In ion chromatography ions are separated in an ion exchanger column with low capacity. Afterwards, the suppressor reduces the conductivity of the eluent to improve the sensitivity of detection. The analytes having a higher conductivity after the suppressor were detected via a conductivity cell for anions and cations. The sugar measurements were carried out using a chromatography column without suppressor since they were detected electrochemically. All PM 10 and PM 1 samples were analysed for cations, anions and sugars. The parameters used for the different methods are given in Table 8.

Table 8: Parameters of chromatographic systems.

	Anions	Cations	Sugars
System	Dionex ICS-1100	Dionex ICS-3000	Dionex ICS-3000
Eluate	Na_2CO_3 (4.5 mM), $NaHCO_3$ (1.4 mM)	Methane sulfonic acid (MSA – 38 mM)	1 M NaOH (52 %) gradient with Milli-Q-water (48 %)
Column	Dionex IonPac AS22 Carbonate Eluate Anion-Exchange Column	IonPac CS16 Cation-Exchange Column	CarboPac MA1 Carbohydrate Column
Detector	Conductivity	Conductivity	Electrochemical (Au/Ag/AgCl)
Suppressor current	30 mA	112 mA	no suppression
Flow	1 mL/min	1 mL/min	0.4 mL/min

Standards and samples were measured with the systems described above. Measured concentration values (in ppm) were calculated further to get an atmospheric concentration of each ion (in µg/m³). Therefore, the peaks of each analyte were integrated with Chromeleon. The calibration curve was obtained by measurements of external standards (Table 9 and Table 10). Chromeleon gave the concentration of each sample in ppm (equivalent to µg/mL). Values below 1 ppm were calculated with a calibration curve excluding standard 4 and 5 (for cations and anions). Concentration values were corrected with the mean of blank values. Then, the values were multiplied with the volume of the eluate and divided through the filter area used to get the loading of the filters in µg/cm² (see Equation 13). The filter loading was transferred into an atmospheric concentration by multiplying with the active sampling area and dividing through the normalised volume (Equation 14).

$$B\ \left[\frac{\mu g}{cm^2}\right] = (value[ppm] - m_{BL}[ppm]) \times \frac{eluate\ [mL]}{\pi \cdot r^2}$$

Equation 13

B .....filter loadings [µg/cm²].
value .....measured concentration in ppm (=µg/mL).
m_{BL} .....mean value of field blanks concentration in ppm (=µg/mL).
eluate .....volume to elute filter material [mL]
r .....radius of the filter area eluted [cm].

$$c\ \left[\frac{\mu g}{m^3}\right] = B\left[\frac{\mu g}{cm^2}\right] \times \frac{d^2 \cdot \pi}{4 \cdot \dot{V}}$$

Equation 14

C .....concentration of sample in µg/m³.
B .....loading of the filters in µg/cm².
d.....diameter of whole sampled filter area in cm (14 for PM 10, 3.7 for PM 1).
$\dot{V}$ .....volume in m³ (normalized) sucked through filter during sampling.

LOD for cations and anions was calculated concerning the measurements of field blanks (Equation 3). Filter blanks for sugars were measured for PM 1 filters only and the calculated LOD for Levoglucosan was also taken for PM 10 Levoglucosan measurements. Due to low concentrations, only Inositol, Levoglucosan, Arabitol, Glucose and Sucrose LODs of PM 1 were calculated. For other sugars no LOD could be calculated based on the field blanks.

3.5.8.1. Cations

Cation chromatography measured Na^+, NH_4^+, Mg^{2+}, K^+ and Ca^{2+}. Therefore, seven standards were used for calibration (amounts given in Table 9). If a value was more than 1 ppm above the highest standard, the sample was diluted and measured again to get a value inside the calibration range. In accordance with interlaboratory surveys the calibration curve was fitted through zero.

Table 9: Concentrations [ppm] of used standards for cation chromatography.

Standard	Natrium	Ammonium	Magnesium	Potassium	Calcium
1	0.1	0.1	0.1	0.1	0.1
2	0.5	0.5	0.5	0.5	0.5
3	1	1	1	1	1
4	2	3	2	2	3
5	5	7	5	5	7
6	0.8	0.8	0.8	0.8	0.8
7	0.05	0.05	0.05	0.05	0.05
9 (control standard 2)	0.2	0.25	0.25	0.5	0.5
11 (control standard 4)	2	2.5	2.5	5	5

For analysis 12 mm punches, one for each sample of PM 10 and PM 1, were taken. The punch was placed in a PP test tube and 3 mL of 38 mmol MSA were added. After shaking it, the sample was placed in an ultrasonic bath (at 30 °C, full power grade 9) for 20 min. The test tube with PM 10 filters was centrifuged at 4000 rpm for 10 min (3500 rpm for 2.5 min for PM 1 filters). 1.1 to 1.5 mL of PM 10 eluate (1 mL of PM 1 eluate) was pipetted into a vial, which could be used within the autosampler. After

centrifugation at 13 400 rpm for 5 min the tube was placed in the automatic sampler and measured with ion chromatography (parameters given in Table 8).

Some chromatograms of PM 10 cations were recorded for a too short time in the end and therefore, the Ca^{2+}-peak was cut off. This data was eliminated and not further processed (week of 28.9.2017 and 30.11.2017). A repetition of these samples is possible due to remaining filter material of PM 10 samples.

3.5.8.2. Anions

Anion chromatography measured chloride, nitrite, nitrate, sulphate and oxalate. Therefore, seven standards were used for calibration (amounts given in Table 10). If a value was more than 1 ppm above the highest standard, the sample as diluted and measured again to get a value inside the calibration range. In accordance with interlaboratory surveys the calibration curve was fitted through zero.

Table 10: Concentrations [ppm] of used standards for anion chromatography.

Standard	Chloride (Cl^-)	Nitrite (NO_2^-)	Nitrate (NO_3^-)	Sulphate (SO_4^{2-})	Oxalate
1	0.1	0.1	0.1	0.1	0.1
2	0.5	0.5	0.5	0.5	0.5
3	1	1	1	2	1
4	2	2	4	4	2
5	4	4	12	12	5
6	0.8	0.8	0.8	0.8	0.8
7	0.05	0.05	0.05	0.05	0.05
9 (control standard 2)	0.5	0.5	0.5	0.5	0.5
11 (control standard 4)	3	3	3	3	3

For analysis of anions, 12 mm punches were taken out of PM 10 filters. For PM 1 filters the remaining area of the filter half (equal to 274.508 mm² as displayed in Figure 1) was taken for anion and sugar measurement (exact treatment of PM 1 filters for anion and sugar measurements see chapter 3.5.8.3). Filter material was eluted with 3 mL of milli-Q-water in a PP test tube. After shaking it, the sample was placed in an ultrasonic bath (at 30 °C, full power grade 9) for 20 min. The test tube with PM 10 filters was centrifuged at 4000 rpm for 10 min (3500 rpm for 2.5 min for PM 1 filters). 1.1 mL of PM 10 eluate (1 mL of PM 1 eluate) was pipetted into a vial, which could be used within the autosampler. After centrifugation at 13 400 rpm for 5 min the tube was placed in the automatic sampler and measured with ion chromatography (parameters given in Table 8).

3.5.8.3. Sugars

As the samples have low concentrations, additional standards with low levels were prepared (see Table 11). All standards were diluted out of paternal solutions. These were prepared with a concentration around 1000 ppm and stored in the freezer. For preparation date and exact concentrations see Table 11 and Table 12.

Table 11 concentrations of additional sugar standards for low concentration range given in ppm.

Standard	Concentration [ppm]	Flask volume [mL]	Stock solution [µL]
N1	0.06	250	15
N2	0.5	100	50
N3	2	100	200
N4	5	50	250
N5	10	50	500
N6	1	100	100
N7	0.05	(1:10 dilution of N2)	-
N8	0.2	(1:10 dilution of N3)	-
N9	0.01	(1:50 dilution of N2)	-

Table 12: Sugars of stock solution with their concentration and preparation date.

Sugar	Concentration [ppm]	Preparation date
Erytritol	1000	09.03.2007
Inositol	1000	05.2017
Levoglucosan	1018	04.07.2018
Arabitol	1014	04.07.2018
Mannosan	1003	04.07.2018
Trehalose	1000	03.03.2017
Mannitol	1008	04.07.2018
Galactosan	1010	04.07.2018
Glucose	1000	03.07.2017
Fructose	1000	03.07.2017
Sucrose	1000	03.07.2017

For PM 10 samples, four 12 mm punches per filter were eluted with 2 mL milli-Q-water in the ultrasonic bath (at 30 °C, full power grade 9) for 20 min. Then, the PP test tube was centrifuged at 4000 rpm for 10 min. 1 mL of supernatant was transferred into a vial and centrifuged at 13 400 rpm for 5 min.

For PM 1 filters the remaining material of one half of the filter was placed in the PP test tube (equal to 274 mm² as displayed in Figure 1) and 3 mL milli-Q-water were added. Shaking of the test tube guaranteed that the filter was covered with water. The test tube was put in the ultrasonic bath at 30 °C and full power for 20 min. Filter material was centrifuged at 4000 rpm for 10 min and 2-times 510 µL of supernatant was pipetted into two vials, one for sugars, the other for anions. Vials were centrifuged at 13 400 rpm for 5 min and if filter residues could be seen, 1 mL of supernatant was pipetted into a new vial and centrifuged at 13 400 rpm again.

4. Results and Discussion

This section is split in two parts where the first one covers results concerning the comparison of methods. The second part deals with time trends of the sample period of nearly two years, PM 1/PM 10 ratios and a comparison of results with measurements performed at SBO in 1991-1993.

4.1. Method comparison

4.1.1. Comparison of Ca, Mg and K concentrations determined by ion chromatography and X-ray fluorescence

To compare IC and XRF measurement, a time series of Ca is shown in Figure 19. The measurements were quite equal except during three weeks in March 2017, where IC measurements showed markedly higher concentration than XRF.

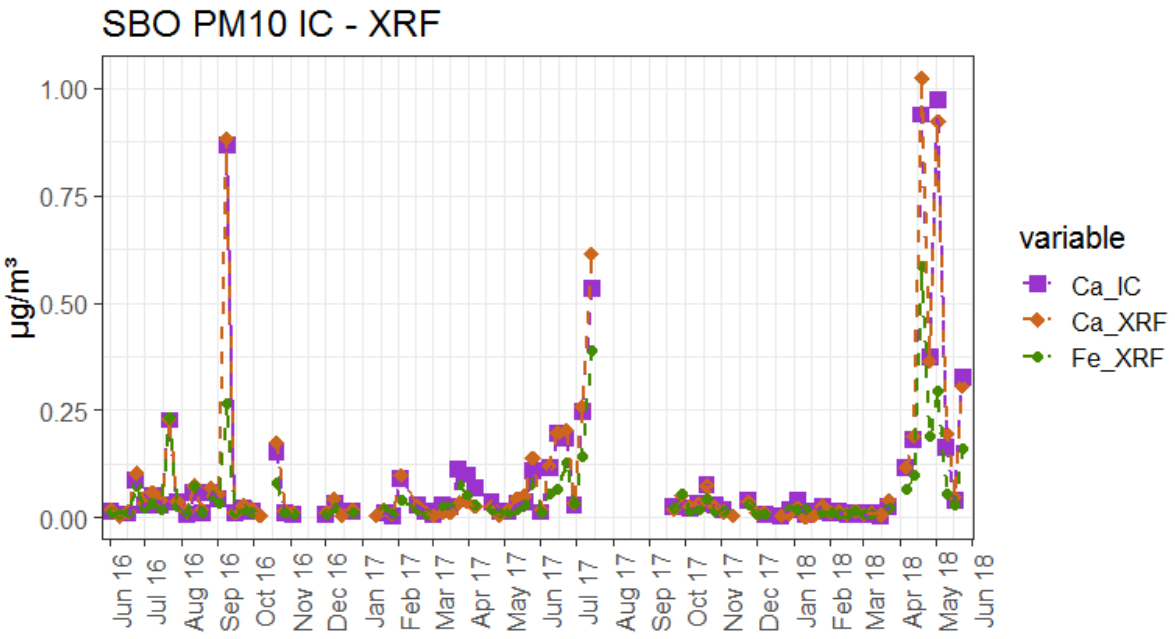

Figure 19: Time series of Ca measured with IC and XRF and Fe measured with XRF (June 2016 to May 2018).

The linear correlation of Ca measured with IC and XRF in Figure 20 shows that IC and XRF measurements resulted in matching Ca concentrations. In addition, Mg and K were also measured with both methods and these measurements correlated as well (see Figure 21 and Figure 22). Intercepts of these correlations lay below the atmospheric LODs of XRF measurements (Ca: 6.7 ng/m³; Mg: -17.0 ng/m³; K: 7.5 ng/m³). For Ca, the slope is nearly 1, whereas for Mg and K the slope is higher (approximately 3 and 7, respectively). This suggests that, for Mg and K in 38 mM MSA, insoluble components are present, which therefore can only be detected in XRF and not in IC.

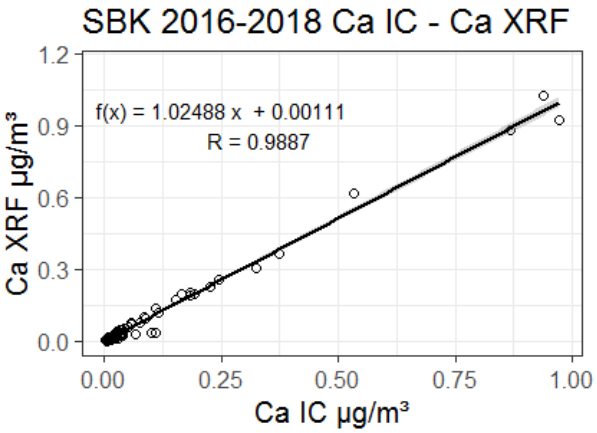

Figure 20: Correlation of Ca between measurement with IC and XRF.

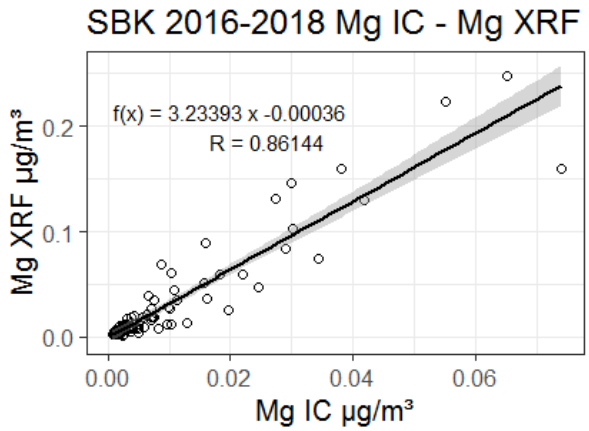

Figure 21: Correlation of Mg between measurement with IC and XRF.

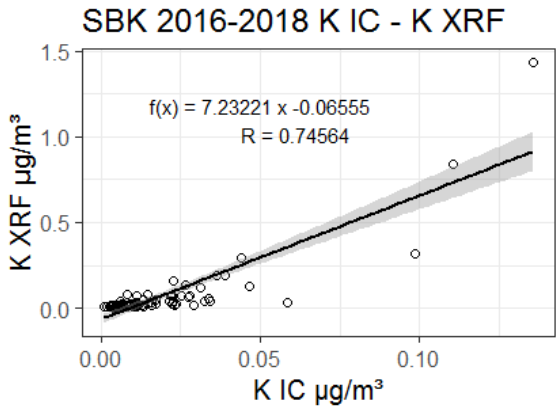

Figure 22: Correlation of K between measurement with IC and XRF.

Assuming that calcium is a marker of mineral dust like iron, the concentration of Ca^{2+} was correlated to Fe to estimate a contribution of mineral dust with IC measurements alone, if XRF measurements are not available. Figure 23 shows the correlation between Ca^{2+} and Fe. The one calculated out of XRF measurement of Ca (R = 0.8666) is better as the one where Ca^{2+} is measured with IC (R = 0.83365). These correlations show, that an approximation of Fe and in second step of mineral dust is possible, but XRF measurement itself is better. The time series of Ca^{2+} (or correlating CO_3^{2-}, assuming that $CaCO_3$ is present) to Fe is presented in Figure 19. Also, comparison of Mg^{2+} and K^+ determined by IC with Fe (XRF) was done and fits quite well (Figure 24 and Figure 25). The lower value of R for K is reasonable, as other sources of K (e.g. wood combustion) are well known (e.g. Pio et al, 2008) [39]. The intercept of these correlations lay below the LOD of Fe (80.3 ng/m³).

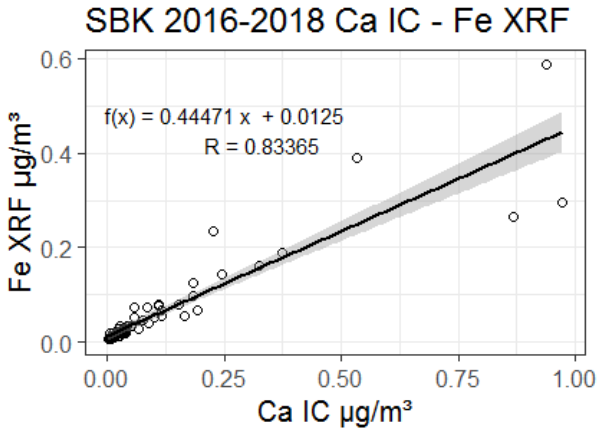

Figure 23: Correlation between Ca^{2+} (IC) and Fe (XRF).

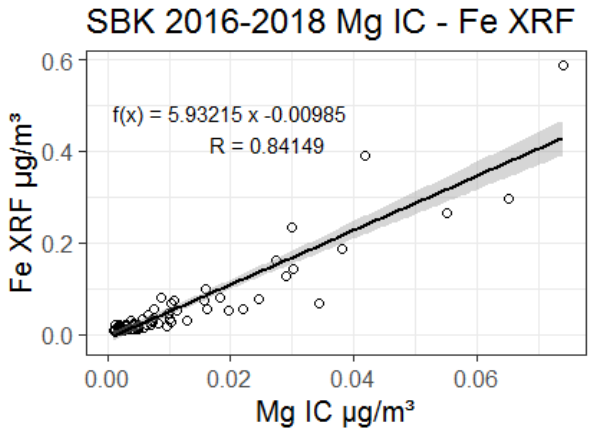

Figure 24: Correlation between Mg^{2+} (IC) and Fe (XRF).

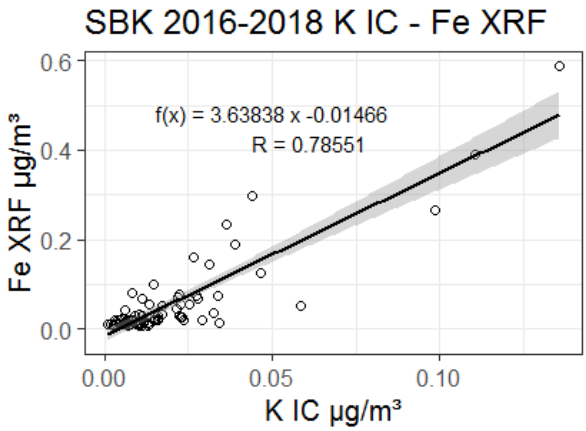

Figure 25: Correlation between K^+ (IC) and Fe (XRF).

High Ca and Fe points to SD, which should give elevated TSP. To check this, time series with independently marked SDEs were considered. Some events show this behaviour - high TSP concentrations and corresponding elevated Fe and Ca concentrations can actually be related to SDEs (see Figure 26). On the other hand, there were events with high concentrations of TSP, calcium and iron,

but without an SDE. Until January 2018 three weeks with especially high Fe and Ca values were noticeable: 21.7.2016; 8.9.2016 and 14.7.2017. For the week of 21.7.2016 an SDE was found in the SBO report. The week of 8.9.2016 showed elevated TSP, Fe and Ca concentrations, but no SDE in the SBO report. Nevertheless, an influence of SD is possible if the model of SD in the atmosphere is combined with the trajectories for SBO, as the trajectories of this week point directly at SD rich atmospheric regions. Obviously, the SD-Index was not set due to limited availability of online data during this week. A different situation occurs for the week of 14.7.2017, when relatively low TSP concentrations, but high Fe and Ca concentrations were observed. An influence of SD can be excluded for this week, but the assumption of local influence of mineral dust [28] due to construction work is enhanced. For the week of 14.7.2017 it was recorded, that the sampling system of Digitel was shut down due to construction work. This week lay shortly before the start of the construction work and shutdown of sampling. Therefore, it is likely, that early commenced work may had started in this week.

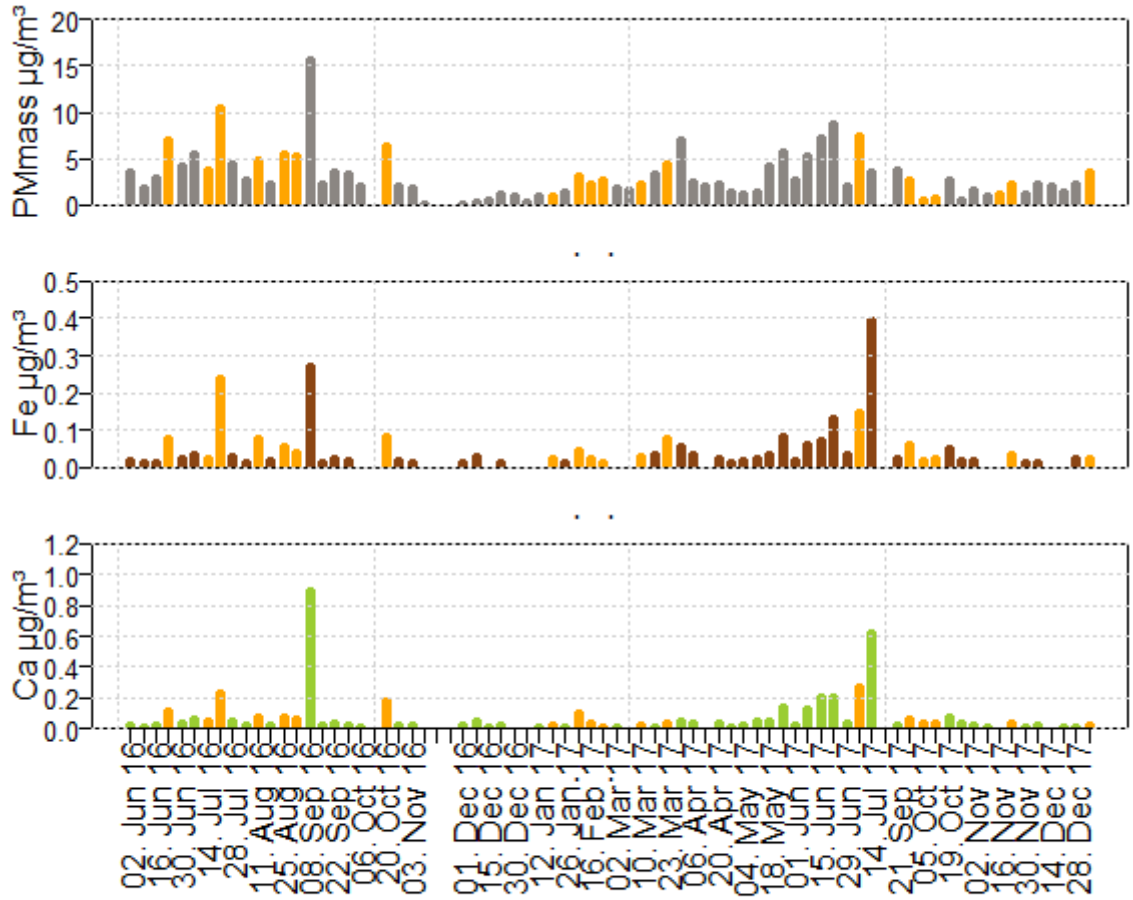

Figure 26: PM 10 mass compared with Fe and Ca measurements of XRF. SDE are marked in orange.

4.1.2. Comparison of EBC, BC and EC determined by Aethalometer, Transmissometer and Sunset

Refractory carbon content, especially the fraction of EC or BC, has been analysed with different methods. Optical methods like the Aethalometer and the Transmissiometer focus on optical properties and determine the BC content, whereas the Sunset as a primary thermal method measures the so-called EC. In difference to the optical methods determining BC, the term EC focuses on the thermal properties of carbon. Nevertheless, the carbon content measured with different systems should be about the same amount. Therefore, correlations between these measurements were calculated to recognize similarities as well as differences. This procedure has already been addressed in chapter 3.5.7, when the determination of the split point was explained.

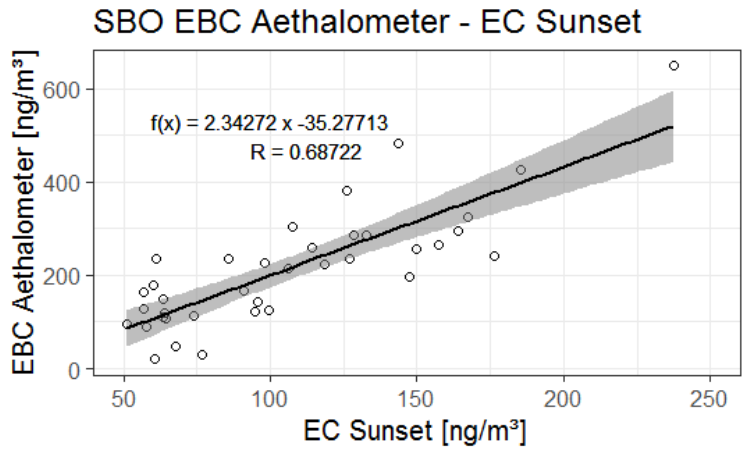

Figure 27: Correlation of EBC measurement on Aethalometer compared to EC measurement on Sunset shows 2-fold elevated BC Aethalometer concentrations compared to EC Sunset.

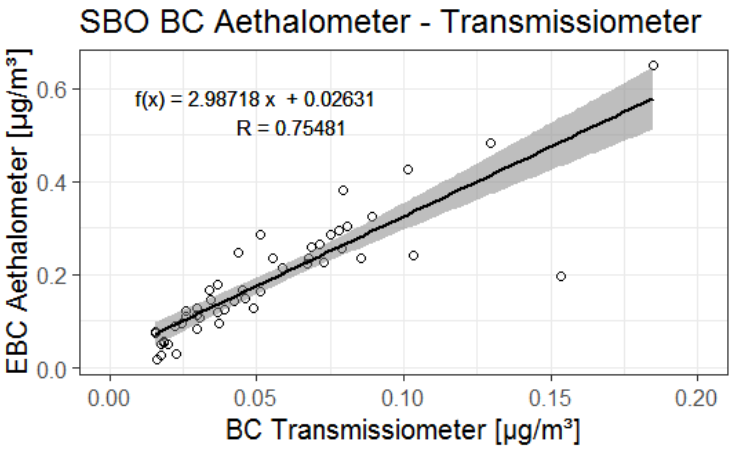

Figure 28: Correlation of BC measurements on Transmissometer and Aethalometer. EBC shows threefold concentrations of BC measured with Transmissometer.

The concentrations measured with the Aethalometer (EBC) was twice the concentrations measured with Sunset (EC) and threefold the ones measured with transmissometry (Figure 27, Figure 28). For the Sunset measurements one has to note, that here a slightly different set of data (values below the LOD were excluded) was used than in the previous chapter concerning the description of the analytical methods, when all values were used. This leads to slight differences of the regression analysis. The marked scatter of the data as well as the slope being markedly higher than 1 (Figure 27), points to the presence of light absorbing species in addition to EC. Note that the Aethalometer was installed behind the whole air inlet, while the Sunset measurements described here refer to PM 10 filters collected with a HiVol sampler installed independently.

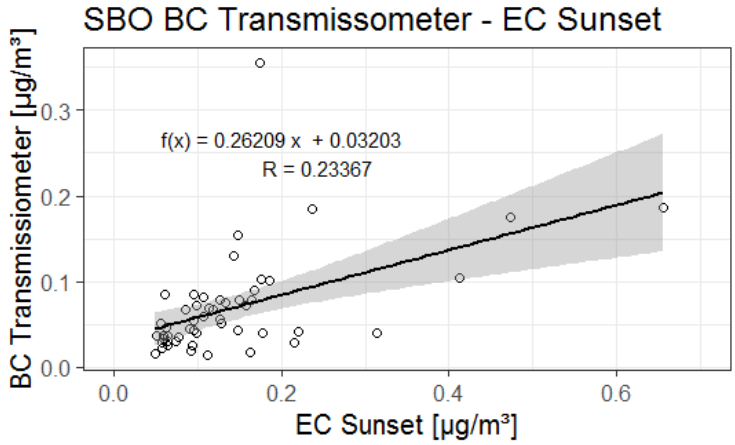

Figure 29: BC measured with Transmissometer shows approximately the same concentration compared to EC Sunset measurements.

Comparing Sunset and transmissometer measurements a slope close to 1, but a large scatter was observed (Figure 29). This bad correlation between EC (Sunset) and BC (Transmissometer) may be due to the calculation procedure chosen for EC, i.e. the manual setting of the split-point, which adjusted EC calculation to the Aethalometer signal. BC values for transmissometry were calculated using a conversion factor determined by Greilinger et al (2019) for SBO. In the cited paper the determination of EC was based on an automatically set split point. The correlation of BC (Transmissometer) and EC (Sunset) is better (see Figure 30), when the split point for EC determination is set automatically (in difference to the calculation in the present thesis, where peak 3 and 4 are used to estimate EC). This again shows, that comparisons of BC and EC measurements performed with different methods, have to be interpreted with care.

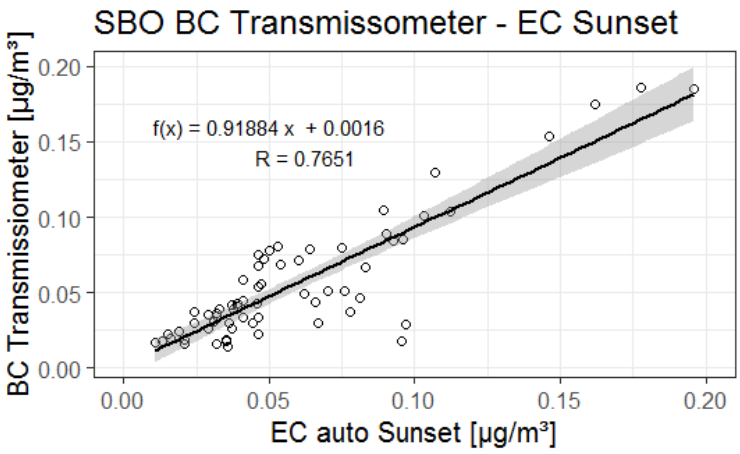

Figure 30: BC measured with Transmissometer shows approximately the same concentration compared to EC Sunset measurements with automatically set split point.

Since there is a difference in BC and EC correlation depending on whether EC is calculated with automatically set split point or out of peak 3 and 4, it has to be noted, that within the present work EC was always calculated out of peak 3 and 4, if not noted differently.

4.2. Time Trends

Here concentrations of metals, ions and carbon compounds are presented starting from June 2016 to May 2018. Time trends for each measurement method are displayed and compared between PM 10 and PM 1 fractions, if possible. In the end the averages of summer and winter periods of this two-year period is compared to the concentrations measured at SBO in the 1990ies [20].

4.2.1. Concentrations of elements – Fe, Ca, Mg, K, Al

Calibration curves are shown in chapter 3.5.6. Fe, Ca and K showed a good calibration curve with an R^2 greater than 0.99. Mg, Al, S and P also showed a good calibration curve with an R^2 above 0.8.

Out of 88 measured PM 10 filters the number of values below the LOD is given in Table 13. For most of the metals no relevant number of samples are below LOD. Exceptions are Fe and P, as for Fe approximately 10 % of the samples are below LOD and for P approximately 20 % of the samples are below LOD. As given above, only the calibrations for Fe, Ca and K showed a correlation coefficient above 0.9, the others had a correlation coefficient above 0.8. As most of the elements lay below the lowest standard, a more appropriate calibration for SBO samples is needed, if XRF is further used for samples of small filter loadings. The aperture of the sample holder (27 mm or 20 mm) was not relevant as the aperture for the beam was limited to 20 mm in the used method.

Table 13: Number of values below LOD out of 88 PM 10 values analysed.

Analyte	Number of values below LOD
Fe	10
Ca	2
Mg	4
Al	1
K	6
S	0
P	17

The timeline of metal compounds measured with XRF shows a low background concentration with about five periods with higher values (July 2016, September 2016, June/July 2017, April 2018) as shown in Figure 31 and Figure 32. In most of the cases Al concentrations exceeds the others. Just at the end of March 2018 Fe concentration is higher than Al. Fe, Ca, Mg, K and Al seem to have a similar trend in concentrations. S seems to have another trend as the metals measured due to different sources. S concentrations are more variable due to mixture and anthropogenic influence, which is enhanced during the summer period.

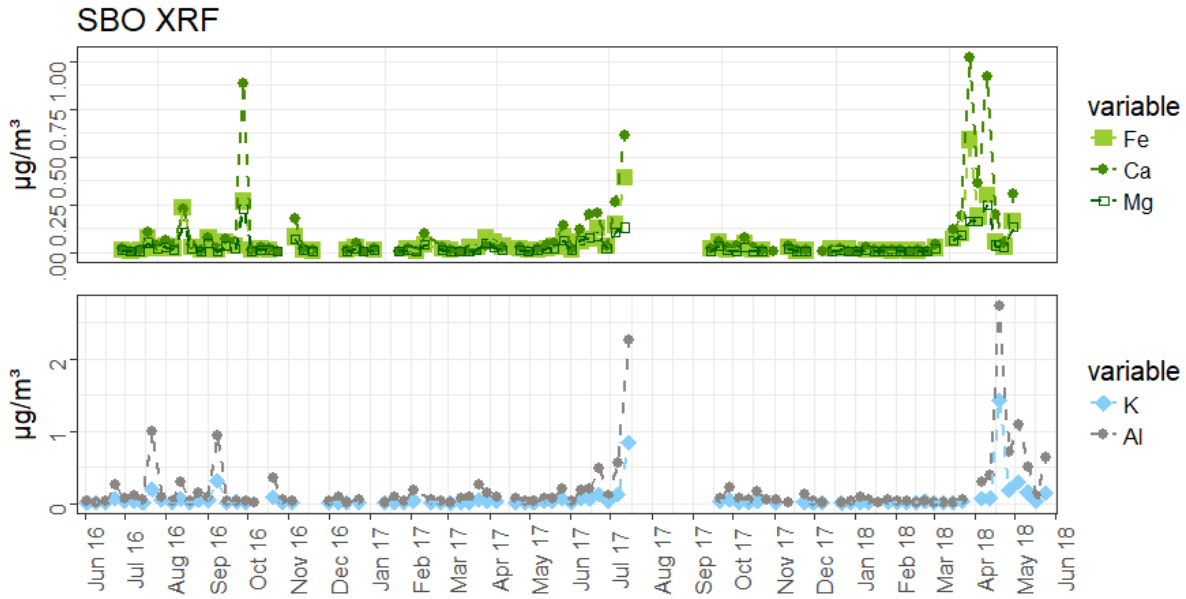

Figure 31: Fe, Ca, Mg, K and Al measured with XRF from June 2016 to May 2018.

P shows the most constant concentrations considering the XRF-measurements. It only shows elevated concentrations during summer 2016, July 2017 and April 2018 (see Figure 32). The other compounds show greater variability over the years, except during winter periods from November to January, where the concentration of all compounds stays rather low. This may be also due to the mixing of the

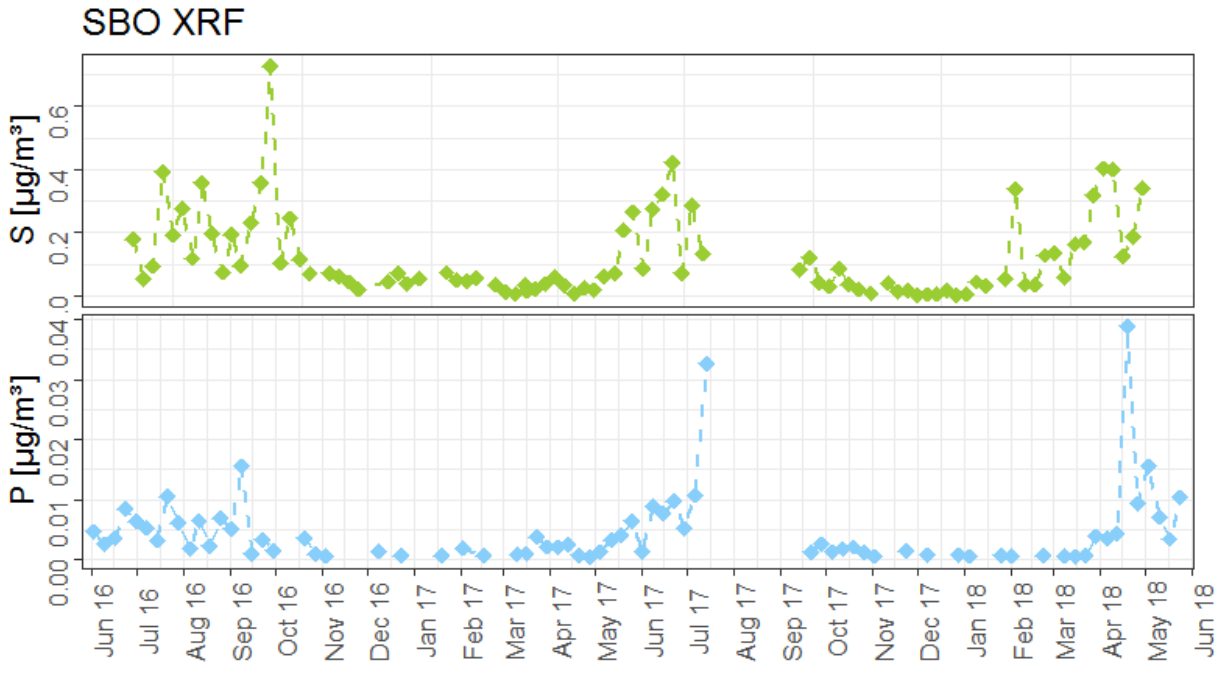

Figure 32: S and P measured with XRF from June 2016 to May 2018.

atmosphere, which augments during summer times due to turbulences. S shows greater variations than the other compounds. Therefore, compounds like Fe, Ca, K, Mg and Al are more likely to be related to SDEs than S as it shows a variability in concentration over the whole year.

Underlining the statement, that P may be part of SDEs in contrast to S, P shows good correlation (R above 0.7) to Al, Fe and K concentrations (see Figure 33 to Figure 36), whereas a low correlation with S (R about 0.3) was observed (see Figure 37). As K^+ also was determined by IC, there are two correlations of P to K. K^+ determined by IC shows a poorer correlation compared to K determined by XRF. This could be cue to an incomplete solution of K compounds by IC measurement, as mentioned above. On the other hand, it has to be held in mind, that the correlation with K determined by XRF is strongly driven by a small number of data point only.

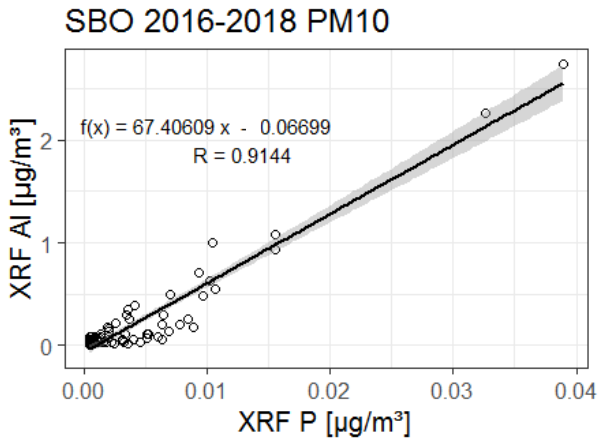

Figure 33: Correlation of P and Al measured with XRF.

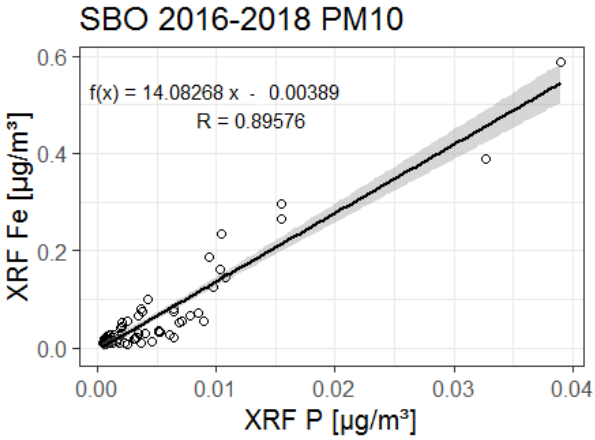

Figure 34: Correlation of P and Fe measured with XRF.

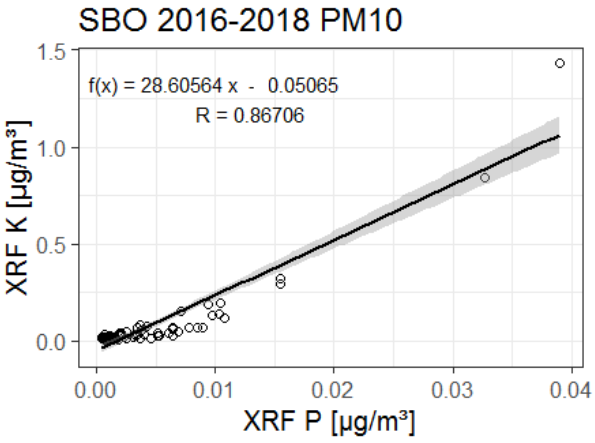

Figure 35: Correlation of P and K measured with XRF.

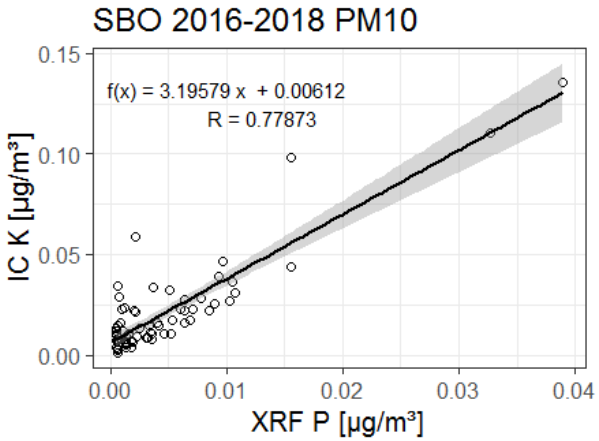

Figure 36: Correlation of P measured with XRF and K^+ measured with IC.

For PM 1 no XRF measurements were undertaken due to limited area. For comparison with metals between PM 10 and PM 1 the half of the PM 1 filter is reserved for ICP-MS measurements. Measurements of PM 10 with ICP-MS are also possible as filter material is still left as well.

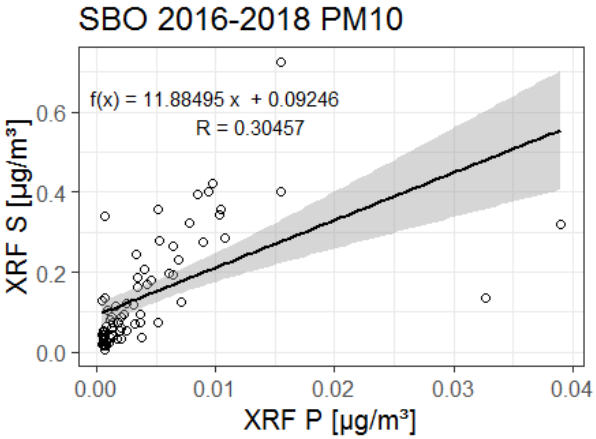

Figure 37: Correlation of P and S measured with XRF.

4.2.2. Carbonaceous Particulate Matter – EBC, BC and EC

The carbon content measured with the aethalometer (EBC) was available for TSP solely. EBC is in reasonable correlation with BC (transmissiometer) and EC (Sunset) (Figure 38) but pronounced differences in absolute concentrations values become visible as discussed before (chapter 4.1.2). 79% of PM 10 BC values lay above the LOD (this corresponds to 18 of 85).

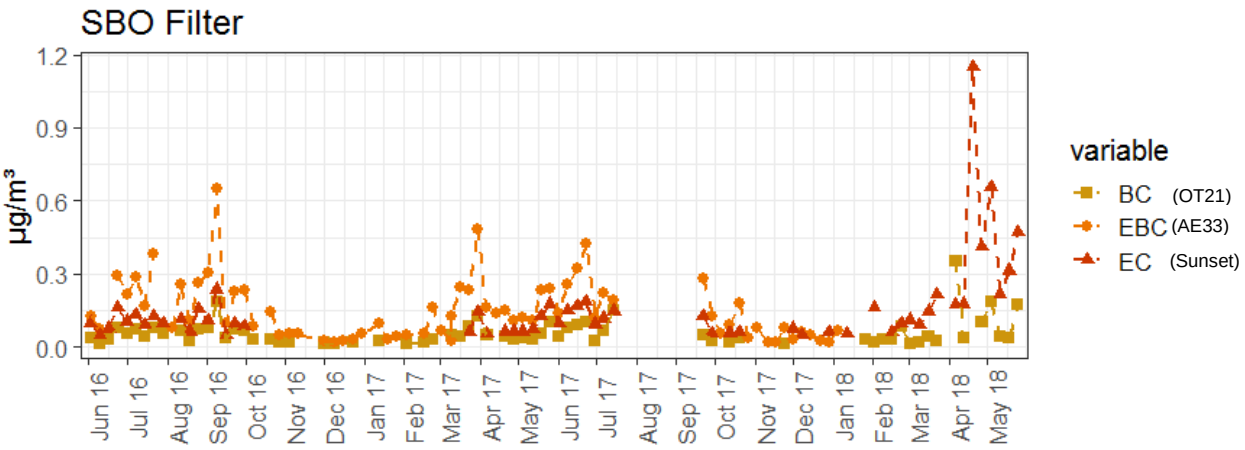

Figure 38: PM 10 concentrations of EBC of aethalometer, BC of transmissometer and EC of Sunset measurements starting from June 2016 to end of May 2018 (EBC measurements values were only available until January 2018).

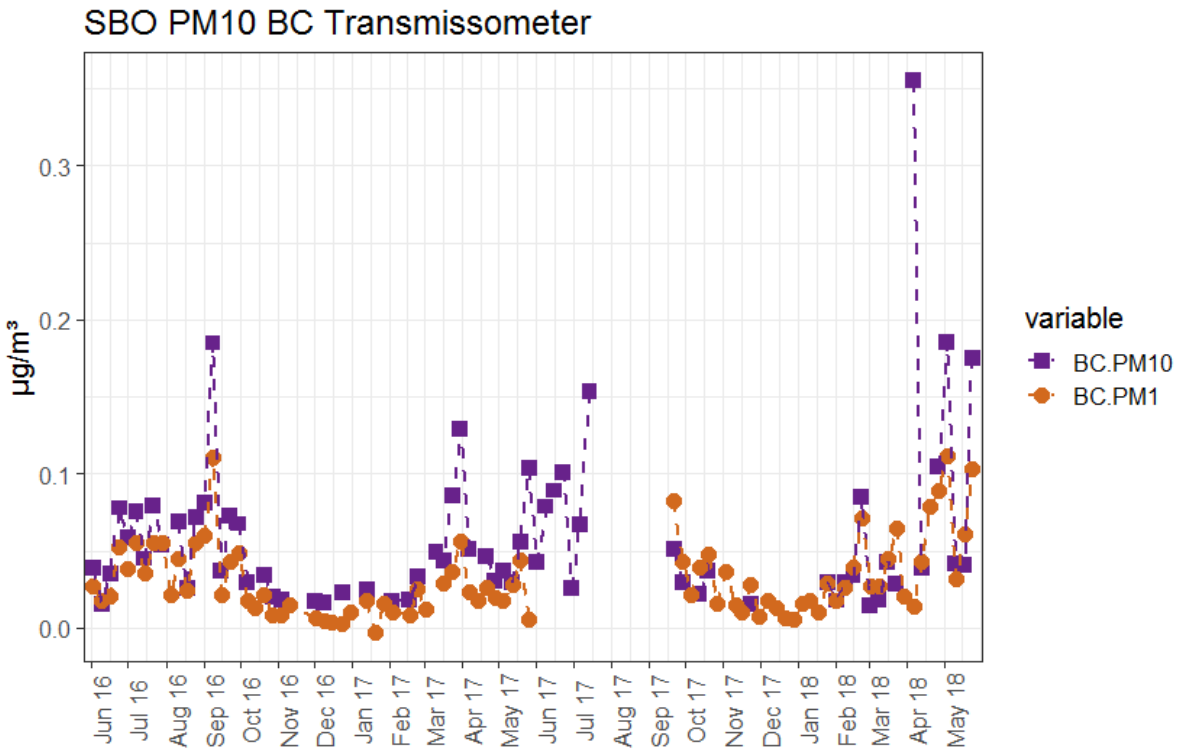

Figure 39: PM 10 and PM 1 BC concentrations in µg/m³ from June 2016 to May 2018.

PM 1 measurements of BC are shown in Figure 39. Nearly all measurements lay below the ones of PM 10 fraction, as expected. 89% of PM 1 BC values lay above the LOD (this corresponds to 76 out of 85 measurements).

Higher concentrations in summer periods compared to winter are observable for carbonaceous components as well. These seasonal variations are due to differing mixing of the atmosphere as described in chapter 4.2.1. Seasonal variation in concentrations are called annual cycles henceforth.

While PM 10 concentrations of EC are shown in Figure 38 over the period of time from June 2016 to May 2018 together with BC and EBC concentrations. PM 10 concentrations of TC, OC and EC are displayed in Figure 40. 92 % of OC and TC concentrations lay above LOD. EC concentrations are lower than OC concentrations. Hence, only 67 % lay above LOD. Annual variations between summer and winter are observable here as well. OC accounts for 79 % of TC.

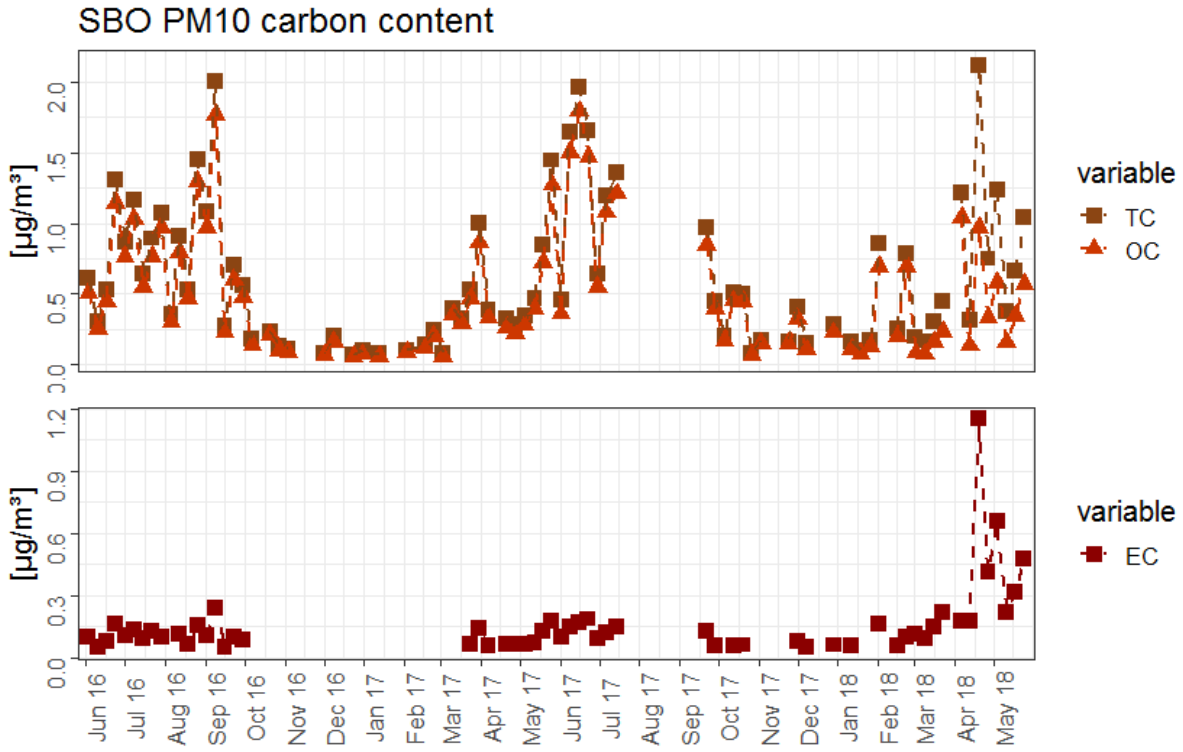

Figure 40: PM 10 carbon concentrations measured with Sunset in µg/m³ from June 2016 to May 2018.

PM 1 concentrations of TC, OC and EC are displayed in Figure 41. 99 % of TC, OC and EC concentrations lay above LOD. The higher percentage of PM 1 EC values above the LOD is most likely due to the greater filter area used for analysis, because the loadings (µg/cm²) of PM 1 and PM 10 samples as well as the blank measurements are similar. Annual variations between summer and winter are observable here as well. OC accounts for 79 % of TC, which is the same contribution as in PM 10.

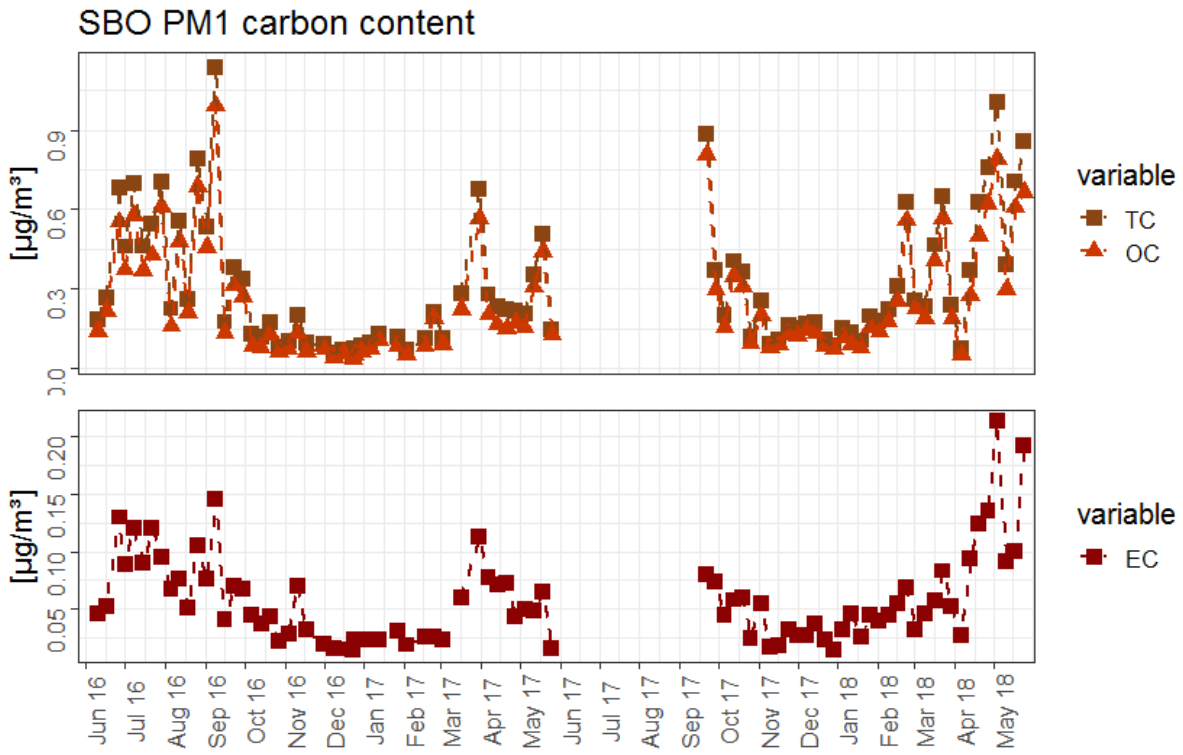

Figure 41: PM 1 carbon concentrations measured with Sunset in µg/m³ from June 2016 to May 2018.

PM 1 concentration is lower than PM 10 concentration as seen in Figure 42. Interesting are two high EC concentrations in PM 10 in April 2018. As no difference to other measurements were observed, these elevated concentrations are most likely due to the first activities related to construction work in Summer 2018 connected to the renewal of the cable car to the Observatory.

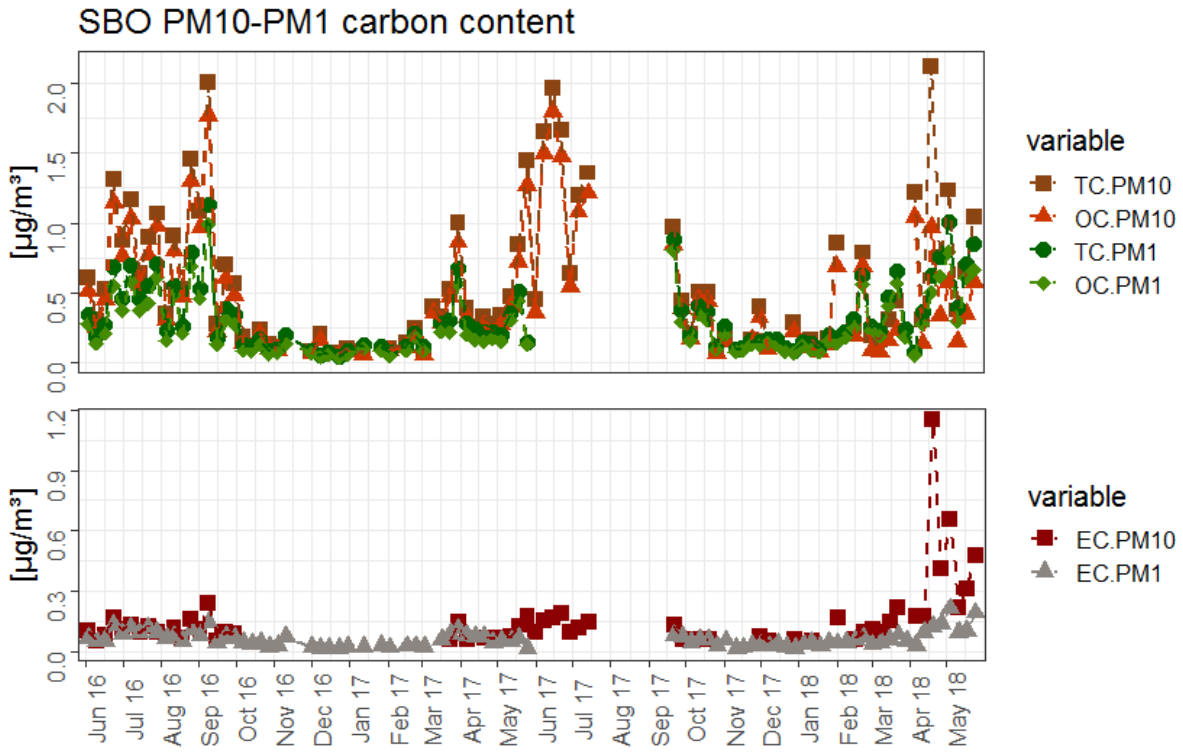

Figure 42: PM 10 and PM 1 carbon concentrations measured with Sunset in µg/m³ from June 2016 to May 2018.

4.2.3. NH_4^+, Ca^{2+}, Na^+, Mg^{2+} and K^+

PM 10 concentrations of cations are shown in Figure 43. The annual trend, which is described for XRF and Sunset measurements in chapter 4.2.1 and 4.2.2, of higher concentrations in summer times compared to winter can be seen here as well as the highest concentrations in this period in September 2016, June/July 2017 and April 2018. These periods of higher concentration are seen for Ca^{2+}, Na^+, Mg^{2+} and K^+. For NH_4^+ the general seasonal trend is visible, but the elevated concentrations mentioned above are not observed. This most likely is due to different sources of NH_4^+ compared to the other analytes, which could be part of SD (or mineral dust related to construction work) as well. And SDEs are more common in spring and autumn, which are the periods where higher concentrations are observed. 83 % of NH_4^+ concentrations lay above the LOD. The other cation concentrations showed an even higher percentage of values above the LOD (Na^+: 90 %, Ca^{2+}: 92 %; K^+: 99 %; Mg^{2+}: 100 %).

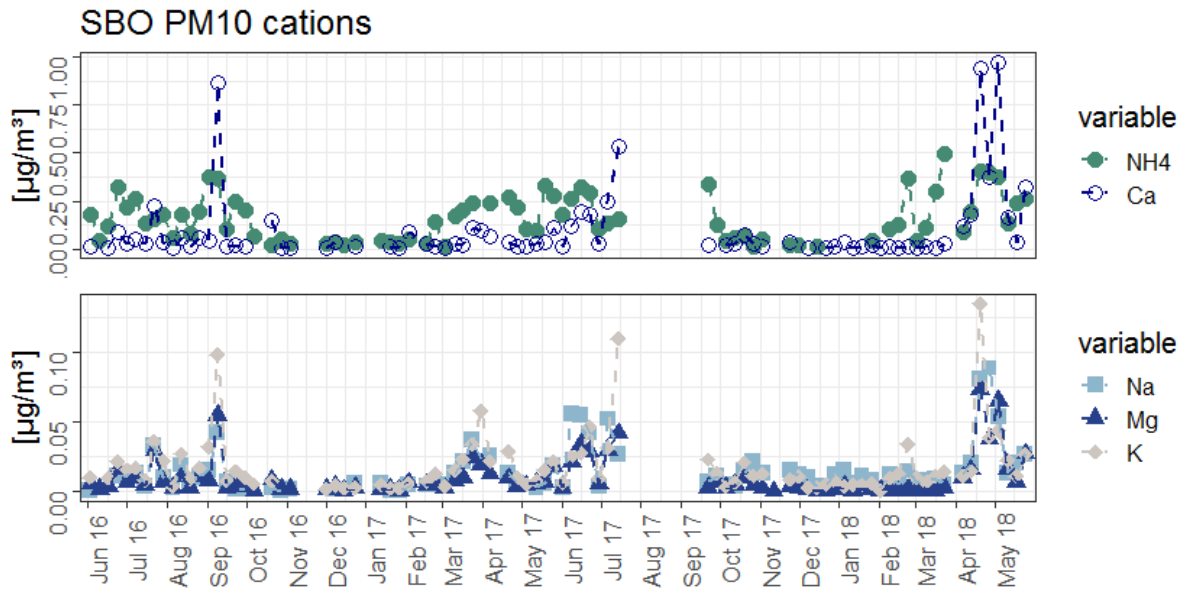

Figure 43: PM 10 concentrations of cations (NH_4^+, Ca^{2+}, Na^+, Mg^{2+}, K^+) from June 2016 to May 2018.

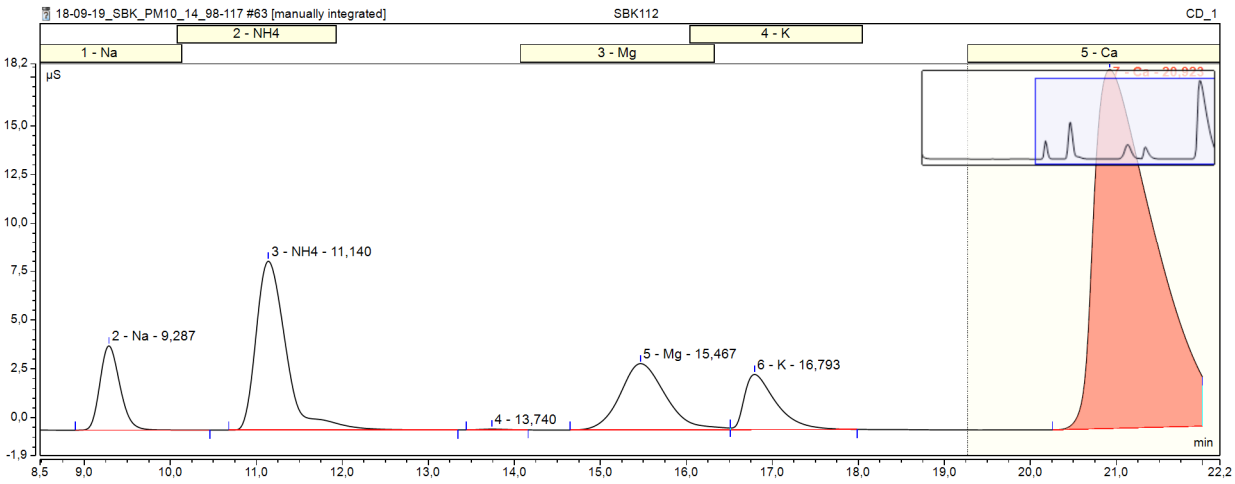

Figure 44: Typical chromatogram of PM 10 filters showing a relatively high Ca^{2+} peak compared to other measured cations (Na^+, NH_4^+, Mg^{2+}, K^+).

Some chromatograms of PM 10 (from week 15.03.2018 to 24.05.2018) showed additional peaks at around 13.6 min, 18.3 min and 19.6 min. BL7 showed the same additional peaks. Therefore, the contamination may be due to the filter material or transportation. Most of the cation chromatograms showed the additional peak at around 13.5 min, which could not be identified yet. Two chromatograms do not include the whole Ca^{2+}-peak at the end of the measurement time and therefore these Ca^{2+}-values with incomplete peaks were excluded from calculation (week of 28.09.2017 and 30.11.2017) as already mentioned before (Analytical Methods). In addition, the measurement time was prolonged for further measurements. Number of values below LOD are given in Table 14 and a typical chromatogram of PM 10 samples in Figure 44.

Table 14: Number of values lying below LOD out of 89 PM 10 values analysed.

Analyte	Number of values below LOD
Na^+	9
NH_4^+	15
Mg^{2+}	0
K^+	1
Ca^{2+}	7

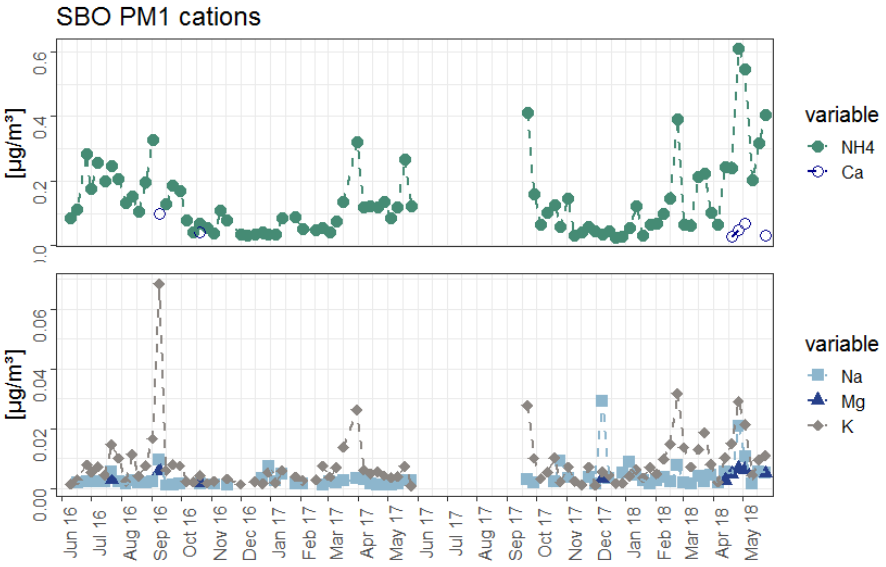

Figure 45: PM 1 concentrations of cations (NH_4^+, Ca^{2+}, Na^+, Mg^{2+}, K^+) from June 2016 to May 2018.

PM 1 concentrations of cations are shown in Figure 45. The annual trend of higher concentrations in summer times compared to winter can be seen here as well as the highest concentrations in this period in September 2016, March to May 2017 and April 2018. Only 6 % of Ca^{2+} and 9 % of Mg^{2+} concentrations lay above the LOD, suggesting that the greater amount of Ca^{2+} and Mg^{2+} lay in the PM coarse fraction, as expected of analytes originating from SD or mineral dust. The other cation concentrations showed a higher percentage of values above the LOD (Na^+: 81 %, K^+: 97 %, NH_4^+: 99 %). Note that the NH_4^+ concentrations in PM 1 exceeds the PM 10 NH_4^+ concentration sometimes. As the LOD of NH_4^+ for PM 10 is higher compared to PM 1, no contamination of PM 1 filters with ammonium after sampling (i.e. during storage within the Observatory) is likely. Blank values used for correction of PM 10 filters were higher compared to PM 1 filters. Applying the blank values of PM 1 would yield in approximately 0.012 µg/m³ higher PM 10 concentrations, which would explain a number of the mismatch of PM 10 and PM 1 observed presently.

For PM 1 samples a typical chromatogram is given in Figure 47. The chromatogram showed a high NH_4^+ peak relative to the other peaks. As NH_4^+ values are the highest of measured cations, they are also the ones mostly over the LOD. Ca^{2+} and Mg^{2+} had such a small concentration, that they could only be qualitatively observed, but not quantitatively (for exact numbers of values below LOD see Table 15).

Table 15: Number of values lying below LOD out of 87 PM 1 values analysed.

Analyte	Number of values below LOD
Na^+	16
NH_4^+	1
Mg^{2+}	78
K^+	3
Ca^{2+}	81

The differing contribution of cations to the PM 1 and PM 10 fraction is also visible from the chromatograms. In PM 10 samples Ca^{2+} typically showed the highest peak (Figure 44), whereas in PM 1 the NH_4^+ peak was highest compared to other peaks in the chromatogram (Figure 47). The number of values below LOD shows, that the concentration on the filter of PM 1 is lower than that on the PM 10 filter. The atmospheric concentrations of cations in PM 1 and PM 10 fractions in the air is represented in Figure 46.

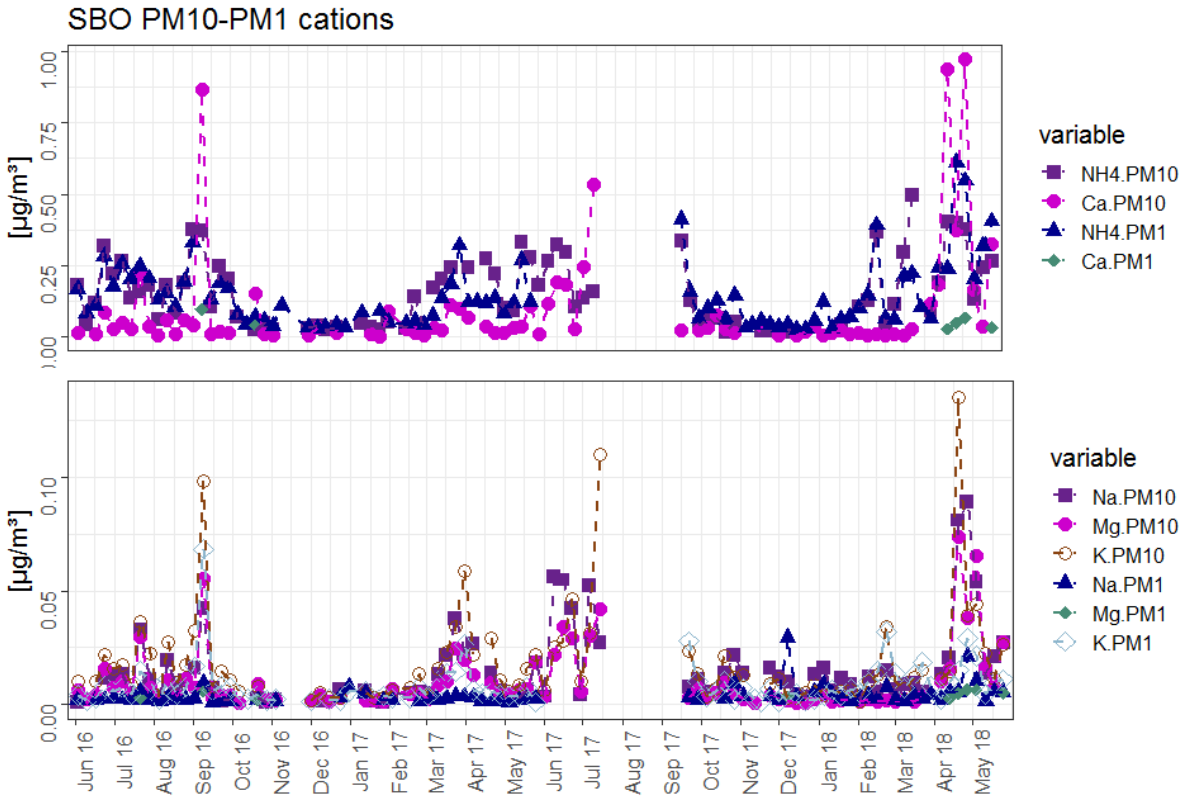

Figure 46: PM 10 and PM 1 concentrations of cations from June 2016 to May 2018.

Bearing in mind, that Ca^{2+} and Mg^{2+} show lesser concentrations above LOD in PM 1 compared to PM 10 and comparing PM 10 to PM 1 concentrations of cations (see Figure 46), Ca^{2+} an Mg^{2+} are enriched in PM coarse. This underlines the assumption, that mineral dust, which contains Ca^{2+} and Mg^{2+}, and particles of mechanical erosion are found in the coarse fraction.

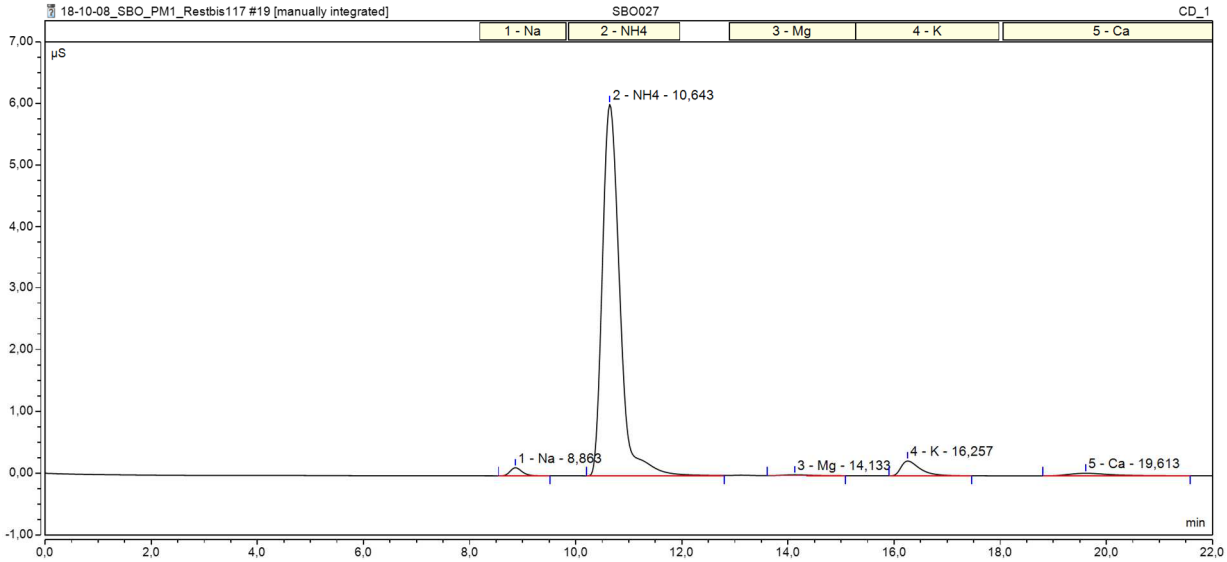

Figure 47: Typical chromatogram of PM 1 filters showing a relatively high NH_4^+ peak compared to other measured cations (Na^+, Mg^{2+}, K^+, Ca^{2+}).

4.2.4. SO_4^{2-}, NO_3^-, NO_2^- and Cl^- determined by anion chromatography

PM 10 concentrations of anions are shown in Figure 48. The annual trend of higher concentrations in summer times compared to winter could be observed here as well with an exception of Cl^-. There are only few concentrations of Cl^- lying above the LOD (11 %) and all show similar concentration in summer and winter. The highest concentrations in this period in September 2016, June/July 2017 and April 2018 could be observed for SO_4^{2-} and NO_3^-. NO_3^- and NO_2^- concentrations showed a similar percentage of values above the LOD (NO_3^-: 43 %; NO_2^-: 57 %), whereas all measured values of SO_4^{2-} lay above the LOD.

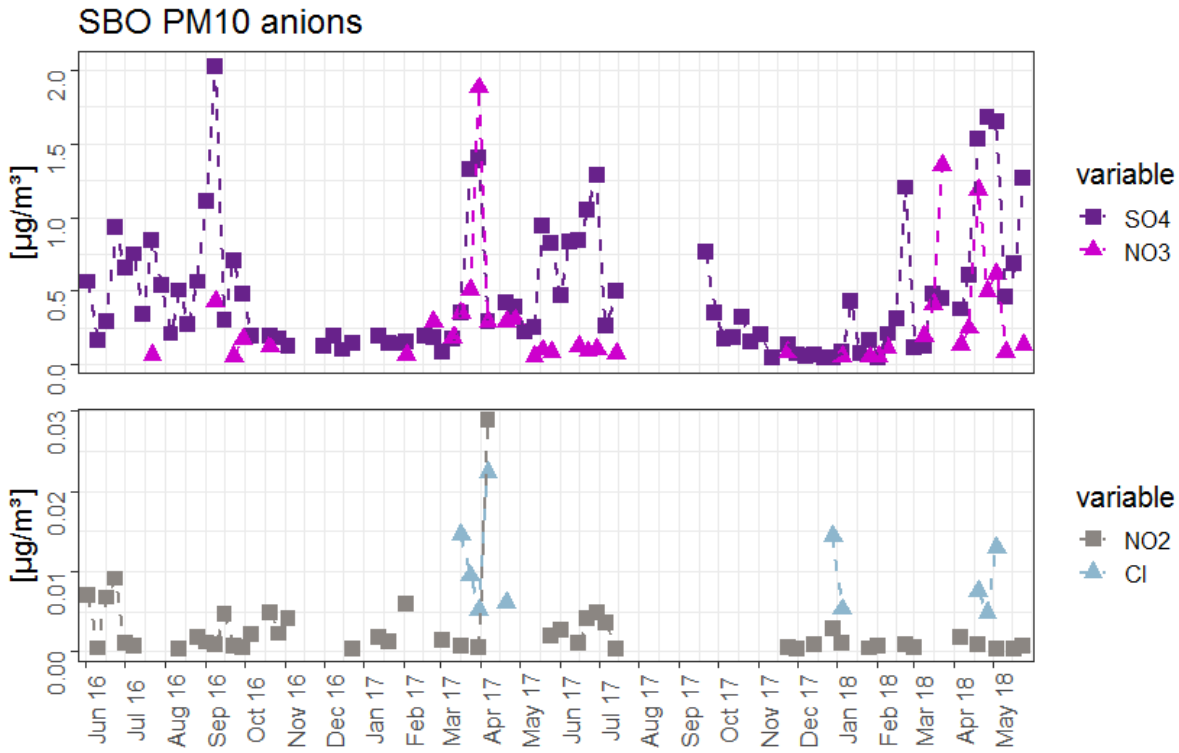

Figure 48: PM 10 concentrations of anions (SO_4^{2-}, NO_3^-, NO_2^-, Cl^-) from June 2016 to May 2018.

In anions chromatograms additional signals eluting before chloride were observed sometimes. These peaks could be due to presence of organic acids or fluoride. Additionally, a peak between NO_2^- and NO_3^-

occurred a number of times. These additional peaks were approximately at 4.1 min, 8.2 min (correlated with the fourth peak of the control standard, which should be bromide) and 12.0 min (correlated with the sixth peak of the control standard, which should be phosphate). The first peak of the control standard (fluoride) was at approximately 3.5 min and therefore before the first peak in the sample. Moreover, NO_2^- often occurred as a double peak and was rather broad (example given week 15.09.2016 or 30.03.2017).

When PM 1 samples were analysed, retention times were slightly shorter, due to the performance of the chromatographic system at that time. Consequently, another signal eluting later than sulphate was observed for PM 1 samples and could be identified as oxalate. Oxalate will have been present in PM 10 as well, but was not detectable because of the set time of analysis. As the peaks eluted late, it couldn't be seen. As PM 1 is a fraction of PM 10 it is assumed, that PM 10 has at least the same amount/concentration of Oxalate.

PM 1 concentrations of anions are shown in Figure 49. The annual trend of higher concentrations in summer times compared to winter could be observed here as well with an exception of Cl^-. There are only few concentrations of Cl^- lying above the LOD (13 %) and all show similar concentration in summer and winter. For NO_2^- only 6 % of the concentrations lay above the LOD. Therefore, no trend could be seen for NO_2^-. The highest concentrations in this period for SO_4^{2-} and NO_3^- could be observed in September 2016, March/April 2017, December 2017 and March/April 2018. NO_3^- and SO_4^{2-} concentrations showed a similar percentage of values above the LOD (NO_3^-: 97 %; SO_4^{2-}: 99 %).

Comparing PM 10 and PM 1 concentrations of anions (see Figure 50), concentrations of PM 1 lay below the ones of PM 10 for SO_4^{2-} and NO_3^-. For NO_2^- and Cl^-no real trend could be seen, as too few values of PM 1 are available.

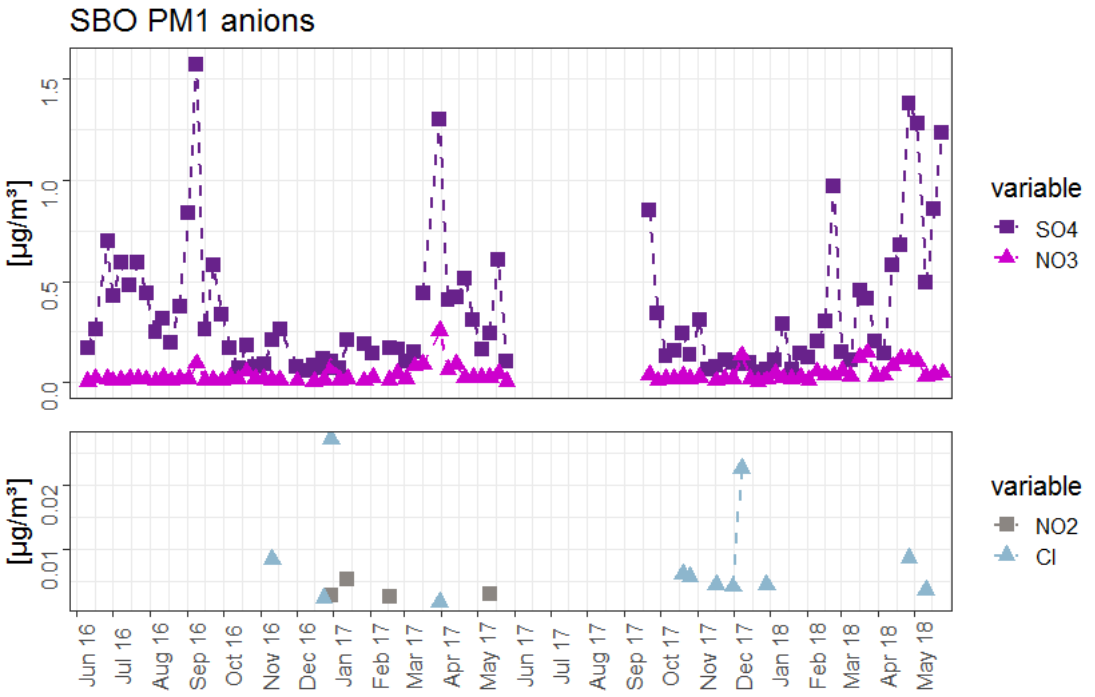

Figure 49: PM 1 concentrations of anions (SO_4^{2-}, NO_3^-, NO_2^-, Cl^-) from June 2016 to May 2018.

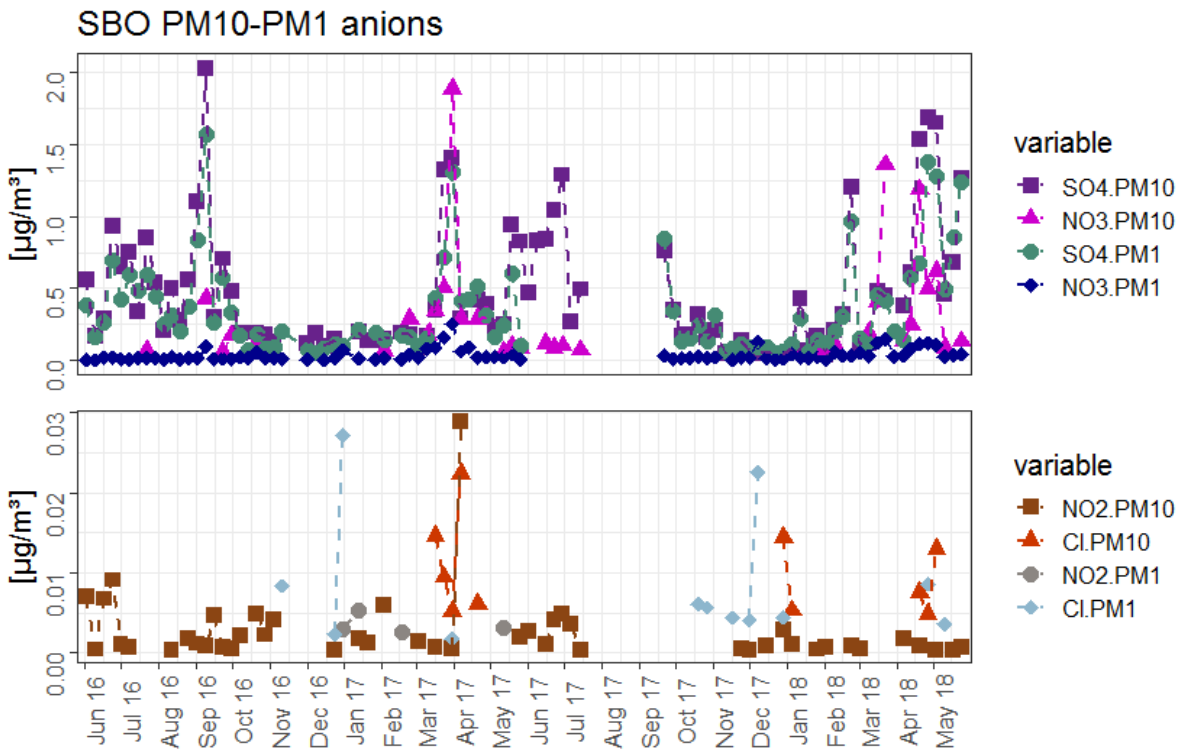

Figure 50: PM 10 and PM 1 concentrations of anions from June 2016 to May 2018.

4.2.5. Levoglucosan, Inositol, Arabitol, Glucose and Sucrose

Within PM 10 only Levoglucosan was measured. 90 % of measured concentrations lay above the LOD. Nevertheless, nearly all samples of March 2017 lay below the LOD. The time trend of Levoglucosan of PM 10 is displayed in Figure 52 in comparison with the Levoglucosan concentration of PM 1. In September 2016, as well as in February and March 2018 elevated concentrations were observed.

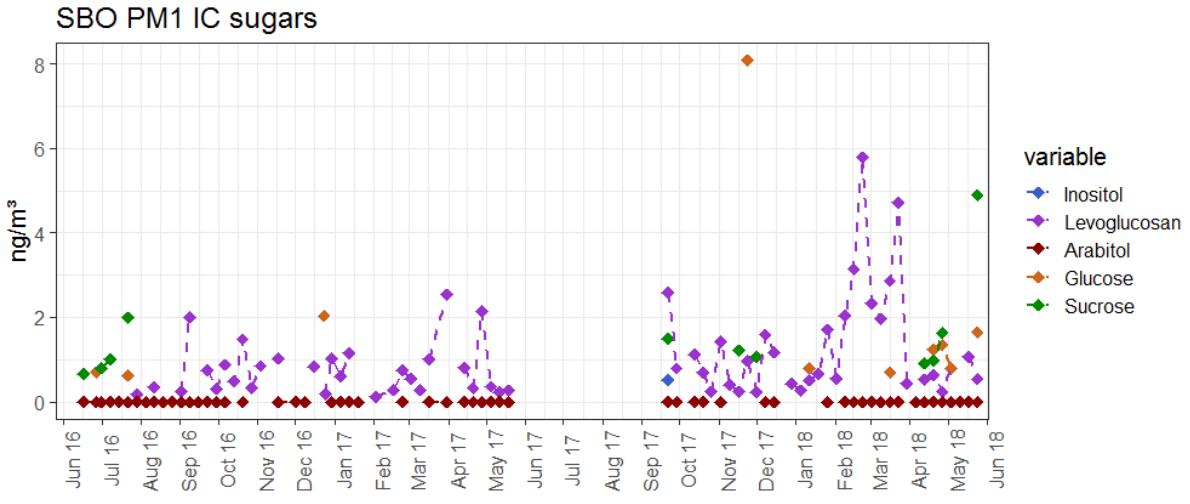

Figure 51: PM 1 sugar measurements. Atmospheric concentration in ng/m³ of Inositol, Levoglucosan, Arabitol, Glucose and Sucrose are given starting from June 2016 to end of May 2018.

As the concentrations were very small, only a few samples showed sugar concentrations above LOD. For PM 1 1 % of Inositol 11 % of Glucose, 12% of Sucrose, 61 % of Arabitol and 66 % of Levoglucosan concentrations lay above the LOD. One relatively high glucose concentration and several elevated Sucrose concentrations occurred. Levoglucosan can be found in most of the samples in the range from 0.15 to 3 ng/m³, whereas Arabitol did not rise above 0.8 ng/m³ (Figure 51). In some samples Mannosan, Trehalose, Mannitol, Galactosan or Fructose could be quantitatively observed as well.

PM 1 concentrations were, as usually expected, lower compared to PM 10 values. Just one value of PM 1 was noticeable high compared to PM 10 (Figure 52). It was the week of 21.9.2017, where measurements have been resumed after a summer pause. Maybe the sampling systems had been differently cleaned before sampling again. As Inositol in PM 1 was also only present above LOD in this week, it may be due to accumulated particles in the PM 1 sampling inlet during the break of sampling in summer 2017. In March 2017 the measurements of PM 10 Levoglucosan lay below the LOD.

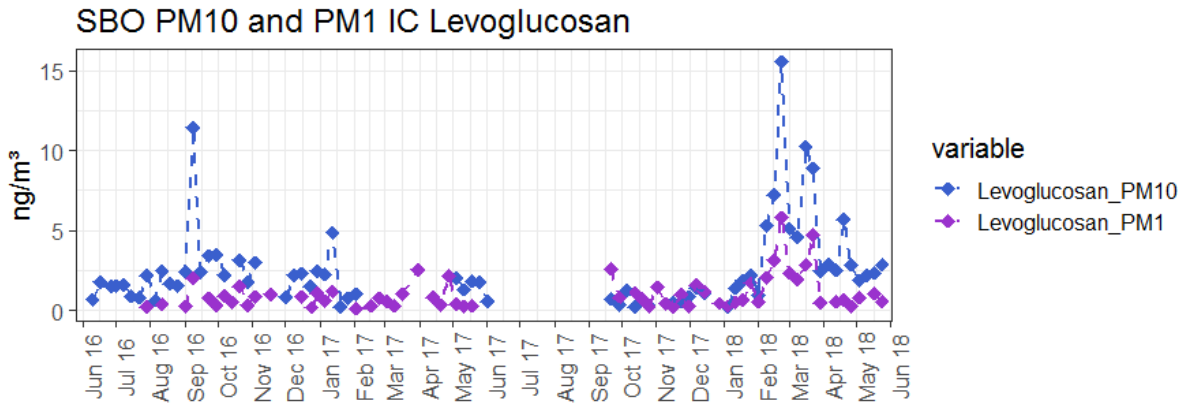

Figure 52: Levoglucosan concentration in ng/m³ of PM 1 and PM 10 filters.

4.3. Comparison of concentrations in summer and winter and PM 1 to PM 10 ratios

The average of concentrations for each analyte for summer and winter periods were calculated. For summer, weeks from June to August were averaged. Starting from November to January, the winter period is averaged. Exact dates from the two winter and summer periods are listed in Table 16. In addition, all summer weeks of both years and all winter weeks of both years were averaged for summer 2016-2018 and winter 2016-2018. PM 10 averages are displayed in Table 17. Table 18 shows averages of PM 1 samples.

Table 16: Dates of summer and winter periods for average of concentrations.

Name of period	Start	End
Summer 2016	02.06.2016	31.08.2016
Winter 2016	03.11.2016	01.02.2017
Summer 2017	01.06.2017	27.07.2017
Winter 2017	02.11.2017	31.01.2018

Generally, concentrations were higher in summer compared to winter (see Table 17 and Table 18). Only Levoglucosan showed a lower concentration for summer than for winter in PM 10 and in PM 1. The lower concentrations of aerosols during winter compared to summer at the mountain top is contrary to the observations in valleys, where concentrations in winter are usually higher than in summer. This effect of higher concentrations in summer is due to the enhanced influence of boundary layer air masses, due to stronger mixing of the troposphere in summer. During winter vertical mixing is less pronounced and PM accumulates closer to the ground. During winter periods, sometimes almost free tropospheric concentrations can be observed at SBO.

Table 17: PM 10 averages of analytes for summer and winter periods. If no values are available, the field is filled with NA (not available). Values measured only for PM 10 are shaded in grey.

	Summer 2016	Summer 2017	Summer	Winter 2016	Winter 2017	Winter	Summer-winter ratio	LOD
BC [µg/m³]	0.054	0.080	0.063	0.020	0.023	0.021	3.1	NA
Fe [µg/m³]	0.045	0.118	0.071	0.013	0.016	0.015	4.8	0.0803
Ca-XRF [µg/m³]	0.056	0.208	0.109	0.016	0.014	0.014	7.6	0.0067
Mg-XRF [µg/m³]	0.030	0.069	0.044	0.009	0.008	0.008	5.4	-0.0170
Al [µg/m³]	0.164	0.547	0.298	0.038	0.040	0.039	7.6	0.0146
K-XRF [µg/m³]	0.042	0.181	0.091	0.010	0.013	0.012	7.8	0.0075
S [µg/m³]	0.189	0.229	0.203	0.053	0.015	0.030	6.7	0.0036
P [µg/m³]	0.005	0.011	0.007	0.001	0.001	0.001	9.5	0.0006
OC [ng/m³]	715	1136	863	111	160	137	6.3	173.1
EC [ng/m³]	107	137	118	67.5	60.1	61.6	1.9	66.5
TC [ng/m³]	818	1273	977	140	202	173	5.6	173.1
SO_4^{2-} [µg/m³]	0.510	0.748	0.593	0.145	0.117	0.128	4.6	0.0014
NO_3^- [µg/m³]	0.064	0.095	0.089	NA	0.060	0.060	1.5	0.0563
Cl^- [µg/m³]	NA	NA	NA	NA	0.010	0.010	NA	0.0051
Ca^{2+} [µg/m³]	0.051	0.187	0.101	0.012	0.018	0.016	6.3	0.0057
NH_4^+ [µg/m³]	0.165	0.210	0.180	0.032	0.030	0.032	5.7	0.0288
Mg^{2+} [µg/m³]	0.009	0.024	0.014	0.002	0.002	0.002	7.1	0.0002
Na^+ [µg/m³]	0.011	0.034	0.020	0.003	0.010	0.008	2.6	0.0034
K^+ [µg/m³]	0.017	0.037	0.024	0.003	0.007	0.005	4.5	0.0023
Lev [ng/m³]	1.40	1.75	1.52	2.03	1.12	1.60	1.0	0.174

Table 18: PM 1 averages of analytes for summer and winter periods. If no values are available, the field is filled with NA (not available).

	Summer 2016	Summer 2017	Summer	Winter 2016	Winter 2017	Winter	Summer-winter ratio	LOD
PM 1 [µg/m³]	3.15	NA	3.15	1.20	NA	1.20	2.6	NA
BC [µg/m³]	0.039	NA	0.039	0.009	0.016	0.013	3.1	NA
OC [ng/m³]	391	NA	391	71.5	115	94.3	4.1	104.6
EC [ng/m³]	85.1	NA	85.1	26.5	30.8	28.7	3.0	8.4
TC [ng/m³]	476	NA	476	98	146	123	3.9	104.6
SO_4^{2-} [µg/m³]	0.399	NA	0.399	0.128	0.121	0.124	3.2	0.0047
NO_3^- [µg/m³]	0.198	NA	0.198	0.016	0.029	0.023	0.6	0.0033
Cl^- [µg/m³]	NA	NA	NA	0.013	0.009	0.011	NA	0.0020
Ca^{2+} [µg/m³]	NA	NA	NA	NA	NA	NA	NA	0.0276
NH_4^+ [µg/m³]	0.178	NA	0.178	0.054	0.056	0.055	3.2	0.0016
Mg^{2+} [µg/m³]	0.003	NA	0.003	NA	0.003	0.003	0.9	0.0020
Na^+ [µg/m³]	0.002	NA	0.002	0.003	0.006	0.005	0.5	0.0015
K^+ [µg/m³]	0.006	NA	0.006	0.003	0.004	0.004	1.8	0.0014
Lev [ng/m³]	0.268	NA	0.268	0.809	0.800	0.804	0.3	0.268

Table 19: PM 1 to PM 10 ratios of summer and winter averages show that PM 1 is a subfraction of PM 10 and hence shows PM 1/PM 10 ratios below one.

PM 1/PM 10 ratio	summer	winter	PM 1/PM 10 ratio	summer	winter
BC [µg/m³]	0.6	0.6	NH_4^+ [µg/m³]	1.0	1.7
OC [ng/m³]	0.5	0.7	Mg^{2+} [µg/m³]	0.2	1.6
EC [ng/m³]	0.7	0.5	Na^+ [µg/m³]	0.1	0.6
TC [ng/m³]	0.5	0.7	K^+ [µg/m³]	0.3	0.7
SO_4^{2-} [µg/m³]	0.7	1.0	Lev [ng/m³]	0.2	0.5
NO_3^- [µg/m³]	0.2	0.4			
Cl^- [µg/m³]	NA	1.1			

The contribution of PM 1 to PM 10 was calculated for summer and winter averages (see Table 19). As expected, PM 1 concentrations are generally lower than PM 10 concentrations, as PM 1 is a subset of PM 10. Interpreting this comparison, we want to highlight, that a number of samples of PM 1 are missing, compared to PM 10, and thus data sets are slightly different. The excess concentrations of Cl^- and Mg^{2+} in PM 1 in winter, point to the very low concentration range and different LODs as well as measurement uncertainties. This argument however is not applicable to NH_4^+, where concentrations are twice as much h in PM 1 compared to PM 10 during winter. As explained before (chapter 4.2.3), this is most likely due to problems of the blank values determined for PM 10. The difference of blank filters between PM 10 and PM 1 would yield in approximately 0.012 µg/m³ higher PM 10 concentrations. If this amount of blank value is added to the PM 10 values, the ratios of PM 1 to PM 10 decline to 0.9 for summer and 1.3 for winter, which seems more reasonable. Nevertheless, NH_4^+ seems to be enriched in the PM 1 fraction.

PM 10 values were compared to averages from 1991-1993 discussed by Kasper-Giebl et al (1998). The concentrations are given in Table 20. Concentrations from 2016-2018 were smaller in summer periods and for SO_4^{2-} also in winter. Only NO_3^- concentration in winter 2016-2018 is higher compared to 1991-1993. Generally, concentrations in a similar range to the 1990ies could be found.

Table 20: PM 10 SO_4^{2-} and NO_3^- concentrations from 2016-2018 compared with measurements from 1991-1993.

	Summer 2016-2018	Summer 1992-1993	Winter 2016-2018	Winter 1991-1993
SO_4^{2-} [µg/m³]	0.593	2.289	0.128	0.293
NO_3^- [µg/m³]	0.089	0.385	0.060	0.036

5. Summary and Outlook

For the measurement period 2016-2018 a very good correlation of IC and XRF measurements of Ca could be found. Regarding Mg and K the correlation was reasonably good as well, but concentrations determined with XRF were higher, indicating that not all of the compounds are soluble and measured by ion chromatography. . In addition, it could be shown, that an estimate for Fe, which is a possible marker for SDEs, can be accomplished due to acceptable correlation of IC measurements of Ca^{2+}, Mg^{2+} and K^{+} with XRF measurements of Fe. Concerning carbon measurements, a reasonable correlation of Aethalometer, Transmissometer and Sunset measurements were observed as well (regarding the correlation coefficient R), but severe concentration differences in absolute values need further investigation.

Time trends were displayed for nearly two years from June 2016 to May 2018 for all compounds. Some analytes (S, SO_4^{2-}, NO_3^{-}, NH_4^{+}, TC, BC, EBC, TSP) follow the annual trend observed at this height since the 1990ies [20], where lower concentrations of aerosols during winter compared to summer were observed at SBO. Other analytes (Levoglucosan, Fe, Ca, Mg, K, Al, P, EC) seem to follow specific events rather than annual cycles. Some of these events could be traced back to SDEs or construction work at the sampling station.

Gernerally PM 1 concentrations are below PM 10 concentration, what could be expected as PM 1 is a fraction of PM 10. Still the PM 1/PM 10 ratios are quite different for the single compounds and represent the preferred occurrence of the respective compounds in the fine or the coarse aerosol fraction. Cases when PM 1 concentrations exceed PM 10 concentrations can be traced back to rather low concentrations (NO_2^{-}, Cl^{-} and Mg^{2+}) as well as measurement and calculation uncertainties (NH_4^{+}).

PM 10 values were compared to averages from 1991-1993 discussed by Kasper-Giebl et al (1998). Concentrations of SO_4^{2-} and NO_3^{-} from 2016-2018 were smaller in summer periods and for SO_4^{2-} also in winter. Only NO_3^{-} concentration in winter 2016-2018 is higher compared to 1991-1993.

Further analyses of acquired data may allow a deeper insight in composition of SD laden air masses or estimates of source regions of SD by comparing ratios of Mg, Ca and Al [40].

List of References

[1] "Dustfall - Zamg." [Online]. Available: https://www.zamg.ac.at/cms/de/forschung/klima/klimafolgen/dustfall. [Accessed: 18-Sep-2018].

[2] "Aerosol." [Online]. Available: http://www.chemie.de/lexikon/Aerosol.html. [Accessed: 18-Sep-2018].

[3] T. C. Bond, S. J. Doherty, D. W. Fahey, P. M. Forster, T. Berntsen, B. J. DeAngelo, M. G. Flanner, S. Ghan, B. Kärcher, D. Koch, S. Kinne, Y. Kondo, P. K. Quinn, M. C. Sarofim, M. G. Schultz, M. Schulz, C. Venkataraman, H. Zhang, S. Zhang, N. Bellouin, S. K. Guttikunda, P. K. Hopke, M. Z. Jacobson, J. W. Kaiser, Z. Klimont, U. Lohmann, J. P. Schwarz, D. Shindell, T. Storelvmo, S. G. Warren, and C. S. Zender, "Bounding the role of black carbon in the climate system: A scientific assessment," *J. Geophys. Res. Atmos.*, vol. 118, no. 11, pp. 5380–5552, Jun. 2013.

[4] K. Baumann-Stanzer, M. Greilinger, A. Kasper-Giebl, C. Flandorfer, A. Hieden, C. Lotteraner, M. Ortner, J. Vergeiner, G. Schauer, and M. Piringer, "Evaluation of WRF-Chem model forecasts of a prolonged Sahara dust episode over the Eastern Alps," *inPress*, 2019.

[5] L. Smith, "Strange 'orange snow' phenomenon reported across eastern Europe," *Independent*. [Online]. Available: https://www.independent.co.uk/news/science/orange-snow-russia-romania-ukraine-weather-environment-sand-sahara-a8272961.html. [Accessed: 28-Nov-2018].

[6] M. Berger and H. F. Krug, "Aerosole," 2012. [Online]. Available: https://roempp.thieme.de/roempp4.0/do/data/RD-01-00934. [Accessed: 08-Dec-2018].

[7] O. Boucher, D. Randall, P. Artaxo, C. Bretherton, G. Feingold, P. Forster, V.-M. Kerminen, Y. Kondo, H. Liao, U. Lohmann, P. Rasch, S. K. Satheesh, S. Sherwood, B. Stevens, and X. Y. Zhang, "Clouds and Aerosols," in *Climate Change 2013: The Physical Science Basis. Contribution of Working Group I to the Fifth Assessment Report of the Intergovernmental Panel on Climate Change [Stocker, T.F., D. Qin, G.-K. Plattner, M. Tignor, S.K. Allen, J. Boschung, A. Nauels, Y. Xia,* Cambridge., Cambridge, United Kingdom and New York, NY, USA, 2013.

[8] R. SWAP, M. GARSTANG, S. GRECO, R. TALBOT, and P. KALLBERG, "Saharan dust in the Amazon Basin," *Tellus B*, vol. 44, no. 2, pp. 133–149, Apr. 1992.

[9] V. A, F. K, and V. T., "Airborne particulate matter and human health: toxicological assessment and importance of size and composition of particles for oxidative damage and carcinogenic mechanisms.," *J. Environ. Sci. Heal.*, vol. 26, no. 4, pp. 339–62, 2008.

[10] T. Eikmann, "Bloß keinen Staub aufwirbeln," in *Chemie über den Wolken*, 1st ed., Weinheim, 2011, pp. 120–123.

[11] WHO, *Air quality guidelines global update 2005 : particulate matter, ozone, nitrogen dioside and sulfur dioxide*. Copenhagen: World Health Organization. Regional Office for Europe, 2006.

[12] H. R. Anderson, R. W. Atkinson, J. L. Peacock, L. Marston, and K. Konstantinou, "meta-analysis of time-series and panel studies of Particulate Matter (PM) and Ozone (O3): report of a WHO task group," Copenhagen, 2004.

[13] J. Ayres, "COMEAP: cardiovascular disease and air pollution," 2005.

[14] C. Braun-Fahrländer, J. C. Vuille, F. H. Sennhauser, U. Neu, T. Künzle, L. Grize, M. Gassner, C. Minder, C. Schindler, H. S. Varonier, and B. Wüthrich, "Respiratory health and long-term exposure to air pollutants in Swiss schoolchildren. SCARPOL Team. Swiss Study on Childhood Allergy and Respiratory Symptoms with Respect to Air Pollution, Climate and Pollen.," *Am. J. Respir. Crit. Care Med.*, vol. 155, no. 3, 1997.

[15] S. Siddique, M. R. Ray, and T. Lahiri, “Effects of air pollution on the respiratory health of children: A study in the capital city of India,” *Air Qual. Atmos. Heal.*, vol. 4, no. 2, pp. 95–102, 2011.

[16] H. E. Wichmann, “Schützen umweltzonen unsere gesundheit oder sind sie unwirksam?,” *Umweltmedizin Forsch. und Prax.*, vol. 13, no. 1, pp. 7–10, 2008.

[17] W. Schober and H. Behrendt, “Einfluss von Umweltfaktoren auf die Allergieentstehung,” *HNO*, vol. 56, no. 8, pp. 752–758, 2008.

[18] M. R. Heal, P. Kumar, and R. M. Harrison, “Particles, air quality, policy and health,” *Chem. Soc. Rev.*, vol. 41, no. 19, pp. 6606–6630, 2012.

[19] R. R. Helmholtz, A. Schneider, S. Breitner, J. Cyrys, and A. Peters, “Health effects of particulate air pollution: A review of epidemiological evidence,” *Inhal. Toxicol.*, vol. 23, no. 10, pp. 555–592, 2011.

[20] A. Kasper-Giebl and H. Puxbaum, “Seasonal variation of SO2, HNO3, NH3 and selected aerosol components at Sonnblick (3106 m a.s.l.),” *Atmos. Environ.*, vol. 32, no. 23, pp. 3925–3939, 1998.

[21] I. Chiapello, “Origins of African dust transported over the northeastern tropical Atlantic,” *J. Geophys. Res. Atmos.*, vol. 102, no. D12, pp. 13701–13709, 1997.

[22] S. Caquineau, A. Gaudichet, L. Gomes, M. C. Magonthier, and B. Chatenet, “Saharan dust: Clay ratio as a relevant tracer to assess the origin of soil-derived aerosols,” *Geophys. Res. Lett.*, vol. 25, no. 7, pp. 983–986, 1998.

[23] I. Tegen and I. Fung, “Contribution to the atmospheric mineral aerosol load from land surface modification,” *J. Geophys. Res.*, vol. 100, pp. 18707–18726, 1995.

[24] C. R. N. Rao, L. L. Stowe, E. P. McClain, and J. Sapper, *Development and application of aerosol remote sensing with AVHRR data from the NOAA satellites*. A. Deepak, 1988.

[25] McDonald and W. F., *Atlas of climatic charts of the oceans*. Washington DC: Department of Agriculture, Weather Bureau, 1938.

[26] J. M. Prospero, R. A. Glaccum, and R. T. Nees, “Atmospheric transport of soil dust from Africa to South America,” *Nature*, vol. 289, pp. 570–572, 1981.

[27] J. M. Prospero and R. T. Nees, “Impact of the North African drought and El Niño on mineral dust in the Barbados trade winds,” *Nature*, vol. 320, pp. 735–738, 1986.

[28] C. Exner, “Erläuterungen zur Geologischen Karte der Sonnblickgruppe,” *Geol. BUNDESANSTALT , WIEN III, RASUMOFSKYGASSE 23*, 1964.

[29] B. C. Inc., “Bemis Parafilm,” 2018. [Online]. Available: http://www.bemis.com/na/products/parafilm-floratape/parafilm-lab. [Accessed: 21-Dec-2018].

[30] W. C. Hinds, *Aerosol Technology*, 2nd ed. John Wiley & Sons, 1999.

[31] R Core Team (R Foundation for Statistical Computing), “R: A Language and Environment for Statistical Computing,” 2017. [Online]. Available: https://www.r-project.org/.

[32] P. Redl, “Darstellung des kohlenstoffh ¨ altigen Aerosols und Aethalometermessungen an zwei Hintergrundmessstellen in Osterreich ausgef u,” TU Wien, 2018.

[33] “Model AE33 Aethalometer.” [Online]. Available: https://mageesci.com/our-products/ae33/. [Accessed: 07-Dec-2018].

[34] Magee Scientific, “SootScan TM Model OT21 Transmissometer,” 2015.

[35] M. Greilinger, L. Drinovec, G. Močnik, and A. Kasper-Giebl, “Evaluation of measurements of light transmission for the determination of black carbon on filters from different station types,” *Atmos. Environ.*, vol. 198, no. October 2018, pp. 1–11, 2019.

[36] E. (TU W. Neuwirth, “Optische und Element-basierte Charakterisierung von Staubproben unterschiedlicher Standorte in Österreich,” 2016.

[37] Sunset Laboratory Inc., “Sunset Laboratory Inc. Semi-Continuous OCEC Carbon Aerosol Analyzer,” Portland.

[38] F. Cavalli, M. Viana, K. E. Yttri, J. Genberg, and J. P. Putaud, “Toward a standardised thermal-optical protocol for measuring atmospheric organic and elemental carbon: The EUSAAR protocol,” *Atmos. Meas. Tech.*, 2010.

[39] C. A. Pio, M. Legrand, C. A. Alves, T. Oliveira, J. Afonso, A. Caseiro, H. Puxbaum, A. Sanchez-Ochoa, and A. Gelencsér, “Chemical composition of atmospheric aerosols during the 2003 summer intense forest fire period,” *Atmos. Environ.*, vol. 42, no. 32, pp. 7530–7543, 2008.

[40] C. Telloli, M. Chicca, S. Pepi, and C. Vaccaro, “Saharan dust particles in snow samples of Alps and Apennines during an exceptional event of transboundary air pollution,” *Environ. Monit. Assess.*, vol. 190, no. 1, p. 37, Jan. 2018.

List of figures

List of tables

Appendix

A. Correlation of PM 1 mass to TSP mass and main components of PM 10

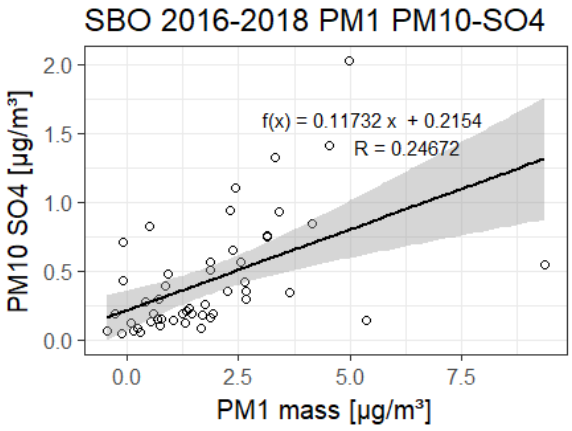

Figure 53: Correlation between mass concentrations of PM 1 [µg/m³] and SO_4^{2-} concentrations of PM 10 [µg/m³].

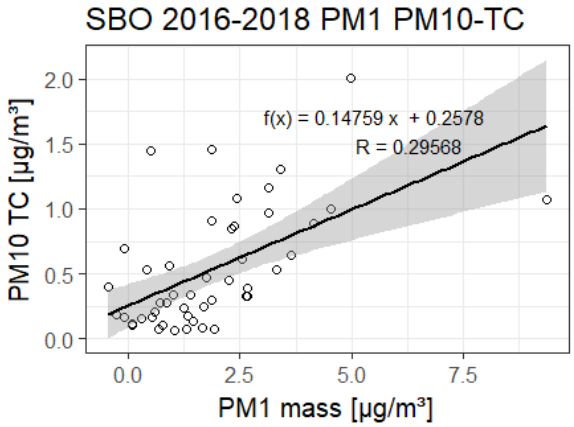

Figure 54: Correlation between mass concentrations of PM 1 [µg/m³] and TC concentrations of PM 10 [µg/m³].

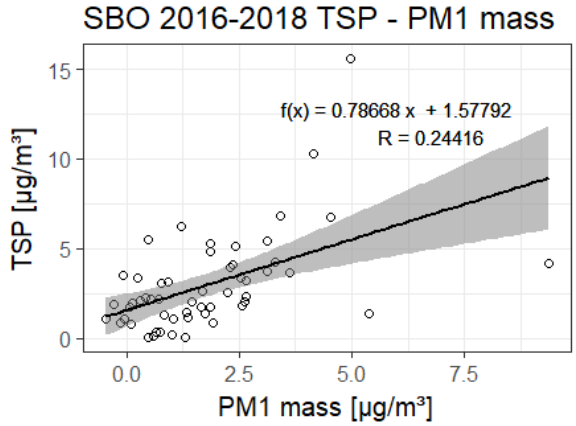

Figure 55: Correlation between mass concentrations of PM 1 [µg/m³] and TSP mass [µg/m³].

Correlation of SO_4^{2-} concentrations of PM 10 and mass concentrations of PM 1 is shown in Figure 53. Correlation of TC concentrations of PM 10 and mass concentrations of PM 1 is shown in Figure 54. Correlation of mass concentrations of TSP and PM 1 is shown in Figure 55. In all three cases a rather poor correlation could be observed.

B. Excluded values due to Digitel sampling malfunction.

One sample (week of 9.3.2017) had been excluded from calculation due to malfunction and error of the sampling system (Digitel) causing an unrealistic value (seen in Figure 57 and Figure 56).

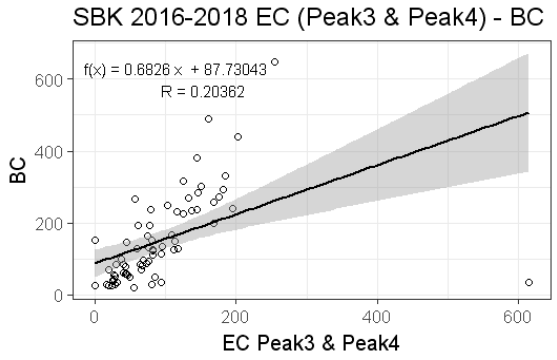

Figure 56: linear regression between EC (Sunset Laboratory) as summary of Peak 3 and Peak 4 and BC (Aethalometer).

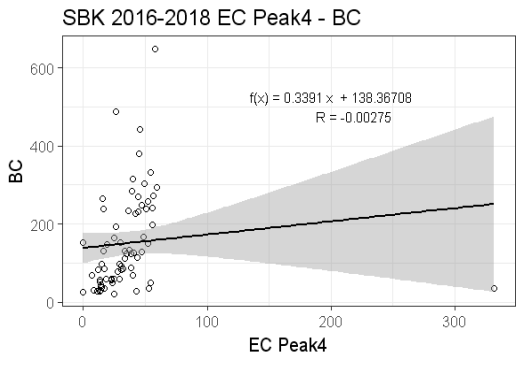

Figure 57: linear regression between EC (Sunset Laboratory) Peak 4 and BC (Aethalometer).

C. Data of PM 10 and PM 1 measurements

If no values are available, the field is filled with #NV (no value).

PM 10	XRF						
	Fe [µg/m³]	Ca [µg/m³]	Mg [µg/m³]	Al [µg/m³]	K [µg/m³]	S [µg/m³]	P [µg/m³]
02.06.2016	0.0129	0.0197	0.0099	0.0332	0.0147	0.1780	0.0046
09.06.2016	0.0073	0.0033	0.0039	0.0152	0.0095	0.0518	0.0025
16.06.2016	0.0107	0.0139	0.0085	0.0242	0.0097	0.0934	0.0036
23.06.2016	0.0723	0.1042	0.0512	0.2600	0.0719	0.3936	0.0084
30.06.2016	0.0219	0.0342	0.0167	0.0608	0.0295	0.1937	0.0064
07.07.2016	0.0329	0.0595	0.0264	0.1075	0.0272	0.2774	0.0053
14.07.2016	0.0188	0.0414	0.0123	0.0463	0.0168	0.1184	0.0031
21.07.2016	0.2341	0.2295	0.1469	0.9961	0.1938	0.3584	0.0105
28.07.2016	0.0276	0.0377	0.0187	0.0833	0.0436	0.1982	0.0060
05.08.2016	0.0112	0.0140	0.0080	0.0318	0.0066	0.0746	0.0018
11.08.2016	0.0739	0.0750	0.0450	0.3032	0.0614	0.1944	0.0064
18.08.2016	0.0117	0.0190	0.0075	0.0291	0.0174	0.0947	0.0023
25.08.2016	0.0515	0.0707	0.0350	0.1440	0.0491	0.2301	0.0069
01.09.2016	0.0354	0.0561	0.0190	0.0784	0.0403	0.3586	0.0051
08.09.2016	0.2659	0.8828	0.2241	0.9382	0.3187	0.7254	0.0155
15.09.2016	0.0101	0.0132	0.0080	0.0298	0.0148	0.1038	0.0009
22.09.2016	0.0208	0.0285	0.0116	0.0349	0.0239	0.2446	0.0033
29.09.2016	0.0125	0.0206	0.0094	0.0274	0.0179	0.1147	0.0016
06.10.2016	#NV	0.0042	0.0020	0.0147	#NV	0.0694	#NV
13.10.2016	#NV	#NV	#NV	#NV	#NV	#NV	#NV
20.10.2016	0.0806	0.1749	0.0687	0.3474	0.0836	0.0727	0.0036
27.10.2016	0.0128	0.0157	0.0088	0.0437	0.0135	0.0630	0.0008
03.11.2016	0.0082	0.0127	0.0075	0.0289	0.0092	0.0442	0.0006
10.11.2016	#NV	#NV	#NV	#NV	#NV	#NV	#NV
17.11.2016	#NV	#NV	#NV	#NV	#NV	#NV	#NV
24.12.2016	#NV	#NV	#NV	#NV	#NV	#NV	#NV
01.12.2016	0.0098	0.0133	0.0059	0.0219	0.0081	0.0445	#NV
08.12.2016	0.0228	0.0458	0.0209	0.0837	0.0131	0.0730	0.0013
15.12.2016	#NV	0.0050	0.0030	0.0152	0.0105	0.0371	#NV
23.12.2016	0.0110	0.0190	0.0118	0.0403	0.0106	0.0550	0.0006
29.12.2016	#NV	#NV	#NV	#NV	#NV	#NV	#NV
05.01.2017	#NV	#NV	#NV	#NV	#NV	#NV	#NV
12.01.2017	#NV	0.0038	0.0042	0.0080	0.0073	0.0737	#NV
19.01.2017	0.0202	0.0184	0.0112	0.0826	0.0162	0.0497	0.0006
26.01.2017	0.0070	0.0071	0.0044	0.0237	0.0074	0.0451	#NV
02.02.2017	0.0415	0.0987	0.0392	0.1771	0.0418	0.0543	0.0019
16.02.2017	0.0182	0.0281	0.0100	0.0580	0.0109	0.0365	0.0005
23.02.2017	0.0099	0.0114	0.0039	0.0221	0.0100	0.0124	#NV
02.03.2017	#NV	0.0044	0.0020	0.0119	0.0049	0.0057	#NV
09.03.2017	#NV	#NV	#NV	#NV	#NV	#NV	#NV
10.03.2017	0.0252	0.0134	0.0085	0.0668	0.0151	0.0158	0.0008
16.03.2017	0.0281	0.0116	0.0128	0.0889	0.0187	0.0212	0.0010
23.03.2017	0.0762	0.0350	0.0476	0.2647	0.0555	0.0380	0.0037
30.03.2017	0.0533	0.0381	0.0257	0.1448	0.0347	0.0594	0.0021
06.04.2017	0.0293	0.0273	0.0142	0.0897	0.0282	0.0332	0.0020
13.04.2017	#NV	#NV	#NV	#NV	#NV	#NV	#NV
20.04.2017	0.0189	0.0265	0.0119	0.0619	0.0194	0.0268	0.0008

PM 10	XRF						
	Fe [µg/m³]	Ca [µg/m³]	Mg [µg/m³]	Al [µg/m³]	K [µg/m³]	S [µg/m³]	P [µg/m³]
27.04.2017	0.0110	0.0060	0.0049	0.0262	0.0129	0.0181	0.0005
04.05.2017	0.0118	0.0178	0.0095	0.0269	0.0145	0.0604	0.0013
12.05.2017	0.0200	0.0438	0.0217	0.0624	0.0300	0.0718	0.0032
18.05.2017	0.0306	0.0501	0.0185	0.0655	0.0346	0.2080	0.0040
25.05.2017	0.0793	0.1398	0.0594	0.2043	0.0716	0.2644	0.0064
01.06.2017	0.0117	0.0199	0.0096	0.0391	0.0133	0.0881	0.0013
08.06.2017	0.0549	0.1213	0.0591	0.1768	0.0687	0.2735	0.0090
15.06.2017	0.0675	0.1989	0.0751	0.2082	0.0692	0.3216	0.0078
22.06.2017	0.1266	0.2050	0.0846	0.4806	0.1311	0.4227	0.0097
29.06.2017	0.0325	0.0345	0.0195	0.1107	0.0269	0.0732	0.0051
06.07.2017	0.1437	0.2598	0.1034	0.5508	0.1205	0.2870	0.0107
14.07.2017	0.3892	0.6158	0.1303	2.2655	0.8403	0.1338	0.0327
27.07.2017	#NV	#NV	#NV	#NV	#NV	#NV	#NV
21.09.2017	0.0211	0.0195	0.0068	0.0628	0.0287	0.0817	0.0012
28.09.2017	0.0557	0.0518	0.0358	0.2197	0.0479	0.1210	0.0026
05.10.2017	0.0164	0.0273	0.0112	0.0683	0.0108	0.0434	0.0013
12.10.2017	0.0193	0.0320	0.0083	0.0519	0.0140	0.0312	0.0018
19.10.2017	0.0450	0.0754	0.0290	0.1639	0.0384	0.0861	0.0021
26.10.2017	0.0139	0.0262	0.0078	0.0428	#NV	0.0354	0.0011
02.11.2017	0.0145	0.0134	0.0060	0.0489	0.0149	0.0203	0.0005
11.11.2017	#NV	0.0047	#NV	0.0111	#NV	0.0073	#NV
16.11.2017	#NV	#NV	#NV	#NV	#NV	#NV	#NV
23.11.2017	0.0286	0.0362	0.0186	0.1184	0.0215	0.0410	0.0013
30.11.2017	0.0079	0.0102	0.0032	0.0243	0.0085	0.0123	#NV
07.12.2017	0.0081	0.0130	0.0042	0.0166	0.0080	0.0158	0.0007
14.12.2017	#NV	#NV	#NV	#NV	#NV	0.0038	#NV
21.12.2017	#NV	0.0037	#NV	0.0100	0.0046	0.0045	#NV
28.12.2017	0.0180	0.0098	0.0045	0.0305	0.0120	0.0060	0.0007
04.01.2018	0.0188	0.0222	0.0141	0.0818	0.0149	0.0165	0.0005
11.01.2018	0.0196	0.0027	0.0069	0.0450	0.0093	0.0022	#NV
18.01.2018	#NV	0.0050	0.0021	0.0135	#NV	0.0062	#NV
25.01.2018	0.0114	0.0278	0.0095	0.0429	0.0219	0.0441	0.0007
01.02.2018	0.0101	0.0113	0.0064	0.0366	0.0102	0.0324	0.0006
08.02.2018	0.0100	0.0139	0.0066	0.0376	0.0121	0.0426	0.0005
15.02.2018	0.0066	0.0088	0.0035	0.0124	0.0161	0.0518	#NV
22.02.2018	0.0142	0.0156	0.0080	0.0297	0.0368	0.3384	0.0006
01.03.2018	0.0079	0.0085	0.0054	0.0176	0.0160	0.0351	#NV
08.03.2018	0.0087	0.0115	0.0071	0.0120	0.0141	0.0366	0.0006
15.03.2018	#NV	0.0065	0.0033	0.0079	0.0174	0.1278	0.0005
22.03.2018	0.0217	0.0398	0.0181	0.0527	0.0313	0.1342	0.0006
29.03.2018	#NV	#NV	#NV	#NV	#NV	#NV	#NV
06.04.2018	0.0674	0.1178	0.0609	0.2952	0.0687	0.1637	0.0035
12.04.2018	0.0993	0.1897	0.0892	0.3974	0.0765	0.1683	0.0042
19.04.2018	0.5876	1.0236	0.1599	2.7405	1.4330	0.3196	0.0390
26.04.2018	0.1881	0.3643	0.1597	0.7046	0.1883	0.4023	0.0094
03.05.2018	0.2968	0.9232	0.2482	1.0801	0.2951	0.4004	0.0155
10.05.2018	0.0556	0.1957	0.0369	0.4958	0.1557	0.1242	0.0071
17.05.2018	0.0292	0.0483	0.0278	0.1088	0.0356	0.1857	0.0034
24.05.2018	0.1612	0.3051	0.1307	0.6350	0.1377	0.3423	0.0103

PM 10	online		OT21	Sunset			chromatography
	SHARP	AE33					
	TSP [µg/m³]	EBC [µg/m³]	BC [µg/m³]	OC [ng/m³]	EC [ng/m³]	TC [ng/m³]	Levoglucosan [ng/m³]
02.06.2016	3.3963	126.2	0.0393	509.6	99.4	609.0	0.950
09.06.2016	1.7761	74.7	0.0156	251.2	49.7	300.9	0.679
16.06.2016	2.7661	#NV	0.0352	448.4	77.4	525.9	1.793
23.06.2016	6.8048	293.5	0.0779	1141.6	164.2	1305.8	1.462
30.06.2016	4.0751	213.6	0.0587	765.2	106.4	871.5	1.523
07.07.2016	5.4086	287.0	0.0752	1030.0	132.8	1162.8	1.624
14.07.2016	3.6515	166.8	0.0451	551.8	91.2	643.0	0.891
21.07.2016	10.3103	380.2	0.0794	766.8	126.1	892.9	0.809
28.07.2016	4.2004	#NV	0.0537	972.1	96.1	1068.2	2.160
05.08.2016	2.5908	81.7	#NV	300.5	#NV	353.3	0.618
11.08.2016	4.8209	257.6	0.0687	796.6	114.3	910.9	2.477
18.08.2016	2.2426	111.1	0.0260	465.9	63.7	529.5	1.667
25.08.2016	5.2877	266.4	0.0715	1297.5	157.2	1454.7	1.517
01.09.2016	5.1331	303.5	0.0810	971.0	107.7	1078.7	2.420
08.09.2016	15.5913	649.2	0.1849	1765.1	237.5	2002.6	11.428
15.09.2016	2.2122	95.3	0.0372	226.5	51.2	277.8	2.391
22.09.2016	3.4942	226.2	0.0727	601.3	98.3	699.6	3.390
29.09.2016	3.1288	235.5	0.0675	476.8	85.8	562.7	3.445
06.10.2016	1.8929	84.8	0.0297	137.2	#NV	182.8	2.221
13.10.2016	#NV	#NV	#NV	#NV	#NV	#NV	#NV
20.10.2016	6.2581	145.5	0.0343	209.0	#NV	236.3	3.139
27.10.2016	1.9050	49.9	0.0197	101.9	#NV	132.9	1.729
03.11.2016	1.7409	57.8	0.0183	88.3	#NV	110.6	2.962
10.11.2016	0.0732	57.1	#NV	#NV	#NV	#NV	#NV
17.11.2016	#NV	#NV	#NV	#NV	#NV	#NV	#NV
24.12.2016	#NV	#NV	#NV	#NV	#NV	#NV	#NV
01.12.2016	0.0553	26.5	0.0173	67.4	#NV	78.4	0.821
08.12.2016	0.1496	17.9	0.0160	164.0	#NV	202.5	2.210
15.12.2016	0.3712	23.6	#NV	#NV	#NV	#NV	2.298
23.12.2016	1.1230	29.4	0.0225	55.2	#NV	68.7	1.492
29.12.2016	0.8173	53.5	#NV	74.5	#NV	102.6	2.446
05.01.2017	0.2358	47.6	#NV	269.1	67.5	336.6	2.249
12.01.2017	0.8670	94.9	0.0245	58.8	#NV	79.5	4.859
19.01.2017	0.7825	33.8	#NV	#NV	#NV	#NV	0.209
26.01.2017	1.3494	43.3	#NV	#NV	#NV	#NV	0.740
02.02.2017	3.0881	51.4	0.0174	85.4	#NV	104.7	1.019
16.02.2017	2.0470	54.6	0.0182	114.0	#NV	140.0	#NV
23.02.2017	2.6312	165.4	0.0337	200.4	#NV	243.5	#NV
02.03.2017	1.7306	70.6	#NV	54.4	#NV	80.9	#NV
09.03.2017	1.4975	27.3	#NV	#NV	#NV	#NV	#NV
10.03.2017	2.2389	127.0	0.0490	357.0	#NV	396.7	#NV
16.03.2017	3.2370	248.3	0.0439	290.1	#NV	329.7	#NV
23.03.2017	4.2377	234.4	0.0856	467.8	60.9	528.7	#NV
30.03.2017	6.7895	483.7	0.1294	860.8	143.5	1004.3	#NV
06.04.2017	2.3257	163.6	0.0512	331.3	57.0	388.4	#NV

PM 10	online		OT21	Sunset			chromatography
	SHARP	AE33					
	TSP [µg/m³]	EBC [µg/m³]	BC [µg/m³]	OC [ng/m³]	EC [ng/m³]	TC [ng/m³]	Levoglucosan [ng/m³]
13.04.2017	1.8277	141.6	#NV	#NV	#NV	#NV	#NV
20.04.2017	2.0785	150.0	0.0461	262.8	63.5	326.2	#NV
27.04.2017	1.2985	107.3	0.0306	217.0	64.5	281.5	#NV
04.05.2017	1.1303	120.2	0.0367	278.0	64.0	341.9	2.044
12.05.2017	1.3544	112.4	0.0298	398.1	73.8	471.9	1.287
18.05.2017	3.9728	235.3	0.0556	720.6	126.8	847.5	1.825
25.05.2017	5.5307	240.3	0.1034	1269.6	176.5	1446.2	1.725
01.06.2017	2.6191	141.6	0.0425	360.1	95.6	455.7	0.530
08.06.2017	5.0522	257.3	0.0789	1497.8	150.0	1647.8	2.562
15.06.2017	7.0254	323.4	0.0891	1793.6	167.3	1960.9	3.178
22.06.2017	8.5986	426.9	0.1013	1472.0	185.5	1657.6	2.705
29.06.2017	2.0264	122.3	0.0258	546.0	94.6	640.6	1.325
06.07.2017	7.4005	224.4	0.0672	1075.4	118.7	1194.1	0.133
14.07.2017	3.3860	195.3	0.1536	1210.0	147.3	1357.3	1.799
27.07.2017	#NV	#NV	#NV	#NV	#NV	#NV	#NV
21.09.2017	3.7464	284.5	0.0512	844.8	128.6	973.4	0.712
28.09.2017	2.5689	128.7	0.0295	390.9	57.1	448.0	0.330
05.10.2017	0.3885	53.4	#NV	173.7	#NV	202.4	1.209
12.10.2017	0.5927	88.7	0.0221	452.0	58.0	510.0	0.195
19.10.2017	2.6642	179.6	0.0369	443.6	60.2	503.8	#NV
26.10.2017	0.3432	38.2	#NV	70.2	#NV	78.6	0.348
02.11.2017	1.4679	82.4	#NV	151.6	#NV	174.4	#NV
11.11.2017	0.8488	23.3	#NV	#NV	#NV	#NV	#NV
16.11.2017	1.1159	22.5	#NV	#NV	#NV	#NV	0.518
23.11.2017	2.1761	77.3	0.0158	148.8	#NV	161.6	0.565
30.11.2017	1.0652	30.9	#NV	327.4	76.9	404.3	0.860
07.12.2017	2.1340	63.1	#NV	103.2	48.4	151.6	1.380
14.12.2017	1.9880	51.7	#NV	#NV	#NV	#NV	1.077
21.12.2017	1.3033	25.9	#NV	#NV	#NV	#NV	#NV
28.12.2017	2.1005	22.2	#NV	227.8	60.6	288.4	#NV
04.01.2018	3.3661	65.0	#NV	#NV	#NV	#NV	0.229
11.01.2018	#NV	#NV	#NV	111.1	54.6	165.7	1.387
18.01.2018	#NV	#NV	#NV	80.2	#NV	102.7	1.849
25.01.2018	#NV	#NV	0.0296	131.9	#NV	171.0	2.184
01.02.2018	#NV	#NV	0.0178	689.7	163.4	853.1	0.975
08.02.2018	#NV	#NV	0.0298	#NV	#NV	#NV	5.297
15.02.2018	#NV	#NV	0.0339	195.3	59.9	255.2	7.193
22.02.2018	#NV	#NV	0.0845	692.9	95.9	788.9	15.536
01.03.2018	#NV	#NV	0.0142	84.7	112.4	197.1	5.118
08.03.2018	#NV	#NV	0.0185	74.5	92.5	167.0	4.562
15.03.2018	#NV	#NV	0.0428	157.7	148.4	306.1	10.234
22.03.2018	#NV	#NV	0.0287	231.3	216.0	447.2	8.866
29.03.2018	#NV	#NV	#NV	NA	NA	NA	2.450
06.04.2018	#NV	#NV	0.3553	1044.0	174.1	1218.1	2.857
12.04.2018	#NV	#NV	0.0393	135.7	176.9	312.6	2.515
19.04.2018	NA	NA	#NV	966.7	1149.6	2116.4	5.677
26.04.2018	NA	NA	0.1046	337.5	413.1	750.6	2.858
03.05.2018	NA	NA	0.1857	576.8	655.7	1232.5	1.872
10.05.2018	NA	NA	0.0415	155.3	219.9	375.2	2.176
17.05.2018	NA	NA	0.0407	346.4	313.4	659.8	2.341
24.05.2018	NA	NA	0.1749	572.8	472.9	1045.8	2.842

PM 10	Cation chromatography					Anion chromatography			
	Ca [µg/m³]	NH_4^+ [µg/m³]	Mg^{2+} [µg/m³]	Na^+ [µg/m³]	K^+ [µg/m³]	SO_4^{2-} [µg/m³]	NO_3^- [µg/m³]	NO_2^- [µg/m³]	Cl^- [µg/m³]
02.06.2016	0.0150	0.1826	0.0060	0.0008	0.0103	0.5616	#NV	0.0070	#NV
09.06.2016	#NV	0.0448	0.0021	#NV	#NV	0.1648	#NV	0.0005	#NV
16.06.2016	0.0083	0.1200	0.0040	#NV	0.0103	0.2920	#NV	0.0068	#NV
23.06.2016	0.0853	0.3195	0.0157	0.0114	0.0219	0.9284	#NV	0.0091	#NV
30.06.2016	0.0281	0.2197	0.0071	0.0119	0.0159	0.6538	#NV	0.0010	#NV
07.07.2016	0.0504	0.2643	0.0100	0.0133	0.0172	0.7494	#NV	0.0007	#NV
14.07.2016	0.0292	0.1375	0.0049	0.0042	0.0084	0.3417	#NV	#NV	#NV
21.07.2016	0.2263	0.1597	0.0300	0.0329	0.0363	0.8469	0.0641	#NV	#NV
28.07.2016	0.0364	0.1789	0.0073	0.0109	0.0226	0.5409	#NV	#NV	#NV
05.08.2016	0.0055	0.0596	0.0027	0.0028	0.0037	0.2069	#NV	#NV	#NV
11.08.2016	0.0577	0.1795	0.0107	0.0192	0.0276	0.5029	#NV	0.0003	#NV
18.08.2016	0.0109	0.0844	0.0033	0.0064	0.0093	0.2758	#NV	#NV	#NV
25.08.2016	0.0583	0.1910	0.0112	0.0105	0.0174	0.5619	#NV	0.0018	#NV
01.09.2016	0.0418	0.3778	0.0076	0.0160	0.0325	1.1044	#NV	0.0012	#NV
08.09.2016	0.8673	0.3700	0.0552	0.0423	0.0984	2.0245	0.4291	0.0009	#NV
15.09.2016	0.0112	0.1068	0.0029	0.0069	0.0080	0.2988	#NV	0.0046	#NV
22.09.2016	0.0196	0.2457	0.0042	0.0016	0.0147	0.7054	0.0555	0.0008	#NV
29.09.2016	0.0126	0.2032	0.0040	0.0019	0.0107	0.4756	0.1734	0.0006	#NV
06.10.2016	#NV	0.0687	0.0008	#NV	0.0057	0.1883	#NV	0.0022	#NV
13.10.2016	#NV	#NV	#NV	#NV	#NV	#NV	#NV	#NV	#NV
20.10.2016	0.1522	0.0245	0.0088	0.0029	0.0081	0.1934	0.1246	0.0049	#NV
27.10.2016	0.0097	0.0480	0.0018	0.0007	#NV	0.1776	#NV	0.0023	#NV
03.11.2016	0.0076	0.0251	0.0019	0.0022	#NV	0.1276	#NV	0.0042	#NV
10.11.2016	#NV	#NV	#NV	#NV	#NV	#NV	#NV	#NV	#NV
17.11.2016	#NV	#NV	#NV	#NV	#NV	#NV	#NV	#NV	#NV
24.12.2016	#NV	#NV	#NV	#NV	#NV	#NV	#NV	#NV	#NV
01.12.2016	0.0058	0.0310	0.0017	#NV	0.0020	0.1223	#NV	#NV	#NV
08.12.2016	0.0329	0.0398	0.0042	0.0015	0.0050	0.1888	#NV	#NV	#NV
15.12.2016	#NV	0.0242	0.0010	#NV	0.0029	0.0992	#NV	#NV	#NV
23.12.2016	0.0143	0.0333	0.0030	0.0066	0.0027	0.1452	#NV	0.0004	#NV
29.12.2016	#NV	#NV	#NV	#NV	#NV	#NV	#NV	#NV	#NV
05.01.2017	#NV	#NV	#NV	#NV	#NV	#NV	#NV	#NV	#NV
12.01.2017	#NV	0.0464	0.0016	0.0061	0.0052	0.1947	#NV	0.0018	#NV
19.01.2017	0.0115	0.0339	0.0020	0.0014	0.0030	0.1422	#NV	0.0012	#NV
26.01.2017	0.0028	0.0259	0.0011	0.0009	0.0027	0.1379	#NV	#NV	#NV
02.02.2017	0.0891	0.0514	0.0067	0.0050	0.0062	0.1514	0.0641	0.0059	#NV
16.02.2017	0.0271	0.0314	0.0047	0.0047	0.0073	0.1931	#NV	#NV	#NV
23.02.2017	0.0142	0.1412	0.0050	0.0054	0.0134	0.1830	0.2872	#NV	#NV
02.03.2017	0.0054	0.0151	0.0024	0.0048	0.0038	0.0827	#NV	0.0014	#NV
09.03.2017	#NV	#NV	#NV	#NV	#NV	#NV	#NV	#NV	#NV
10.03.2017	0.0301	0.1729	0.0082	0.0134	0.0159	0.1727	0.1784	#NV	#NV
16.03.2017	0.0235	0.2027	0.0103	0.0215	0.0231	0.3525	0.3489	0.0008	0.0146
23.03.2017	0.1108	0.2429	0.0246	0.0379	0.0339	1.3217	0.5035	#NV	0.0094
30.03.2017	0.0990	#NV	0.0197	0.0222	0.0586	1.4056	1.8794	0.0005	0.0053
06.04.2017	0.0679	0.2419	0.0128	0.0265	0.0221	0.2932	0.2896	0.0288	0.0224
13.04.2017	#NV	#NV	#NV	#NV	#NV	#NV	#NV	#NV	#NV
20.04.2017	0.0371	0.2733	0.0096	0.0140	0.0293	0.4176	0.2869	#NV	0.0061
27.04.2017	0.0152	0.2201	0.0039	0.0058	0.0108	0.3937	0.3049	#NV	#NV
04.05.2017	0.0133	0.1020	0.0046	#NV	0.0056	0.2259	#NV	#NV	#NV
12.05.2017	0.0312	0.0939	0.0064	0.0031	0.0082	0.2532	0.0537	#NV	#NV
18.05.2017	0.0364	0.3308	0.0070	0.0064	0.0158	0.9421	0.0968	#NV	#NV
25.05.2017	0.1097	0.2795	0.0184	0.0185	0.0221	0.8255	0.0832	0.0020	#NV
01.06.2017	0.0118	0.1808	0.0032	0.0034	0.0064	0.4667	#NV	0.0026	#NV
08.06.2017	0.1165	0.2655	0.0220	0.0564	0.0252	0.8335	#NV	#NV	#NV
15.06.2017	0.1938	0.3237	0.0344	0.0548	0.0280	0.8426	0.1198	0.0011	#NV
22.06.2017	0.1828	0.2948	0.0291	0.0421	0.0464	1.0452	0.0879	0.0042	#NV
29.06.2017	0.0271	0.1057	0.0056	0.0043	0.0103	1.2867	0.1005	0.0048	#NV

PM 10	Cation chromatography					Anion chromatography			
	Ca [µg/m³]	NH_4^+ [µg/m³]	Mg^{2+} [µg/m³]	Na^+ [µg/m³]	K^+ [µg/m³]	SO_4^{2-} [µg/m³]	NO_3^- [µg/m³]	NO_2^- [µg/m³]	Cl^- [µg/m³]
06.07.2017	0.2459	0.1366	0.0302	0.0526	0.0313	0.2653	#NV	0.0036	#NV
14.07.2017	0.5326	0.1606	0.0419	0.0272	0.1103	0.4941	0.0716	0.0004	#NV
27.07.2017	#NV	#NV	#NV	#NV	#NV	#NV	#NV	#NV	#NV
21.09.2017	0.0245	0.3357	0.0030	0.0075	0.0234	0.7598	#NV	#NV	#NV
28.09.2017	#NV	0.1276	0.0074	0.0111	0.0133	0.3489	#NV	#NV	#NV
05.10.2017	0.0220	0.0433	0.0030	0.0055	0.0036	0.1684	#NV	#NV	#NV
12.10.2017	0.0325	0.0591	0.0049	0.0041	0.0070	0.1823	#NV	#NV	#NV
19.10.2017	0.0769	0.0663	0.0098	0.0141	0.0213	0.3220	#NV	#NV	#NV
26.10.2017	0.0269	0.0173	0.0050	0.0215	0.0117	0.1537	#NV	#NV	#NV
02.11.2017	0.0164	0.0518	0.0024	0.0137	0.0130	0.2053	#NV	#NV	#NV
11.11.2017	#NV	#NV	0.0004	#NV	#NV	0.0466	#NV	#NV	#NV
16.11.2017	#NV	#NV	#NV	#NV	#NV	#NV	#NV	#NV	#NV
23.11.2017	0.0399	0.0199	0.0038	0.0160	0.0089	0.1353	0.0820	0.0006	#NV
30.11.2017	#NV	0.0196	0.0026	0.0123	0.0110	0.0690	#NV	0.0004	#NV
07.12.2017	0.0067	#NV	0.0017	0.0099	0.0030	0.0512	#NV	#NV	#NV
14.12.2017	#NV	0.0163	0.0004	0.0040	0.0028	0.0651	#NV	0.0009	#NV
21.12.2017	0.0039	#NV	0.0006	0.0033	0.0052	0.0421	#NV	#NV	#NV
28.12.2017	0.0169	#NV	0.0021	0.0130	0.0082	0.0446	#NV	0.0028	0.0144
04.01.2018	0.0375	#NV	0.0039	0.0161	0.0038	0.0828	0.0516	0.0011	0.0053
11.01.2018	0.0052	#NV	0.0012	0.0059	0.0048	0.4262	#NV	#NV	#NV
18.01.2018	0.0144	#NV	0.0018	0.0115	0.0056	0.0726	#NV	#NV	#NV
25.01.2018	0.0247	0.0438	0.0024	0.0085	0.0063	0.1665	0.0473	0.0005	#NV
01.02.2018	0.0090	#NV	0.0012	0.0026	0.0010	0.0400	0.0564	0.0007	#NV
08.02.2018	0.0126	0.1054	0.0022	0.0121	0.0099	0.2074	0.1098	#NV	#NV
15.02.2018	0.0072	0.1278	0.0011	0.0053	0.0130	0.3150	#NV	#NV	#NV
22.02.2018	0.0117	0.3661	0.0020	0.0150	0.0343	1.2025	#NV	0.0009	#NV
01.03.2018	0.0062	0.0465	0.0011	0.0063	0.0103	0.1112	#NV	0.0005	#NV
08.03.2018	0.0103	0.1148	0.0021	0.0086	0.0069	0.1222	0.1926	#NV	#NV
15.03.2018	0.0042	0.2973	0.0011	0.0093	0.0118	0.4821	0.4048	#NV	#NV
22.03.2018	0.0259	0.4972	0.0032	0.0056	0.0150	0.4447	1.3558	#NV	#NV
29.03.2018	#NV	#NV	#NV	#NV	#NV	#NV	#NV	#NV	#NV
06.04.2018	0.1161	0.0919	0.0104	0.0131	0.0111	0.3750	0.1340	0.0018	#NV
12.04.2018	0.1819	0.1916	0.0159	0.0203	0.0146	0.6086	0.2443	#NV	#NV
19.04.2018	0.9380	0.4026	0.0739	0.0811	0.1355	1.5298	1.1844	0.0009	0.0075
26.04.2018	0.3722	0.3967	0.0381	0.0890	0.0389	1.6821	0.4981	#NV	0.0049
03.05.2018	0.9713	0.3756	0.0652	0.0539	0.0441	1.6481	0.6171	0.0004	0.0130
10.05.2018	0.1636	0.1338	0.0162	0.0137	0.0226	0.4600	0.0864	#NV	#NV
17.05.2018	0.0387	0.2434	0.0071	0.0210	0.0113	0.6843	#NV	0.0004	#NV
24.05.2018	0.3248	0.2655	0.0273	0.0274	0.0266	1.2624	0.1331	0.0007	#NV

PM 1	OT21	Sunset			chromatography				
	BC [µg/m³]	OC [ng/m³]	EC [ng/m³]	TC [ng/m³]	Inositol [ng/m³]	Levoglucosan [ng/m³]	Arabitol [ng/m³]	Glucose [ng/m³]	Sucrose [ng/m³]
02.06.2016	0.0269	280.2	65.1	345.3	#NV	#NV	0.14	#NV	#NV
09.06.2016	0.0175	139.2	46.4	185.7	#NV	#NV	#NV	#NV	#NV
16.06.2016	0.0202	215.1	52.7	267.9	#NV	#NV	0.08	#NV	0.66
23.06.2016	0.0525	552.0	129.6	681.7	#NV	#NV	0.24	0.70	#NV
30.06.2016	0.0385	371.9	88.3	460.2	#NV	#NV	0.16	#NV	0.79
07.07.2016	0.0554	578.5	119.8	698.3	#NV	#NV	0.33	#NV	1.01
14.07.2016	0.0361	370.7	89.8	460.4	#NV	#NV	0.15	#NV	#NV
21.07.2016	0.0552	426.5	120.0	546.4	#NV	#NV	0.36	0.63	1.99
28.07.2016	0.0549	609.3	95.5	704.8	#NV	0.19	0.16	#NV	#NV
05.08.2016	0.0220	158.9	66.8	225.7	#NV	#NV	0.15	#NV	#NV
11.08.2016	0.0451	480.1	76.0	556.2	#NV	0.35	0.31	#NV	#NV
18.08.2016	0.0242	210.3	50.8	261.1	#NV	#NV	0.11	#NV	#NV
25.08.2016	0.0553	686.2	105.2	791.4	#NV	#NV	0.31	#NV	#NV
01.09.2016	0.0598	458.0	75.9	533.9	#NV	0.23	0.19	#NV	#NV
08.09.2016	0.1106	989.8	145.0	1134.8	#NV	2.01	0.55	#NV	#NV
15.09.2016	0.0219	136.0	40.3	176.4	#NV	#NV	0.04	#NV	#NV
22.09.2016	0.0433	311.7	69.8	381.5	#NV	0.74	0.28	#NV	#NV
29.09.2016	0.0486	272.9	67.0	339.9	#NV	0.31	0.16	#NV	#NV
06.10.2016	0.0180	85.8	44.6	130.4	#NV	0.88	0.06	#NV	#NV
13.10.2016	0.0128	82.0	37.6	119.5	#NV	0.48	#NV	#NV	#NV
20.10.2016	0.0213	130.9	42.8	173.7	#NV	1.48	0.14	#NV	#NV
27.10.2016	0.0083	60.8	22.1	83.0	#NV	0.33	#NV	#NV	#NV
03.11.2016	0.0083	72.5	28.5	100.9	#NV	0.85	#NV	#NV	#NV
10.11.2016	0.0150	132.9	70.0	202.9	#NV	#NV	#NV	#NV	#NV
17.11.2016	0.0127	65.7	32.1	97.8	#NV	1.02	0.06	#NV	#NV
24.12.2016	0.0097	52.8	22.7	75.4	#NV	0.17	#NV	#NV	#NV
01.12.2016	0.0066	71.8	19.3	91.1	#NV	#NV	0.03	#NV	#NV
08.12.2016	0.0044	43.4	15.2	58.6	#NV	#NV	0.03	#NV	#NV
15.12.2016	0.0037	57.5	15.1	72.6	#NV	0.83	#NV	#NV	#NV
23.12.2016	0.0027	34.7	14.8	49.5	#NV	#NV	#NV	2.03	#NV
29.12.2016	0.0104	62.8	23.2	85.9	#NV	1.03	0.47	#NV	#NV
05.01.2017	0.0090	72.3	23.4	95.7	#NV	0.59	0.09	#NV	#NV
12.01.2017	0.0176	105.0	23.0	128.0	#NV	1.16	0.06	#NV	#NV
19.01.2017	-0.0033	#NV	#NV	#NV	#NV	#NV	0.13	#NV	#NV
26.01.2017	0.0157	86.4	30.7	117.2	#NV	#NV	#NV	#NV	#NV
02.02.2017	0.0103	51.9	18.8	70.8	#NV	0.12	#NV	#NV	#NV
16.02.2017	0.0086	87.1	25.8	112.8	#NV	0.28	#NV	#NV	#NV
23.02.2017	0.0252	188.4	25.3	213.8	#NV	0.75	0.05	#NV	#NV
02.03.2017	0.0121	90.8	23.5	114.3	#NV	0.53	#NV	#NV	#NV
09.03.2017	#NV	#NV	#NV	#NV	#NV	0.29	#NV	#NV	#NV
10.03.2017	#NV	#NV	#NV	#NV	#NV	#NV	#NV	#NV	#NV
16.03.2017	0.0288	223.2	59.4	282.6	#NV	1.02	0.10	#NV	#NV
23.03.2017	0.0367	219.9	85.8	305.8	#NV	0.16	#NV	#NV	#NV
30.03.2017	0.0562	565.5	112.1	677.7	#NV	2.54	0.17	#NV	#NV
06.04.2017	0.0238	202.8	77.7	280.5	#NV	#NV	#NV	#NV	#NV
13.04.2017	0.0179	165.5	70.7	236.2	#NV	0.81	0.09	#NV	#NV
20.04.2017	0.0263	151.1	72.3	223.4	#NV	0.32	0.07	#NV	#NV
27.04.2017	0.0196	173.8	43.7	217.5	#NV	2.15	0.39	#NV	#NV

PM 1	OT21	Sunset			chromatography				
	BC [µg/m³]	OC [ng/m³]	EC [ng/m³]	TC [ng/m³]	Inositol [ng/m³]	Levoglucosan [ng/m³]	Arabitol [ng/m³]	Glucose [ng/m³]	Sucrose [ng/m³]
04.05.2017	0.0182	154.6	49.9	204.4	#NV	0.36	0.18	#NV	#NV
12.05.2017	0.0278	307.7	48.2	355.9	#NV	0.22	0.04	#NV	#NV
18.05.2017	0.0445	441.0	64.5	505.5	#NV	0.27	0.17	#NV	#NV
25.05.2017	0.0053	128.9	15.5	144.4	#NV	#NV	#NV	#NV	#NV
01.06.2017	#NV	#NV	#NV	#NV	#NV	#NV	#NV	#NV	#NV
08.06.2017	#NV	#NV	#NV	#NV	#NV	#NV	#NV	#NV	#NV
15.06.2017	#NV	#NV	#NV	#NV	#NV	#NV	#NV	#NV	#NV
22.06.2017	#NV	#NV	#NV	#NV	#NV	#NV	#NV	#NV	#NV
29.06.2017	#NV	#NV	#NV	#NV	#NV	#NV	#NV	#NV	#NV
06.07.2017	#NV	#NV	#NV	#NV	#NV	#NV	#NV	#NV	#NV
14.07.2017	#NV	#NV	#NV	#NV	#NV	#NV	#NV	#NV	#NV
27.07.2017	#NV	#NV	#NV	#NV	#NV	#NV	#NV	#NV	#NV
21.09.2017	0.0822	804.8	80.0	884.8	0.52	2.58	0.29	#NV	1.50
28.09.2017	0.0433	297.3	73.3	370.6	#NV	0.79	0.07	#NV	#NV
05.10.2017	0.0214	155.0	45.1	200.1	#NV	#NV	#NV	#NV	#NV
12.10.2017	0.0395	347.8	57.8	405.7	#NV	1.12	0.29	#NV	#NV
19.10.2017	0.0479	306.7	60.0	366.8	#NV	0.70	0.05	#NV	#NV
26.10.2017	0.0159	96.4	24.5	120.9	#NV	0.24	#NV	#NV	#NV
02.11.2017	0.0365	202.4	55.3	257.7	#NV	1.43	0.06	#NV	#NV
11.11.2017	0.0150	77.1	17.0	94.1	#NV	0.40	#NV	#NV	#NV
16.11.2017	0.0100	88.1	18.7	106.8	#NV	0.24	#NV	#NV	1.22
23.11.2017	0.0279	130.2	32.1	162.4	#NV	0.97	#NV	8.08	#NV
30.11.2017	0.0078	123.5	27.1	150.6	#NV	0.23	#NV	#NV	1.07
07.12.2017	0.0176	144.3	26.5	170.8	#NV	1.58	0.11	#NV	#NV
14.12.2017	0.0127	136.1	37.4	173.5	#NV	1.17	0.03	#NV	#NV
21.12.2017	0.0067	83.6	23.4	107.0	#NV	#NV	#NV	#NV	#NV
28.12.2017	0.0058	71.6	14.1	85.8	#NV	0.43	#NV	#NV	#NV
04.01.2018	0.0162	118.2	32.3	150.5	#NV	0.26	#NV	#NV	#NV
11.01.2018	0.0176	89.9	46.0	136.0	#NV	0.51	#NV	0.80	#NV
18.01.2018	0.0106	79.9	25.8	105.7	#NV	0.67	#NV	#NV	#NV
25.01.2018	0.0290	154.1	44.5	198.6	#NV	1.71	0.07	#NV	#NV
01.02.2018	0.0174	137.7	39.5	177.2	#NV	0.55	#NV	#NV	#NV
08.02.2018	0.0263	179.7	45.1	224.8	#NV	2.04	0.04	#NV	#NV
15.02.2018	0.0396	255.0	54.8	309.7	#NV	3.14	0.12	#NV	#NV
22.02.2018	0.0713	557.8	68.2	625.9	#NV	5.79	0.21	#NV	#NV
01.03.2018	0.0269	225.9	32.4	258.3	#NV	2.34	0.08	#NV	#NV
08.03.2018	0.0276	190.2	45.6	235.9	#NV	1.96	0.14	#NV	#NV
15.03.2018	0.0449	408.9	56.9	465.8	#NV	2.86	0.13	0.69	#NV
22.03.2018	0.0643	567.9	83.0	650.9	#NV	4.72	0.27	#NV	#NV
29.03.2018	0.0210	188.8	51.7	240.5	#NV	0.44	#NV	#NV	#NV
06.04.2018	0.0144	51.3	26.6	77.9	#NV	#NV	0.06	#NV	#NV
12.04.2018	0.0431	274.8	93.6	368.4	#NV	0.53	0.09	#NV	0.91
19.04.2018	0.0792	502.6	124.1	626.7	#NV	0.62	0.31	1.24	0.99
26.04.2018	0.0893	622.6	135.2	757.7	#NV	0.24	0.21	1.35	1.64
03.05.2018	0.1114	790.5	213.0	1003.6	#NV	0.78	0.80	0.80	#NV
10.05.2018	0.0323	300.0	91.6	391.7	#NV	#NV	0.09	#NV	#NV
17.05.2018	0.0611	606.5	99.9	706.4	#NV	1.06	0.24	#NV	#NV
24.05.2018	0.1037	662.8	191.8	854.7	#NV	0.55	0.16	1.64	4.89

PM 1	Cation chromatography					Anion chromatography			
	Ca^{2+} [µg/m³]	NH_4^+ [µg/m³]	Mg^{2+} [µg/m³]	Na^+ [µg/m³]	K^+ [µg/m³]	SO_4^{2-} [µg/m³]	NO_3^- [µg/m³]	NO_2^- [µg/m³]	Cl^- [µg/m³]
02.06.2016	#NV	2.3723	#NV	0.0255	0.0580	0.3832	0.1050	#NV	#NV
09.06.2016	#NV	1.2028	#NV	#NV	0.0213	0.1672	0.0403	#NV	#NV
16.06.2016	#NV	1.5799	#NV	0.0288	0.0417	0.2608	0.2985	#NV	#NV
23.06.2016	#NV	4.0407	#NV	0.0316	0.1131	0.6974	0.2734	#NV	#NV
30.06.2016	#NV	2.4991	#NV	0.0353	0.0776	0.4282	0.1123	#NV	#NV
07.07.2016	#NV	3.6829	#NV	0.0310	0.1034	0.5960	0.1572	#NV	#NV
14.07.2016	#NV	2.8792	#NV	0.0298	0.0641	0.4807	0.2426	#NV	#NV
21.07.2016	#NV	3.5245	0.0404	0.0791	0.2105	0.5921	0.2895	#NV	#NV
28.07.2016	#NV	2.9331	#NV	0.0306	0.1443	0.4430	0.2083	#NV	#NV
05.08.2016	#NV	1.9015	#NV	0.0199	0.0329	0.2496	0.1032	#NV	#NV
11.08.2016	#NV	2.1981	#NV	0.0398	0.1636	0.3171	0.3455	#NV	#NV
18.08.2016	#NV	1.4907	#NV	0.0268	0.0597	0.1988	0.0951	#NV	#NV
25.08.2016	#NV	2.7936	#NV	0.0258	0.1084	0.3761	0.2978	#NV	#NV
01.09.2016	#NV	4.7100	#NV	0.0339	0.2378	0.8374	0.2665	#NV	#NV
08.09.2016	1.4100	#NV	0.0833	0.1368	0.9799	1.5723	1.3417	#NV	#NV
15.09.2016	#NV	1.8669	#NV	0.0146	0.0856	0.2629	0.1478	#NV	#NV
22.09.2016	#NV	2.6728	#NV	0.0182	0.1135	0.5770	0.1890	#NV	#NV
29.09.2016	#NV	2.4146	#NV	0.0225	0.1082	0.3324	0.1131	#NV	#NV
06.10.2016	#NV	1.1005	#NV	#NV	0.0332	0.1723	0.3320	#NV	#NV
13.10.2016	#NV	0.6103	#NV	#NV	0.0319	0.0745	0.1919	#NV	#NV
20.10.2016	0.5866	0.9795	0.0255	0.0236	0.0618	0.1823	0.7710	#NV	#NV
27.10.2016	#NV	0.7849	#NV	#NV	0.0248	0.0784	0.2253	#NV	#NV
03.11.2016	#NV	0.5477	#NV	0.0195	0.0341	0.0933	0.3073	#NV	#NV
10.11.2016	#NV	1.5683	#NV	#NV	#NV	0.2082	0.1416	#NV	0.1201
17.11.2016	#NV	1.1266	#NV	0.0183	0.0458	0.2646	0.1275	#NV	#NV
24.12.2016	#NV	0.5496	#NV	#NV	0.0248	0.0698	0.0937	#NV	#NV
01.12.2016	#NV	0.4810	#NV	#NV	0.0197	0.0778	0.0981	#NV	#NV
08.12.2016	#NV	0.4413	#NV	#NV	#NV	0.0553	#NV	#NV	#NV
15.12.2016	#NV	0.5116	#NV	#NV	0.0324	0.0821	0.0786	#NV	#NV
23.12.2016	#NV	0.6113	#NV	0.0459	0.0226	0.1163	0.2135	#NV	0.0345
29.12.2016	#NV	0.4714	#NV	0.1067	0.0771	0.1066	0.9883	0.0417	0.3896
05.01.2017	#NV	0.4950	#NV	0.0353	0.0279	0.0691	0.1673	#NV	#NV
12.01.2017	#NV	1.2143	#NV	0.0676	0.0834	0.2105	0.2318	0.0765	#NV
19.01.2017	#NV	#NV	#NV	#NV	#NV	#NV	#NV	#NV	#NV
26.01.2017	#NV	1.2741	#NV	0.0233	0.0550	0.1884	0.0977	#NV	#NV
02.02.2017	#NV	0.7373	#NV	0.0230	0.0391	0.1438	0.3140	#NV	#NV
16.02.2017	#NV	0.6830	#NV	#NV	0.0412	0.1699	0.1627	0.0369	#NV
23.02.2017	#NV	0.7938	#NV	0.0182	0.1065	0.1668	0.5972	#NV	#NV
02.03.2017	#NV	0.5998	#NV	0.0348	0.0526	0.1060	0.2667	#NV	#NV
09.03.2017	#NV	1.0751	#NV	0.0294	0.0990	0.1516	1.1391	#NV	#NV
10.03.2017	#NV	#NV	#NV	#NV	#NV	#NV	#NV	#NV	#NV
16.03.2017	#NV	1.9646	#NV	0.0373	0.1987	0.4384	1.3077	#NV	#NV
23.03.2017	#NV	2.6508	#NV	0.0536	0.2050	0.7190	2.3087	#NV	#NV
30.03.2017	#NV	4.5741	#NV	0.0473	0.3766	1.3025	3.6273	#NV	0.0256
06.04.2017	#NV	1.7195	#NV	0.0420	0.0892	0.4100	0.8935	#NV	#NV
13.04.2017	#NV	1.7591	#NV	0.0202	0.0702	0.4217	1.2825	#NV	#NV
20.04.2017	#NV	1.6874	#NV	0.0165	0.0785	0.5113	0.3060	#NV	#NV
27.04.2017	#NV	1.9393	#NV	0.0192	0.0613	0.3099	0.3330	#NV	#NV
04.05.2017	#NV	1.1958	#NV	0.0145	0.0515	0.1650	0.3356	#NV	#NV
12.05.2017	#NV	1.6956	#NV	0.0232	0.0576	0.2411	0.3419	0.0447	#NV
18.05.2017	#NV	3.8439	#NV	0.0355	0.1069	0.6076	0.6312	#NV	#NV
25.05.2017	#NV	1.7568	#NV	0.0356	0.0128	0.1029	0.0880	#NV	#NV
01.06.2017	#NV	#NV	#NV	#NV	#NV	#NV	#NV	#NV	#NV
08.06.2017	#NV	#NV	#NV	#NV	#NV	#NV	#NV	#NV	#NV
15.06.2017	#NV	#NV	#NV	#NV	#NV	#NV	#NV	#NV	#NV
22.06.2017	#NV	#NV	#NV	#NV	#NV	#NV	#NV	#NV	#NV

PM 1	Cation chromatography					Anion chromatography			
	Ca^{2+} [µg/m³]	NH_4^+ [µg/m³]	Mg^{2+} [µg/m³]	Na^+ [µg/m³]	K^+ [µg/m³]	SO_4^{2-} [µg/m³]	NO_3^- [µg/m³]	NO_2^- [µg/m³]	Cl^- [µg/m³]
29.06.2017	#NV	#NV	#NV	#NV	#NV	#NV	#NV	#NV	#NV
06.07.2017	#NV	#NV	#NV	#NV	#NV	#NV	#NV	#NV	#NV
14.07.2017	#NV	#NV	#NV	#NV	#NV	#NV	#NV	#NV	#NV
27.07.2017	#NV	#NV	#NV	#NV	#NV	#NV	#NV	#NV	#NV
21.09.2017	#NV	5.8960	#NV	0.0441	0.3991	0.8481	0.5260	#NV	#NV
28.09.2017	#NV	2.2621	#NV	0.0284	0.1444	0.3434	0.1175	#NV	#NV
05.10.2017	#NV	0.9301	#NV	#NV	0.0468	0.1282	0.2439	#NV	#NV
12.10.2017	#NV	1.4355	#NV	#NV	0.0793	0.1555	0.2286	#NV	#NV
19.10.2017	#NV	1.7996	#NV	0.0346	0.1453	0.2415	0.4152	#NV	0.0872
26.10.2017	#NV	0.8467	#NV	0.1307	0.0312	0.1347	0.2699	#NV	0.0814
02.11.2017	#NV	2.0869	#NV	0.0509	0.1010	0.3111	0.3266	#NV	#NV
11.11.2017	#NV	0.4612	#NV	#NV	0.0340	0.0625	#NV	#NV	#NV
16.11.2017	#NV	0.5966	#NV	#NV	0.0169	0.0812	0.0944	#NV	0.0633
23.11.2017	#NV	0.8194	#NV	0.0528	0.1004	0.1109	0.2863	#NV	#NV
30.11.2017	#NV	0.6313	#NV	0.0237	0.0169	0.0960	0.2617	#NV	0.0594
07.12.2017	#NV	0.4788	0.0453	0.4195	0.0772	0.0895	1.8942	#NV	0.3236
14.12.2017	#NV	0.6474	#NV	0.0470	0.0652	0.0956	0.2493	#NV	#NV
21.12.2017	#NV	0.3718	#NV	#NV	0.0229	0.0496	0.0834	#NV	#NV
28.12.2017	#NV	0.3904	#NV	0.0734	0.0267	0.0621	0.2211	#NV	0.0638
04.01.2018	#NV	0.7873	#NV	0.1275	0.0578	0.1121	0.6443	#NV	#NV
11.01.2018	#NV	1.7421	#NV	0.0617	0.0884	0.2915	0.2963	#NV	#NV
18.01.2018	#NV	0.4417	#NV	0.0381	0.0507	0.0629	0.2360	#NV	#NV
25.01.2018	#NV	0.9046	#NV	0.0220	0.1004	0.1444	0.3196	#NV	#NV
01.02.2018	#NV	0.9940	#NV	0.0387	0.0698	0.1238	0.1523	#NV	#NV
08.02.2018	#NV	1.4334	#NV	0.0533	0.1416	0.2027	0.7684	#NV	#NV
15.02.2018	#NV	2.0685	#NV	0.0325	0.2097	0.3018	0.5186	#NV	#NV
22.02.2018	#NV	5.6053	#NV	0.1103	0.4560	0.9688	0.4866	#NV	#NV
01.03.2018	#NV	0.9306	#NV	0.0277	0.1966	0.1484	0.7872	#NV	#NV
08.03.2018	#NV	0.8794	#NV	0.0227	0.1030	0.1087	0.4252	#NV	#NV
15.03.2018	#NV	3.0410	#NV	0.0566	0.1875	0.4533	1.7597	#NV	#NV
22.03.2018	#NV	3.1825	#NV	0.0342	0.2676	0.4126	2.0943	#NV	#NV
29.03.2018	#NV	1.4727	#NV	0.0621	0.1139	0.2041	0.4538	#NV	#NV
06.04.2018	#NV	0.9240	#NV	0.0287	0.0326	0.1455	0.4942	#NV	#NV
12.04.2018	#NV	3.4775	0.0381	0.0772	0.1467	0.5794	1.1470	#NV	#NV
19.04.2018	0.3990	3.4153	0.0694	0.0737	0.2149	0.6784	1.6603	#NV	#NV
26.04.2018	0.6954	8.7318	0.0957	0.2986	0.4173	1.3811	1.7016	#NV	0.1232
03.05.2018	0.9617	7.8160	0.0906	0.1503	0.3065	1.2795	1.4973	#NV	#NV
10.05.2018	#NV	2.9028	#NV	0.0206	0.0631	0.4962	0.3902	#NV	0.0524
17.05.2018	#NV	4.5579	#NV	0.0808	0.1348	0.8602	0.4990	#NV	#NV
24.05.2018	0.4663	5.7935	0.0715	0.0751	0.1580	1.2331	0.6786	#NV	#NV